STRUCTURAL REHABILITATION OF DETERIORATED POST-TENSIONED CONCRETE BRIDGE CANTILEVER WING SLABS UTILIZING POST-TENSIONED CFRP RODS

By

Faraj Shahrstan

Submitted in partial fulfilment of the requirements

for the degree of Master of Applied Science

At

Dalhousie University

Halifax, Nova Scotia

December 2022

DEDICATION

I am dedicating this thesis to my beloved mother, Maram Nasef, my brother, Rinad Shahrstan, my father, Dr. Kamil Shahrstan, and my engineering mentor, Ray Daniels. Thank you for the endless fruitful discussions and conversations we have had and for the much-needed guidance and support in my personal life and professional career path. You have all championed me, fostered me, invested in me, and supported me on various levels, and to you, I owe it all. I will never cease to fight for with the right mindset, tools, virtues, and values, I am unstoppable and will always be victorious. “Stretching out my wings always to soar high with the grace and mercy of God”.

TABLE OF CONTENTS

LIST OF TABLES

LIST OF FIGURES

ABSTRACT

In this thesis, the structural rehabilitation of a deteriorated post-tensioned concrete cantilever wing slab with post-tensioned (PT) carbon-fibre-reinforced polymer (CFRP) rods is investigated. The goal of this research was two-fold: First, to determine the viability and suitability of a proposed mechanical strengthening system for post-tensioning unidirectional pultruded CFRP Rods. Second, to evaluate the performance and feasibility of utilizing post-tensioned CFRP rods with permanent mechanical anchorage to rehabilitate a deteriorated post-tensioned concrete bridge cantilever wing slab. To achieve the first goal, a proposed mechanical split wedge and barrel anchor was machined in-house for a #3 (10 mm) CFRP rod. The anchor features a contoured longitudinal profile consisting of a 1650 mm circular radius to minimize the stress concentrators at the loading end of the anchor, pushing the stress toward the back of the anchor. The anchor also features a competitive 80 mm in-length stainless steel barrel and 80 mm in-length aluminum wedge core. The system strictly relies on friction for load-bearing capacity with no adhesives required. Seven specimens in total were carried out for the experimental assessment of the anchorage system. Pre-setting the anchors was required to eliminate system slippage. At a pre-setting force of 80 kN, the maximum effective jacking force for the selected CFRP rod was determined to be 50 kN. The CFRP anchor was utilized to strengthen an experimental PT concrete bridge cantilever wing slab specimen. Two half-scale bridge cantilever wing slab specimens based on an existing in-service bridge in the Province of Nova Scotia were fabricated and cast. One specimen served as the steel control emulating nominal existing conditions. The second specimen served as the CFRP rehabilitation emulating simulated damage and subsequent PT CFRP rehabilitation. The CFRP rods for rehabilitation were embedded in near-surface-mounted (NSM) grooves in the negative moment region of the experimental PT concrete bridge cantilever wing specimen. The bridge cantilever specimens were tested, and both had flexural concrete crushing failure modes. The proposed CFRP rehabilitation was able to restore the lost structural capacity and reduced deflection under service. An analytical model was created in order to predict the ultimate flexural capacity of the PT bridge cantilever wing slabs and the experienced deflection at simulated service conditions. The model accurately predicted the flexural capacity of the bridge cantilever specimen and slightly overpredicted the service deflection.

LIST OF ABBREVIATIONS AND SYMBOLS USED

Abbreviations

ACI	American Concrete Institute
ASTM	American Society for Testing and Materials
CFRP	Carbon Fibre Reinforced Polymer
CLP	Contoured Longitudinal Profile
CSA	Canadian Standards Association
DLA	Dynamic Load Allowance
FHWA	Federal Highway Administration
fib	Federation International De Beton
FRP	Fibre Reinforced Polymer
LP	Linear Potentiometer
NSDPW	Nova Scotia Department of Public Works
NSM	Near Surface Mounted
NSMR	Near Surface Mounted Rehabilitation
NSTIR	Nova Scotia Transportation and Infrastructure Renewal
PT	Post-Tensioned
PTI	Post-Tensioning Institute
SLS	Serviceability Limit State
ULS	Ultimate Limit State

Symbols

a	Depth of Equivalent Rectangular Concrete Stress Block
As	Mild Steel Cross-Sectional Area

Aps	Prestressing Steel Tendon Cross-Sectional Area
Afrp	FRP Tendon Cross-Sectional Area
Atrans	Transformed Concrete Cross-Sectional Area
b	Width of the Concrete Component Section
c	Concrete Section Neutral Axis
c/c	Centre to Centre
e	Eccentricity
Ec	Modulus of Elasticity of Concrete
Efrp	Modulus of Elasticity of FRP Tendon
Eps	Modulus of Elasticity of Prestressing Steel Tendon
Es	Modulus of Elasticity of Mild Steel
f'c	Specified Compressive Strength of Concrete
fcr	Cracking Strength of Concrete
ffrp	Stress in FRP Tendons
ffu	Guaranteed Tensile Strength of FRP Tendon
fp	Peak Stress of Concrete
fps	Stress in Steel Tendons
fpu	Specified Tensile Strength of Prestressing Steel Tendon
fs	Stress in Mild Steel
ft	Feet
fy	Specified Yield Strength of Reinforcing Bars
GPa	Giga-Pascals
kg	Kilogram

kips	Kilo-pounds
kN	Kilo-Newtons
L	Length
Ld	Development Length
m	Metre
Mcr	Cracking Moment
Mdead	Dead Load Moment
Mlive	Live Load Moment
mm	Millimetre
MPa	Mega-Pascal
Ms	Flexural Moment at the Serviceability Limit State
Mu	Ultimate Moment
n	Modular Ratio
O.D	Outer Diameter
o/c	On Centre
P	Load
Q	First moment of Area
rad	Radians
s	Section Modulus
εc	Strain in Concrete
εcu	Ultimate Design Strain of Concrete
εfrp	Strain in FRP Tendon
εps	Strain in Prestressing Steel Tendon

ε_s	Strain in Reinforcing Bars
ψ	Curvature
Δ	Deflection
ρ	Density
α	Equivalent Concrete Stress Block Factor 1
β	Equivalent Concrete Stress Block Factor 2
φ	Resistance Factor
γ	Unit Weight

ACKNOWLEDGEMENTS

The author of this thesis would first like to thank the tremendous contribution and support of Raymond Daniels, Central District Bridge Engineer with the Nova Scotia Department of Transportation. Secondly, thank all the members of the Nova Scotia Department of Transportation Central Bridge Division for their sustained moral support and for taking care of my bridge specimens. Thirdly, the contribution and support of Paul Matheson, Atlantic Provinces Area Manager with SIKA Corporation, and Bird Stairs regional construction supplier. Fourthly, the generous financial support provided to the author by the American Concrete Institute Foundation and support from the SYPAC committee of the American Concrete Institute. Fifthly, the author's academic supervisor, Dr. Pedram Sadeghian, Associate Professor and Canada Research Chair in Sustainable Infrastructure at Dalhousie University.

The author would also like to highlight his gratitude towards Jordan Maerz (Civil Technician), the general contractor for the research project, and Graham Muirhead, the mechanical engineer/CNC specialist for without their expertise, and support, this research project would not have been successful. Additionally, gratitude to the technicians at Dalhousie University Faculty of Engineering and the Emera IDEA Hub for their contribution and support for this research project including Jesse Keane (Data Acquisition Technician), Dean Grijm (Machinist), and Mark Macdonald (Machinist). Furthermore, the consulting advice of Christopher Dyck, Senior Bridge Engineer with COWI North America. Lastly, the countless discussions, technical expertise, and advice from Dr. John Newhook, Professor at Dalhousie University.

CHAPTER 1 INTRODUCTION

1.1 Motivation

Canada is experiencing a crisis trying to deal with the nation's aging public infrastructure. In 2019, almost 40% of public roads and bridges in Canada were reported to be in worse condition and in need of repair or replacement (Canadian Infrastructure Report Card 2019). Most of Canada is in a frigid climate region where public infrastructure is constantly exposed to harsh ambient environments which include constant freeze and thaw cycles, de-icing salts and chemicals, and exposure to marine air. Additionally, mechanical snowplow damage has put a toll on public infrastructure. These harsh environments have facilitated a haven for corrosion to damage the structural capacity of the steel reinforcement within concrete bridges. Figure 1-1 exemplifies the effect of corrosion on post-tensioned steel tendons in a post-tensioned concrete bridge deck.

Figure 1-1. Corroded Transverse Steel Post-Tensioning (photo taken by Faraj Shahrstan in 2020)

Corrosion is a natural phenomenon that induces the gradual destruction of metal materials due to chemical reactions from the environment. De-icing salts, chemicals, water, and moisture have penetrated through the cracks of concrete bridge decks over the years. The steel cross-section degrades, thereby leading to concrete spalling and the diminishing of the structural capacity of the member. Corrosion has drastically cost public transportation departments in North America

billions of dollars as public infrastructure endures severe environments throughout its service life. In several case studies, Departments of Transportation (DOT) have found compromised post-tensioning steel in bridge slabs where a cost-effective rehabilitation and strengthening strategy is required to fulfill the service life of the bridge structure (NCHRP 2021). The increase in truck sizes and vehicle traffic, the restrictive budgets, the deferred maintenance plans, and the consistent exposure to harsh ambient environments have drastically put a heavy toll on aging infrastructure perpetuating the deterioration of existing highway bridges. In the United States, repair and maintenance issues related to post-tensioned bridges have gained attention in light of instances of serious tendon degradation in structures built before 2000 (NCHRP 2021). Aging infrastructure is in a dire state and needs an eco-conscious viable solution. Bridges in service require corrective maintenance to prolong service life as replacement of existing bridges warrants high capital costs that are presently unavailable and are a burden to taxpayers. Moreover, the closure of existing highway bridges for replacement is logistically challenging as it results in massive detours and prolonged public frustration. A breakthrough in the structural rehabilitation of concrete bridges is the utilization of fiber reinforced polymer (FRP) composites to strengthen deteriorated concrete bridges. Although FRP composites have become a common reinforcement in the construction industry, an emerging method is the utilization of prestressed FRPs as a corrective maintenance solution to restore structural capacity and strengthen concrete bridges. There is a huge demand for increased research in the field of prestressed FRPs. The main concern with prestressing CFRPs specifically is the efficiency of a suitable anchorage system that is required to grip and hold the rod and the capability to transfer the required jacking force (pre-compression) into the concrete. Several researchers have experimented with bonded and mechanical anchorage systems since the 1990s to grip CFRP rods and strips but to the author's knowledge, there are no commercial CFRP anchorage systems nor standardized acceptance criteria for such systems. A particular post-tensioned concrete bridge structure in the Province of Nova Scotia with deteriorated transverse steel post-tensioning within its cantilever wing slab serves as the basis for this experimental research. The main issue at hand is finding a cost-effective rehabilitation strategy to maintain the service life of post-tensioned concrete bridge structures that have experienced deterioration to their post-tensioning steel.

1.2. Research Objectives

The objectives of this research are as follows:

- To determine the viability and suitability of a proposed mechanical strengthening system for post-tensioning unidirectional pultruded CFRP rods.
- To evaluate the performance and feasibility of utilizing post-tensioned CFRP rods near-surface-mounted with permanent mechanical anchorage to rehabilitate deteriorated post-tensioned concrete bridge cantilever wing slabs.
- Conduct an analytical study to predict the ultimate flexural capacity and service deflection for deteriorated cantilever sections of an existing bridge that utilize the proposed CFRP rehabilitation system.

1.3. Research Scope

To achieve the outlined objectives, the first stage of the research project was selecting and developing a design for the proposed mechanical strengthening system that would be utilized for PT unidirectional pultruded CFRP rods. A split wedge and barrel mechanical anchor was developed and machined in-house. Preliminary anchorage testing was conducted on the mechanical anchor to determine the design concept viability and suitability. After preliminary anchorage testing and determining the promising nature of the anchor, the next step was to determine how to implement the system into a PT concrete structure. The anchorage design had to be altered for threading of the barrels was needed to transfer the post-tensioning force to a concrete structure. There were a few other adjustments made to the anchor. After a final design was completed, static anchorage testing was conducted. The static anchorage tests provided the maximum safe effective post-tensioning force that could be applied to a concrete structure. The second stage of the research project was utilizing the proposed developed CFRP mechanical anchor in a post-tensioned concrete bridge cantilever wing slab system. Two half-scale post-tensioned concrete bridge cantilever wing specimens were fabricated and cast based on an existing in-service bridge in the Province of Nova Scotia. One specimen served as the control and the other specimen undertook the proposed PT CFRP mechanical strengthening after enduring simulated damage. The specimens were tested, and their performance was evaluated. The feasibility of the CFRP anchor for the rehabilitation of PT bridge concrete structures was

documented. An analytical study was conducted to predict the ultimate flexural capacity and the service deflection of a unit cantilever wing slab cut out of the existing in-service bridge structure. The analytical model was verified with the experimental data obtained in the laboratory.

1.4. Thesis Layout

The general layout of this thesis consists of an introduction to prestressed/post-tensioned CFRP, a literature review into the utilization of FRPs for the rehabilitation of concrete bridge structures, an in-depth explanation of the comprehensive two-stage experimental program that was conducted, a discussion of the results obtained, an overview of the analytical study conducted, and ending with the conclusions and recommendations. The literature review in Chapter 2 presents applicable literature in the past two decades on the utilization of FRPs for the rehabilitation of concrete bridge structures. The review presents past research conducted on prestressed FRP materials and the implementation of FRPs utilizing the near-surface-mounted method within concrete bridge structures. Additionally, the review discusses past research advances on the development of anchorage systems for CFRP rods and finally research gaps in this scope of research. Chapter 3 presents the CFRP anchorage experimental program that was conducted. This chapter presents the details of the design and material selection of the anchor. Additionally, all details on the preliminary anchorage proof of concept testing, static anchorage testing, and the final anchorage design are presented. The details in the chapter include the test matrices, specimen fabrication, test results, and discussion. Chapter 4 presents the in-depth bridge cantilever experimental program that was conducted. The chapter discusses the materials selected, the system design, the test matrices, specimen fabrication, specimen post-tensioning, specimen instrumentation and test setup, loading protocol, and final test results and discussion. Chapter 5 presents the analytical model that was created to predict the ultimate flexural capacity of the bridge cantilever specimens and the service deflection. Model verification with the experimental data is presented and a parametric study applying the model to a real-life in-service PT concrete bridge cantilever wing slab is presented. Chapter 6 presents the conclusions of this research project and recommendations for future research.

CHAPTER 2 LITERATURE REVIEW

Post-tensioned concrete is a very common approach where concrete bridge deck spans and panels are post-tensioned on-site after the concrete has cured. Historically, high-strength steel has been utilized for pre-stressing applications for concrete bridges, but more recently prestressing FRP material is growing widely. There are many structural benefits to prestressing reinforcement which is as follows (modified from El-Hacha et al. 2001):

- Improve Serviceability
- Reduce dead load deflections
- Reduce crack widths and delay the onset of cracking
- Relieve internal steel reinforcement strains
- Induce compressive stress capable of resisting fatigue failure
- Increase the yielding capacity of internal steel reinforcement
- Increase material efficacy of concrete and FRP
- Increase live load capacity
- Improve fatigue strength by reducing tensile steel stress

Moreover, there are many economic benefits to using prestressing reinforcement during the overall service life of a concrete bridge. Even though the initial capital cost of prestressing is higher than conventional mild reinforcement, the above-mentioned structural benefits offset the initial capital costs throughout the service life of the bridge. Due to the economic and structural benefits of prestressing, the prestressing approach has become popular for implementation with FRP materials. Material for prestressing reinforcement can come in different geometries including wires, strands, and bars. Unlike conventional steel reinforcement, there are no standardized shapes, surface configurations, fibre orientation, constituent materials, and proportions for final FRP products (ACI 440.4 2011). Thus, there is a huge demand for increased research in the field of prestressed FRPs. Due to the significant economic and structural benefits associated with prestressing reinforcement and the ongoing research with FRP materials, there is huge promise in prestressing FRP materials mitigating the structural capacity issues that face concrete bridges. Carbon fibres offer the highest tensile strength and highest stiffness. Carbon FRP is typically used for prestressed applications to fully utilize the efficacy of the material. Moreover, literature has focused on CFRP strands, bars, and strips for prestressing. Although CFRP can be implemented

in non-prestressed applications, the expensive price tag of CFRP underlines prestressing to fully utilize the capacity of the material. CFRP is readily available commercially for new construction and rehabilitation of concrete bridge girders, decks, and piers. This paper will focus on the application of post-tensioned CFRP rods as CFRP tendons. CFRP rods are known for their high strength-to-weight ratio, non-corrosiveness, high durability, and high stiffness offering better ultimate limit state and serviceability conditions for bridge infrastructure.

2.1. FRP Rehabilitation of Concrete Bridge Elements

Fiber-reinforced polymers are high-strength, lightweight, noncorrosive, nonconducting, and nonmagnetic materials that have revolutionized new bridge construction and bridge rehabilitation (ACI 440.4 2011). In new bridge construction, FRP materials have been utilized as the main flexural reinforcement for bridge decks. Additionally, FRP materials, specifically CFRP tendons were deployed as a prestressing material as a substitute for steel tendons with an initiative to enhance the durability and lifespan of newly constructed bridges (Grace et al. 2022). For bridge rehabilitation, FRP materials have been utilized to retrofit and strengthen existing damaged or deteriorated concrete bridge decks, girders, and piers. Current literature presents good promise for FRPs in prestressing applications since by prestressing the FRP reinforcement, the stress in the internal steel reinforcement steel and deflections will decrease; as well as there will be higher utilization of the FRP materials (El-Hacha and Soudki 2013). Prestressed FRP is the same lightweight, non-corrosive materials that are used in non-prestressed applications but by applying a prestress to the FRP, the material may be used more efficiently since a greater portion of its tensile capacity is engaged (El-Hacha et al. 2001). This paper will focus more on the near-surface-mounted application of FRPs for concrete bridge structure rehabilitation. NSM is a technique to retrofit/rehabilitate bridge elements by inserting FRP material into pre-cut grooves that are saw-cut in the strengthened concrete member. The depth of the grooves is limited to the depth of the concrete cover unless a concrete overlay is to be cast to increase the cover, but the high cost associated with such a procedure yields it unlikely. The width and spacing of the grooves are dependent on the amount of strengthening required for the concrete bridge element. FRP bars, strips, and/or rods are placed in grooves, and they are protected by the concrete cover being less exposed to accidental impact, mechanical damage, fire, and vandalism (Lorenzis and Teng 2007). The NSM method relies on either an epoxy-based or a cement-based adhesive or grout to transfer

tensile forces from the reinforcement to the parent concrete member (Lorenzis and Teng 2007). Epoxy resins have been found to deliver a much stronger FRP-concrete bond but at a much higher cost than cement grouts. The NSM method can be applied for both non-prestressed and prestressed applications but to increase the efficacy of the material, a prestressed technique is recommended. Surface preparation is critical yet laborious for near-surface mounted applications. The grooves need to be saw cut as indicated where extreme caution is needed to not interfere with the internal steel reinforcement of the concrete member due to the limitation of the groove depth. The grooves are half-filled with adhesive, and FRP material is placed in the shape of strips or bars followed by final epoxy leveled off at the surface to facilitate the transfer of tensile forces from the FRP to the concrete. Figure 2-1 presents a typical NSM FRP application method where CFRP rods are placed in grooves within the tensile soffit of a bridge deck.

Figure 2-1. NSM FRP Placement in Deck Soffit Side (Taken from Casadei et al. 2006)

The most typical failure mode associated with NSM FRP strengthening is the splitting of the concrete cover as failure progresses, but to mitigate this, the prestressed FRP needs to be anchored. However, unlike conventional steel, there are no commercial anchorage systems for CFRP

prestressed tendons, and the influence of different anchorage configurations remains unknown (Kim et al. 2014). Research remains ongoing for the utilization of NSM CFRP for strengthening. Near-surface-mounted FRPs are used as reinforcement to provide enhanced ultimate and serviceability capacities. A promising NSM application is the utilization of NSM CFRP in a post-tensioning situation to strengthen reinforced concrete beams. An experimental program was conducted by Taljsten and Nordin 2007 where they retrofitted reinforced concrete T-beams with post-tensioned NSM CFRP rods whose performance was compared with that of other beams strengthened with conventional, externally unbonded steel strands. The beam with post-tensioned CFRP showed 100% and 182% increases in yield and ultimate loads, respectively, compared with an unstrengthened control beam. Figure 2-2 presents the placement of the NSM rods within the T-beams used by Taljsten and Nordin in their experimental program.

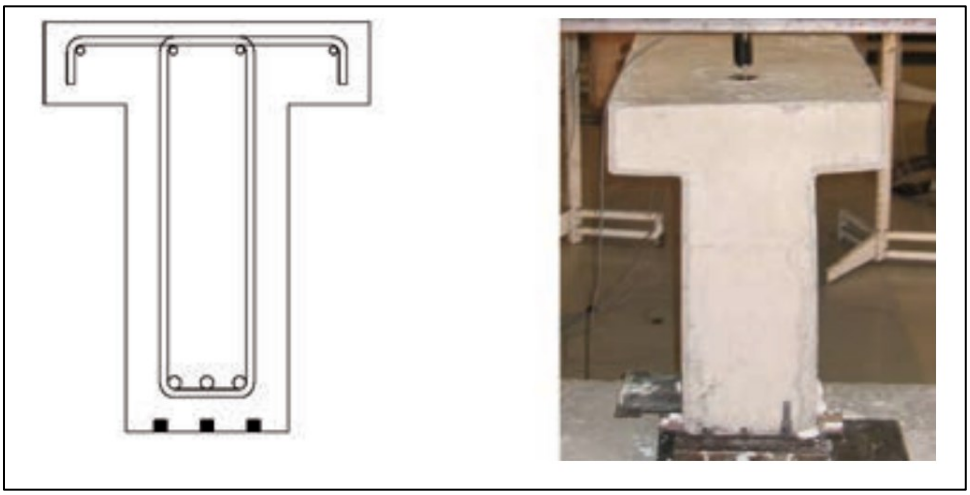

Figure 2-2. Placement of NSM Rods (Taken from Taljsten and Nordin 2007)

In 2011, El-Hacha and Gaafar conducted studies on the load-carrying capacity and strain development of reinforced concrete beams strengthened with post-tensioned NSM CFRP. The level of post-tensioning applied varied from 0% to 60% of the CFRP strength. All strengthened beams exhibited an increase in the flexural load of approximately 75% relative to an un-strengthened control beam, but the failure mode was brittle. They presented the following prestressing system for NSM CFRP bars as shown in Figure 2-3.

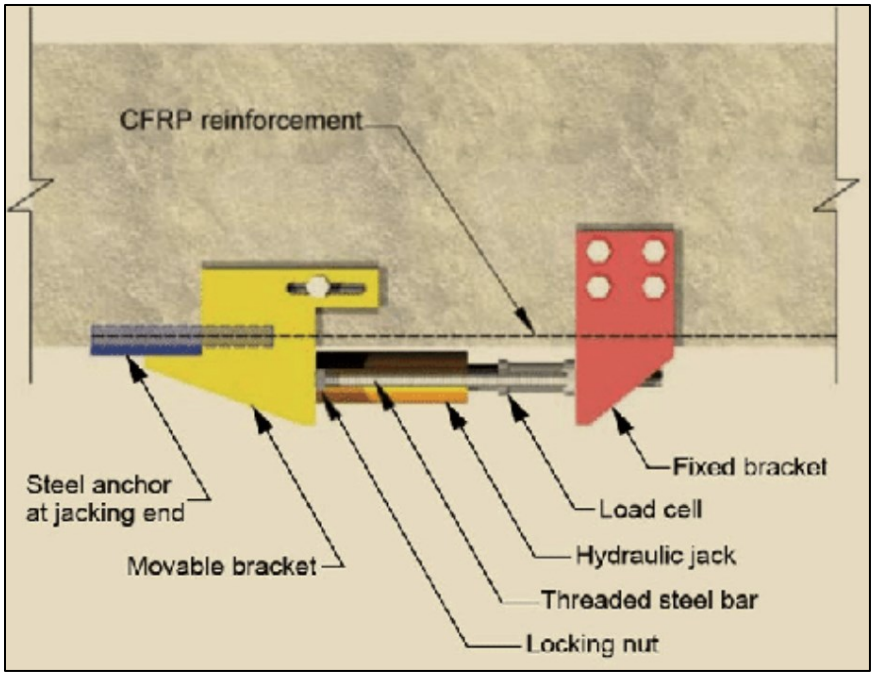

Figure 2-3. Prestressing System for NSM CFRP Bars (Taken from El-Hacha and Gaafar 2011)

In 2014, Kim et al. proposed a now patented anchorage configuration methodology for post-tensioned NSM CFRP upgrading of constructed bridge girders. Figure 2-4 presents their patented (Patent Numbers: 10-1083626, 10-0653632, 10-1005347) application technique:

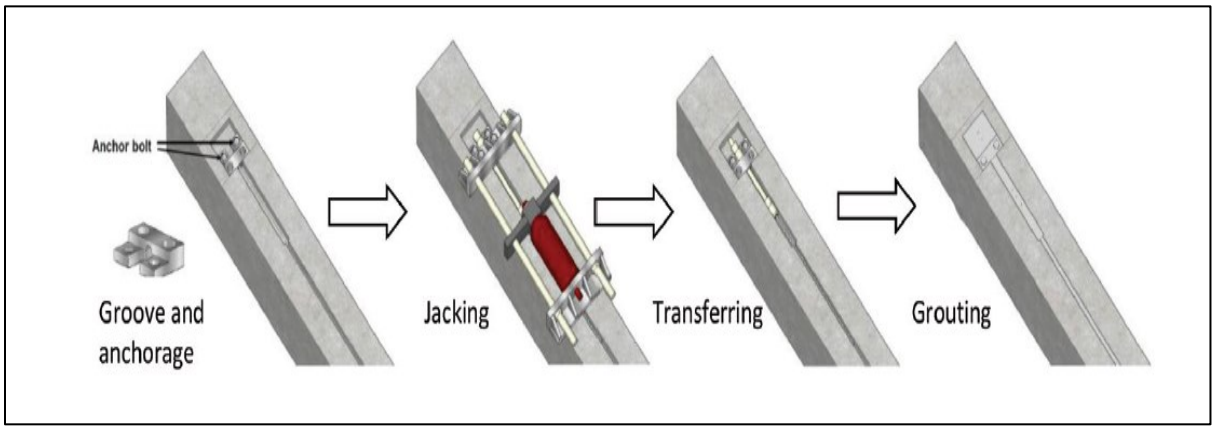

Figure 2-4. Post-Tensioned NSM CFRP Application Method (Taken from Yail Kim et al. 2016)

The technique as portrayed in Figure 2-4 begins by first saw cutting grooves in the tension soffit side of the beam followed by the installation of the temporary anchorage system. Next, jacks are

placed and secured in place to post-tension the FRP material in the groove. The prestressing force is transferred and then slowly released to allow for the removal of the jacks. Finally, the groove is grouted and leveled flush with the parent concrete member. The NSM strengthening technique has been conducted greatly for strengthening reinforced concrete beams, but more research is needed for NSM strengthening experimentation with other concrete bridge elements including bridge decks and piers.

An experimental campaign in the state of Missouri was conducted with the main purpose of proving that the prestressed NSM CFRP upgrade technique could allow not only restoring the original ultimate flexural capacity of the respective damaged girder but also the service performance of the prestressed concrete girder. A pilot research project proceeded with recreating two full-scale size girders that were damaged. The replicated girders were based on two in-service bridges, the first from bridge A10062, St. Louis County, Missouri, and bridge A5657 South of Dixon, Missouri that was both damaged due to impact from over-height vehicles. Figure 2-5 presents the lab setup of the pilot research project:

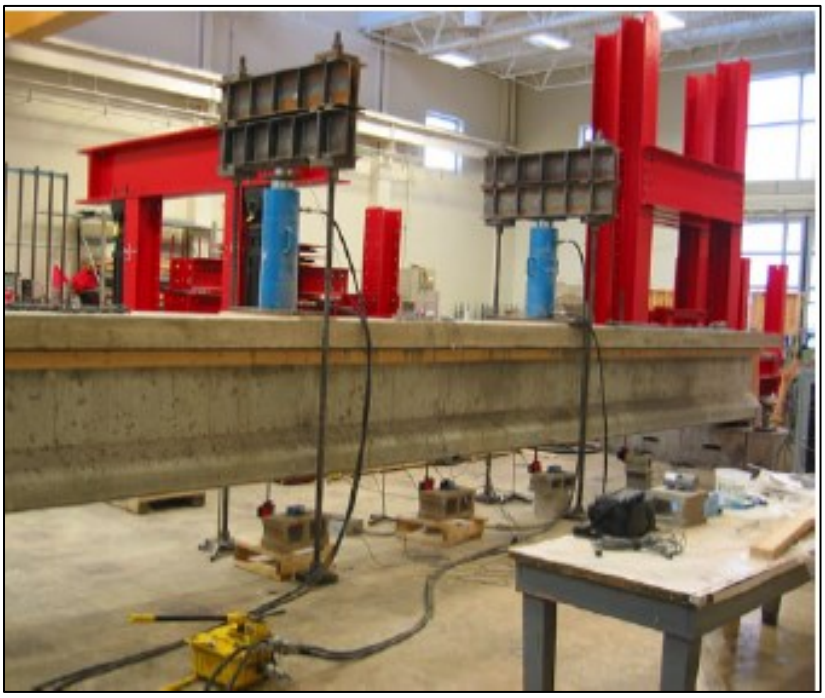

Figure 2-5. Pilot Research Project Full Scale Bridge Girder Lab Setup (Taken from Casadei et al. 2006)

Both girders had similar profiles being 11 m span prestressed concrete I-girders with twelve straight profile low-relaxation steel tendons as flexural reinforcement. The experimental study included a girder that was strengthened with prestressed NSM CFRP. The prestress NSM CFRP application included CFRP bars but with no permanent anchorage. Epoxy adhesives were utilized. To simulate equivalent damage on both bridge girders after the concrete was cast, the team saw cut and chiseled out concrete at the midspan of each girder exposing two steel prestressed tendons. Two prestressed steel tendons were cut on both girders and rapid-set mortar was used to fill in place of the chiseled-out concrete. Each girder was then loaded until failure. The girder strengthened using prestressed NSM CFRP bars failed due to the splitting of the concrete cover which resulted in a debonding failure followed by the progressive failure of the system. However, the NSM CFRP strengthening method was able to restore the ultimate capacity of the original girder based on the simulated damage and failed in a ductile manner. Thus, NSM CFRP for rehabilitation is a very promising rehabilitation scheme. Previous studies have primarily been focused on reinforced concrete beams and decks in their positive bending moment regions, with limited research on concrete slabs for which near-surface-mounted rehabilitation is applied in the negative bending moment area, such as bridge slab overhangs (Lee and Cheng 2011). Therefore, this research project attempts to contribute to the research gap in this field with the utilization of PT CFRP rods in the negative bending moment region of bridge cantilever wing slabs.

2.2. CFRP Anchorage Systems

Steel is isotropic and offers great ductility due to its great post-yielding plastic hardening properties. The major concern with steel that has led to investment in FRP materials is the issues regarding fatigue relaxation and corrosion. CFRP material is an alternative to supplement steel, but it has its Achilles Heel. Due to CFRP material's orthotropic properties, reduced ductility, and reduced ability to withstand sharp stress concentrators, conventional mechanical anchors used for post-tensioning steel strand applications are not suitable. A modification to existing mechanical anchorages is required to better suit CFRP. CFRP is weak in the transverse direction and cannot handle orthogonal compression as greatly as isotropic steel strands. However, when there are concerns related to the long-term durability of prestressed steel in terms of corrosion, fatigue, and relaxation, CFRP materials are a good candidate. CFRP is known for its high strength-to-weight ratio, non-corrosiveness, high durability, and high stiffness offering improved ultimate limit state

and serviceability conditions for bridge infrastructure. Unlike conventional steel strands and bars, to the author's best knowledge, there are no available commercial anchorage systems for CFRP rods. Various researchers have experimented with bonded versus mechanical anchorage systems for CFRP materials. However, a mechanical strengthening system is more suitable for heavy civil infrastructure projects. The main concern with mechanical anchorage systems is how to adequately grip the CFRP rod without premature failure. Various experiments have been conducted in the past two decades with differential angles, contoured longitudinal profiles, and different geometry configurations for an optimum mechanical anchorage system. The contact pressure distribution on the rod surface plays a significant role in controlling the level of tensile loading that can be carried by the CFRP anchorage system. High contact pressure on the rod surface combined with high applied tensile stress induces premature failure due to the stress concentration at the loading end of the anchor. On the other hand, low contact pressure on the rod surface causes it to slip as the tensile load increases. Thus, a balance between contact pressure and tensile load capacity would provide for the ideal anchorage system. Optimum contact pressure is needed for a suitable anchor design to ensure no slippage as required by design codes. The contact pressure can be controlled by the profile geometry and the mechanical properties of the anchor components that are in direct contact with the CFRP rod. The competitiveness of a CFRP anchorage system would be to achieve a minimal anchor barrel and wedge length that is adequate to compete with conventional mechanical systems that grip steel strands. In 2006, Al-Mayah and Soudki found that the performance of the anchor was dependent upon the contact pressure distribution on the rod, especially at the entrance of the anchor where the tensile load was high. In order to reduce the contact pressure at this loading end of the rod, they proposed a design of a novel wedge anchor system in which the contact pressure is distributed in a manner that reduces the stress concentration. The concept is based on smoothly changing the geometric configuration of the barrel-wedge interface. Since the pressure is high at the loading end of the rod, stress concentrations may become particularly damaging because of the highest tensile stress at the same end. Ideally, the lowest contact pressures should be imposed at the loading end with the highest pressures at the free end where little or no tensile stresses are induced in the rod. They introduced the concept of a longitudinal circular profile to balance the required contact pressure and the high tensile stress occurring in the same location. Their design consisted of an alloy steel barrel

(AISI 4140), alloy steel split wedges (AISI 4140), a copper sleeve, and a longitudinal circular profile. Figure 2-6 presents their novel mechanical CFRP anchor.

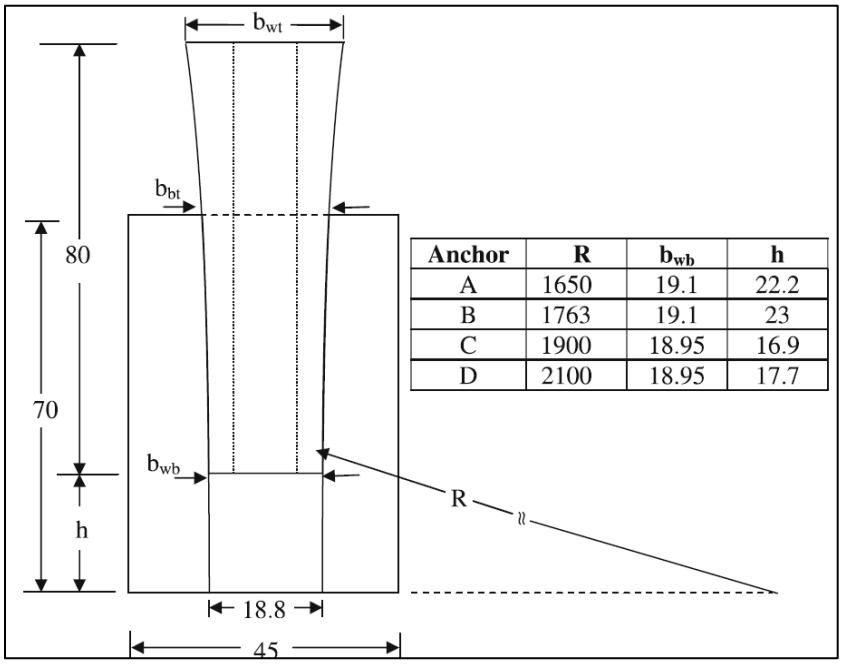

Anchor	R	b_{wb}	h
A	1650	19.1	22.2
B	1763	19.1	23
C	1900	18.95	16.9
D	2100	18.95	17.7

Figure 2-6. Al-Mayah and Soudki Proposed CFRP Anchor (Obtained from Al-Mayah and Soudki 2006)

The tensile strength of the Al-Mayah and Soudki anchorage system exceeded the guaranteed strength of the CFRP rods. Schmidt and Bennintz (2010) proposed a mechanical anchor for CFRP rods but instead of using split wedges and a longitudinal circular profile, they had an integrated wedge system and a constant longitudinal differential angle. Their intention like Al-Mayah was to create higher radial stresses at the back of the anchorage. A longitudinal differential angle of 0.4 deg in the barrel/wedge interface was used to solve the issue of high principal stresses in the anchorage's loaded end. Their mechanical anchor consisted of an alloy steel barrel, a one-piece aluminum wedge, an integrated aluminum sleeve, and a constant differential angle. Their mechanical anchor is portrayed in Figure 2-7.

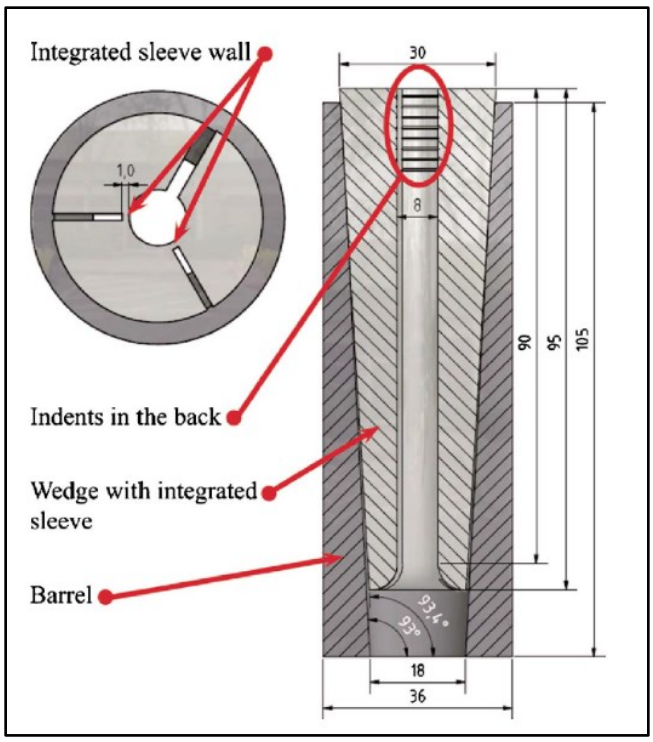

Figure 2-7. Schmidt & Bennintz Proposed CFRP Anchor (Obtained from Schmidt and Bennintz 2010)

Schmidt and Bennintz utilized an 8 mm CFRP rod for their anchor and after various experimental testing were able to overcome the anchorage effect and observed a failure within the CFRP rod's free gauge length which is ideal. In 2013, Al-Mayah and Soudki revisited their proposed CFRP anchor developed in 2006 and improved on it. Their new anchor was comprised of an alloy steel barrel, soft hardness steel split wedges, no sleeve, and a longitudinal circular profile. They note that although softer wedges have the potential to replace the sleeve and protect the rod, they may reduce the contact pressure resulting in less grip. Additionally, the harder wedges undergo limited deformation resulting in reduced movement on average, causing significant slippage of the rod at a load level well below that corresponding to its ultimate tensile strength. Thus, a softer wedge is related to its greater deformability thereby allowing it to conform to the rod profile and minimize the effect of the stress concentration at the loading end of the anchor in contrast with the harder wedges. The main goal remained that stress concentrations at the loading end of the anchor must be avoided in the design of the anchor systems due to the susceptibility of the CFRP rod to stress concentrations. Figure 2-8 presents their new updated CFRP anchor.

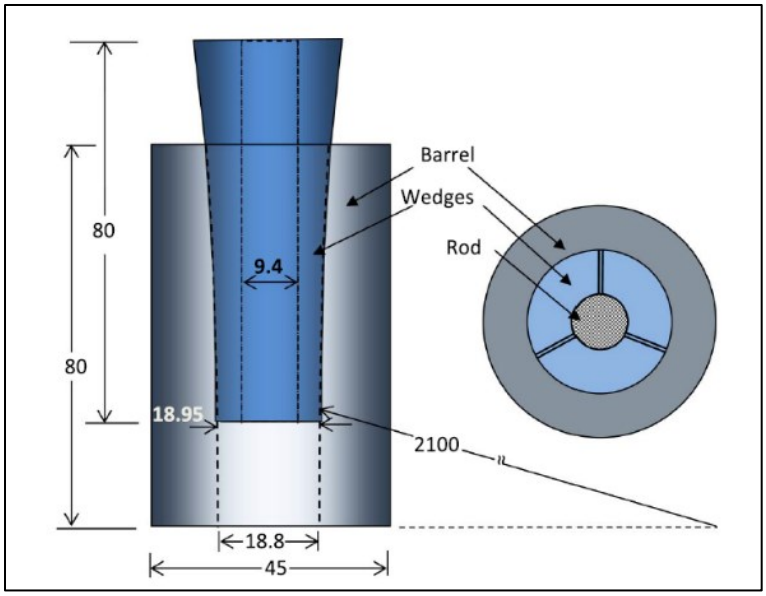

Figure 2-8. Al-Mayah & Soudki Updated CFRP Anchor
(Obtained from Al-Mayah and Soudki 2013)

More recently, researchers from Switzerland at the EMPA laboratory proposed an anchorage design that was a combination of the previously mentioned anchorage designs (Heydarinouri et al. 2021). They found that split wedges were more advantageous than a one-piece wedge as they observed CFRP interlaminar shear failure when not using split wedges. They concurred with Al-Mayah and Soudki 2006 that soft wedges were needed to conform to the profile of the CFRP rather than using high-hardness alloy steel wedges that could be rougher in grip and cause premature failure. In their study, they developed a wedge-barrel anchor with a curved profile. The wedges were made of aluminum and were in direct contact with the CFRP rod, without the need for a sleeve. The use of aluminum wedges reduced the required presetting force because aluminum has a lower stiffness than steel, resulting in an easier insertion into the barrel. They claim that aluminum plasticization that occurs due to the high contact pressure inside the barrel can improve the gripping of the CFRP rod. They were the only researchers to mention if they threaded their barrel. They threaded their barrel at the free end for presetting the anchors. Figure 2-9 presents their developed CFRP mechanical anchor.

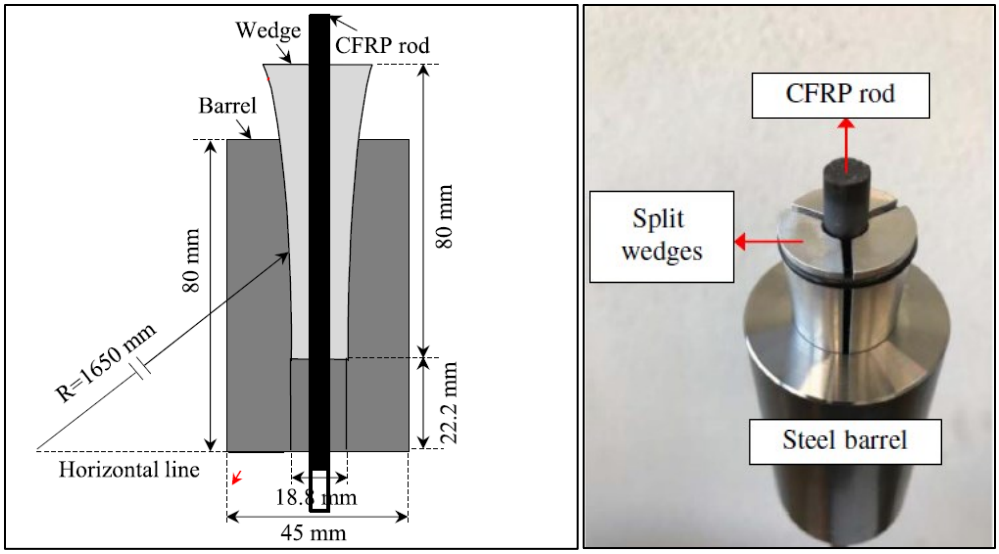

Figure 2-9. EMPA Proposed CFRP Anchor (Obtained from Heydarinouri et al, 2021)

The EMPA researchers utilized an 8 mm unidirectional CFRP rod and conducted static and fatigue anchorage testing. They report the CFRP rod failed within its free gauge length, which is ideal, i.e., they were able to overcome the anchorage effect. Our proposed mechanical anchor for our study would be a combination and adaptation from all the anchors presented above in this literature review.

2.3. Research Gaps

Currently, in the literature, there are many research gaps when it comes to the utilization of post-tensioned CFRP rods for NSM rehabilitation of concrete bridge elements which are detailed below:

- Implementation of post-tensioned CFRP rods is still very novel and state-of-the-art even with two decades of ongoing research.
- There are no commercially available anchorage systems for CFRP rods or strips or any FRP material.
- There are no standardized acceptance criteria for FRP anchorage systems.
- Limited research is available on fatigue performance and the corresponding acceptance criteria of mechanical anchorage systems for FRP material.

- There is limited guidance for the utilization of CFRP or any other FRP material near-surface-mounted in a concrete structure.
- Most CFRP or FRP rehabilitation has mostly occurred on simple rectangular beams or slabs.
- Most NSM rehabilitation research has focused on reinforced concrete beams and decks in their positive bending moment regions.
- There is limited NSM groove detailing requirements within design codes and specifications.
- There is limited in-situ data on in-service concrete elements that have undergone a post-tensioned FRP rehabilitation strategy.
- There is limited data on the long-term creep effect of CFRP or FRP materials in general that have been used within the public infrastructure.

The above list is only a small synopsis of the literature research gap within this field. Our research project attempts to reduce the research gap and contribute to this research field.

CHAPTER 3 CFRP ANCHORAGE EXPERIMENTAL PROGRAM

A proposed CFRP mechanical anchorage system was developed, computer numerical control (CNC) machined, and assessed experimentally to evaluate its suitability and efficacy for the rehabilitation of post-tensioned concrete bridge cantilever wing slabs exhibiting deteriorated transverse steel post-tensioning. The developed CFRP mechanical anchorage system in this research project is a combination/adaptation from a combination of previous researchers including Al-Mayah et al. (2006), Schmidt et al. (2010, 2011), and Heydarinouri et al. (2021). The anchorage system is tailored to anchor and grip a pultruded No.3 (10 mm) unidirectional CFRP rod from Aslan/Geotree. Stage one of the experimental program consisted of firstly, conducting tensile tests on the selected No.3 (10 mm) CFRP rod as per the ASTM D7205-21 standard to verify the material properties of the CFRP rod. Secondly, conducting preliminary proof of concept testing to verify the proposed anchorage design concept in-house. Lastly, conducting static anchorage testing on the anchors per a specified load-controlled loading protocol was obtained from Rostasy (1998). The main objective of the proposed anchorage system is to grip and jack the CFRP rod up to a specified post-tensioning force with no slippage safely and effectively. The specified PT force will subsequently be transferred through a steel bearing plate to the PT concrete bridge cantilever wing slab for rehabilitation. The PT CFRP rod utilized for rehabilitation is near surface mounted on the concrete tensile top slab with permanent mechanical anchorage at the ends. The following sections in this chapter present the details regarding the development and assessment of the proposed CFRP mechanical anchorage system. The presentation of the performance and behavior of a post-tensioned concrete bridge cantilever specimen that underwent rehabilitation with the NSM post-tensioned CFRP rods using the proposed mechanical anchorage system will be discussed in Chapter 4 of this document.

3.1 Anchorage Design and Materials

The developed mechanical anchorage system is based on existing mechanical anchorage systems used for conventional steel strand post-tensioning systems. The conventional steel strand anchorage design is modified and adapted to be suitable for CFRP rods. For this research project, the developed CFRP anchor is comprised of a conical barrel and split wedge system incorporating a contoured longitudinal profile (CLP). The outer surface profile of the split wedges and the inner surface profile of the conical barrel is CNC machined with the same selected longitudinal circular

radius of 1650 mm. The wedges are in direct contact with the CFRP rod and grip the rod relying purely on frictional resistance for load-bearing capacity. The wedges are housed inside a conical barrel that transfers the PT force to the to-be-strengthened concrete structure via a steel bearing plate. To reduce stress concrentrations at the loading end, the tangent to the interface between the wedge and barrel must be small (Al-Mayah et al. 2006). However, the angle should increase smoothly along the length of the anchor to reach its highest value at the free end. The utilization of a contoured longitudinal profile within the anchor facilitates the reduction of stress concentrators at the loaded end of the anchor. The contoured longitudinal profile provides a distribution of the differential angles along the anchor, thus facilitating a balance between the required contact pressure and the imparted high applied tensile stress concentration. Figure 3-1 depicts the contoured longitudinal profile design concept utilized in the proposed CFRP anchorage system.

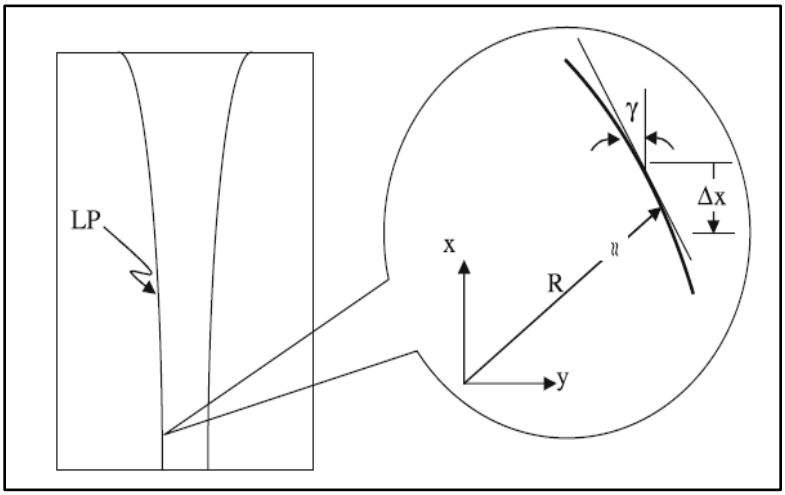

Figure 3-1. Anchor Contoured Longitudinal Profile (Obtained from Al-Mayah et al. 2006)

The equations that describe the above profile are as follows:

$$y^2 + x^2 = R^2 \tag{3-1}$$

$$\frac{dy}{dx} = \frac{-x}{\sqrt{R^2 - x^2}} \tag{3-2}$$

$$|\gamma| = \tan^{-1}\left(\left|\frac{dy}{dx}\right|\right) \tag{3-3}$$

Where x, and y are the Cartesian coordinates, γ is the angle of the tangent of the curve and R is the radius of the circular longitudinal profile.

The CFRP material chosen for this research study is a unidirectional pultruded No.3 (10 mm) CFRP Rod. Table 3-1 presents the material properties of the selected CFRP rod.

Table 3-1. CFRP Rod Material Properties

Nominal Diameter (mm)	Cross Section Area (mm2)	Ultimate Strength (Mpa)	Modulus of Elasticity (Gpa)
10	71.26	2172	124

Material selection for the anchorage components was based on the criteria of utilizing cost-effective, locally sourced, commercially available corrosion-resistant materials. Table 3-2 presents the selected materials for the barrel and wedge components of the anchorage system.

Table 3-2. Anchorage Constituent Materials

Anchorage Component	Material
Barrel	Stainless Steel 316
Wedges	Aluminum 6061

Stainless Steel 316 was selected as the constituent material for the barrel for its exceptionally high resistance in chloride environments and overall corrosion-resistant properties. Stainless 316 is the most corrosion-resistant grade of stainless steel commercially available locally. Aluminum 6061 was selected as the constituent material for the split wedges for its low-cost, corrosion resistance, and good formability as a soft metal. The phenomenon of the plasticization of aluminum as the

contact pressure increases results in the aluminum wedges conforming to the shape of the CFRP rod which increases the grip and friction between the wedges and rod resulting in a higher anchorage system tensile load capacity. Table 3-3 presents the material properties of the selected anchorage components.

Table 3-3. Anchorage Material Properties

Material	**Tensile Strength (Mpa)**	**Modulus of Elasticity (Gpa)**
316 Stainless Steel Barrel	515	193
6061 Aluminum Wedges	310	68

There is a necessity for CFRP mechanical anchorage systems to be as compact as possible to be competitive with existing steel strand post-tensioning anchorage systems. A minimal as possible length for both the conical barrel and the wedge core was selected for the developed anchor similar to the anchorage system developed by Heydarinouri et al. (2021). Figure 3-2 presents the geometric details of the developed split wedge and barrel CFRP anchorage system.

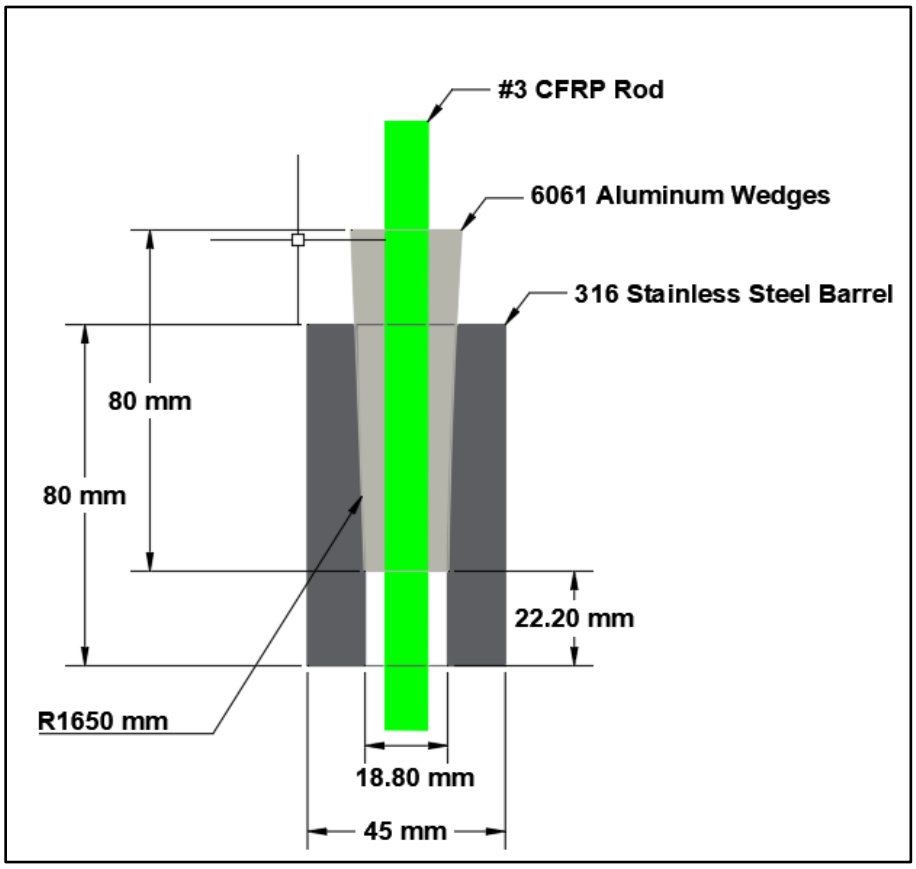

Figure 3-2. Split Wedge and Barrel Anchor Geometric Details

Figure 3-3 presents the cross-section of the developed split wedge and barrel CFRP anchorage system.

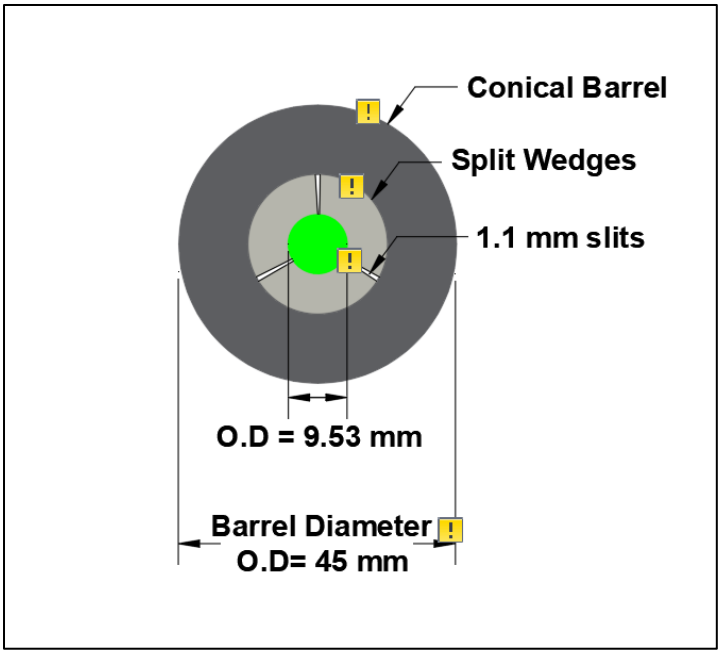

Figure 3-3. Split Wedge and Barrel Anchor Cross Section

3.2 ASTM D7205 FRP Tensile Tests

The tensile strength of the CFRP specimens was verified by following the ASTM D7205-21 standard. This test method determines the quasi-static longitudinal tensile strength and elongation properties of fiber-reinforced polymer matrix (FRP) composite bars commonly used as tensile elements in reinforced, prestressed, or post-tensioned concrete. This test method was chosen as an internationally recognized testing strategy to verify the material properties of the sourced CFRP rod and to cross-check with the manufacturer's reported values. Additionally, the results obtained from the tensile tests would facilitate more refined input parameters to be used for the analytical study presented in Chapter 5 of this document.

3.2.1 Test Matrix and Fabrication

The number of prepared specimens, specimen length, and CFRP free gauge length in between the ends of the anchors were in adherence to the ASTM D7205-21 standard requirements. These requirements are similar in nature to the FRP tensile test method specified in the CSA S806 standard. In total, five specimens were prepared. Table 3-4 presents the observed test matrix.

Table 3-4. ASTM D7205 Tensile Test Matrix

Specimen ID	Material	Anchor Type	Specimen Length (m)
S1	#3 CFRP Rod	Epoxy Potted Steel Pipe	1.8
S2	#3 CFRP Rod	Epoxy Potted Steel Pipe	1.8
S3	#3 CFRP Rod	Epoxy Potted Steel Pipe	1.8
S4	#3 CFRP Rod	Epoxy Potted Steel Pipe	1.8
S5	#3 CFRP Rod	Epoxy Potted Steel Pipe	1.80

To observe the ultimate strength of the CFRP rod where the CFRP rod ruptures within its free gauge length, potted anchors were utilized as the gripping mechanism. Direct gripping of the CFRP rods by the jaws of the testing machine would result in premature failure. The anchors were comprised of ASTM A36 1¼" (32 mm) carbon steel schedule 80 pipes and an in-house developed epoxy resin with silica sand filler matrix as the potting material. Each specimen was 1.8 m in total length. Each anchor was 550 mm in length. The free gauge length of the CFRP rod in between the steel pipe anchors was 650 mm. Two 350-ohm strain gauges were attached at the midpoint of the CFRP rod's free gauge length. Figure 3-4 presents a schematic of the fabricated ASTM specimens for tensile strength testing.

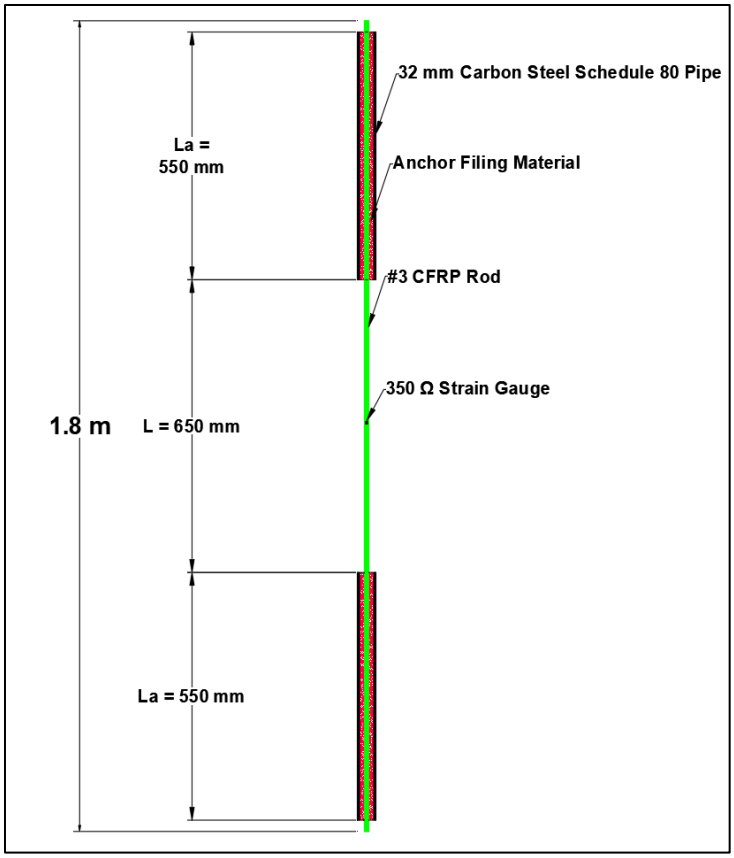

Figure 3-4. ASTM D7205 Tensile Test Specimen

Figure 3-5 presents the cross-section of the steel pipe anchors inclusive of the steel pipe, the potting material, and the concentric CFRP rod.

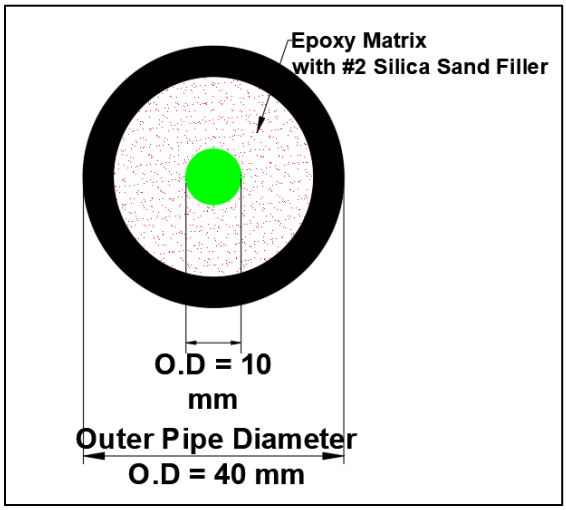

Figure 3-5. ASTM D7205 Tensile Test Specimen Cross-Section

A wooden jig from 19 mm plywood was built to align the fabricated specimens. Alignment of the CFRP rod within the potted anchors is essential to facilitate a pure tensile test with no induced bending. Figure 3-6 presents the aligning jig built for the ASTM tensile tests.

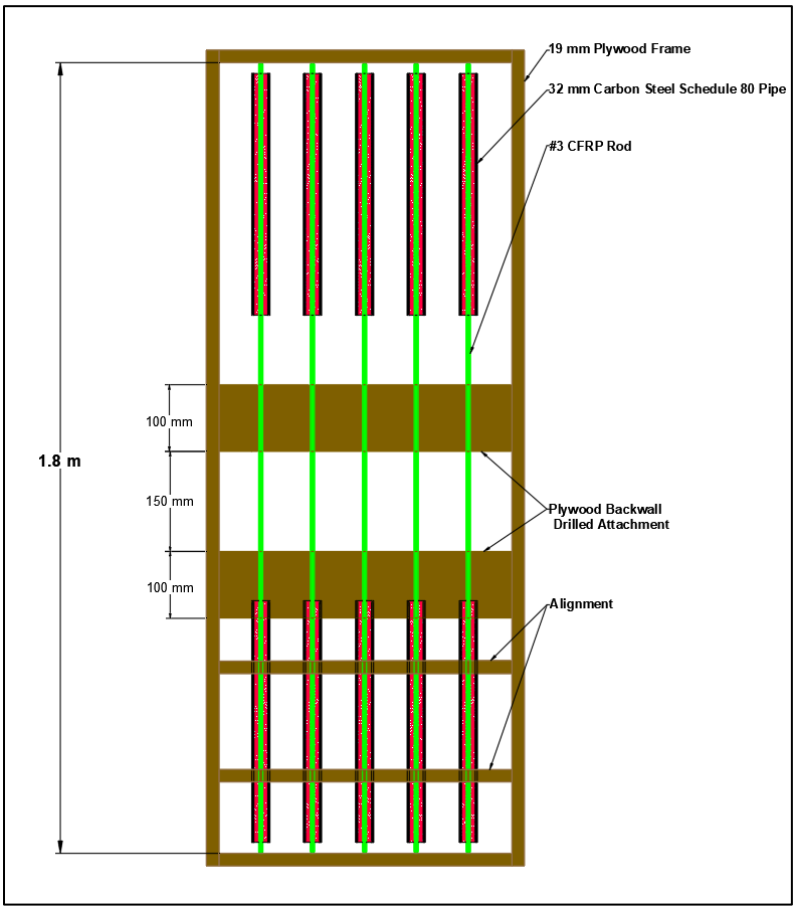

Figure 3-6. Jig for Aligning ASTM Specimens and Anchors

Figure 3-7 presents a cross-sectional view of the built alignment wooden jig showcasing all five steel pipe anchors.

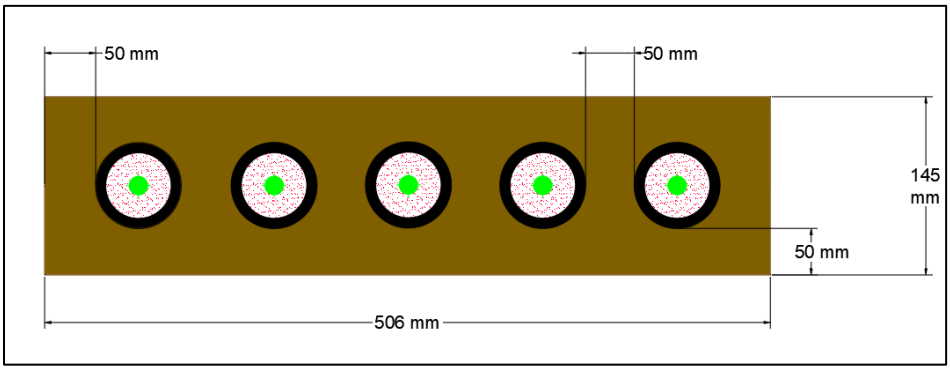

Figure 3-7. Cross-Section of Wooden Alignment

3.2.2 Test Results and Discussion

The 5 specimens were monotonically loaded using a displacement-controlled loading scheme of 2.5 mm/min until ultimate rupture. Table 3-5 presents the results of the ASTM tensile tests.

Table 3-5. ASTM D7205 Tensile Test Results

Specimen ID	Ultimate Load (kN)	Ultimate Strength (MPa)	Elastic Modulus (GPa)
S1	193	2708	135
S2	193	2708	137
S3	191	2680	135
S4	175	2455	132
S5	163	2287	130

The failure mode of all five specimens was the rupture of the CFRP rod within the free gauge length. The obtained results verify that the CFRP rods meet the manufacturer's guaranteed tensile load of 154 kN, the ultimate strength of 2172 MPa, and the elastic modulus of 124 GPa respectively. It was difficult to pin point the reason for the variance as all the selected rods were from the same pultrusion batch. However, we note there was a significant variance in the manufacturer-applied sand/epoxy surface bar coating.

3.3 Preliminary Anchorage Proof of Concept Tests

Preliminary proof of concept testing was conducted on the anchors to verify the proposed design concept of the selected contoured longitudinal profile, the geometric details portrayed in Figure 3-2, and the selected materials for the respective components of the anchorage system.

3.3.1 Test Matrix and Fabrication

The main objectives of the preliminary anchorage proof of concept tests were as follows:

- Verify the selected contoured longitudinal profile design concept.
- Verify the suitability of the anchorage materials.
- Observe the behaviour and performance of each of the anchorage components under a load-controlled stepwise testing protocol.

Ideally, the proposed anchor would be capable of developing the full ultimate tensile strength of the CFRP material with a rupture of the CFRP rod within its free gauge length. However, the mechanical anchorage system imparts a limiting effect on the CFRP rod from the grip of the wedges. Since the application of the proposed CFRP anchorage system is intended for NSM rehabilitation of a post-tensioned concrete bridge cantilever wing slab exhibiting deteriorated transverse steel post-tensioning in Canada, the Canadian Highway Bridge Design Code (CHBDC) will be utilized for anchorage acceptance criteria. The Canadian Standards Association (CSA) CSA S6-19 code, clause 16.8.6.3 on the capacity of FRP anchors stipulates that when tested in an unbonded condition, anchors for post-tensioning tendons shall be capable of developing a tendon force at least 50% higher than the jacking force. Thus, the test criteria for the anchor will be set to meet the CSA S6-19 bridge code. Additionally, after tensioning and seating, anchors shall sustain applied loads without slippage, distortion, or other changes that result in loss of prestress. The ultimate tensile capacity of the anchorage system and the displacements and slippage of the anchorage components will dictate the maximum permissible jacking force. Moreover, as there are no standardized acceptance criteria for CFRP anchorage systems, we adopted certain recommendations and requirements from the American Concrete Institute (ACI) ACI 423.7-14, Post-Tensioning Institute (PTI) Manual 2006, PTI M50.1-1998, PTI M50.3-19, and Rostasy 1998. The adopted recommendations include but are not limited to the following: minimum required number of test specimens, minimum length requirements per test specimen, specimen loading protocol, and loading rate. For the preliminary anchorage proof of concept testing, two specimens were fabricated. No pre-setting load was applied onto the barrel anchors at this stage to monitor the movements of the anchorage components at the loose natural state to record when the slippage and the draw-ins occur. Table 3-6 presents the anchorage proof-of-concept test matrix that was observed.

Table 3-6. Preliminary Proof of Concept Test Matrix

Specimen ID	Anchor Type	Pre-Setting Load (kN)	Specimen Length (m)
S1-Top	Split Wedge & Barrel	None: Loose	1.80
S1-Bottom	Split Wedge & Barrel	None: Loose	
S2-Top	Split Wedge & Barrel	None: Loose	1.80
S2-Bottom	Epoxy Potted Steel Pipe	None: Loose	

The first specimen was comprised of a split wedge and barrel anchor for both the live and dead ends. The second specimen was comprised of a split wedge and barrel anchor for the live end and an epoxy-potted steel anchor for the dead end. Both specimens were 1.8 m in total length with different free gauge lengths of CFRP rod owing to the longer length of the potted dead anchor. The purpose of the second specimen was to detect if there would be a change in performance if a bonded anchor is utilized rather than the proposed mechanical anchor on the dead end. Figure 3-8 presents a schematic of the fabrication of the preliminary anchorage proof of concept test specimens.

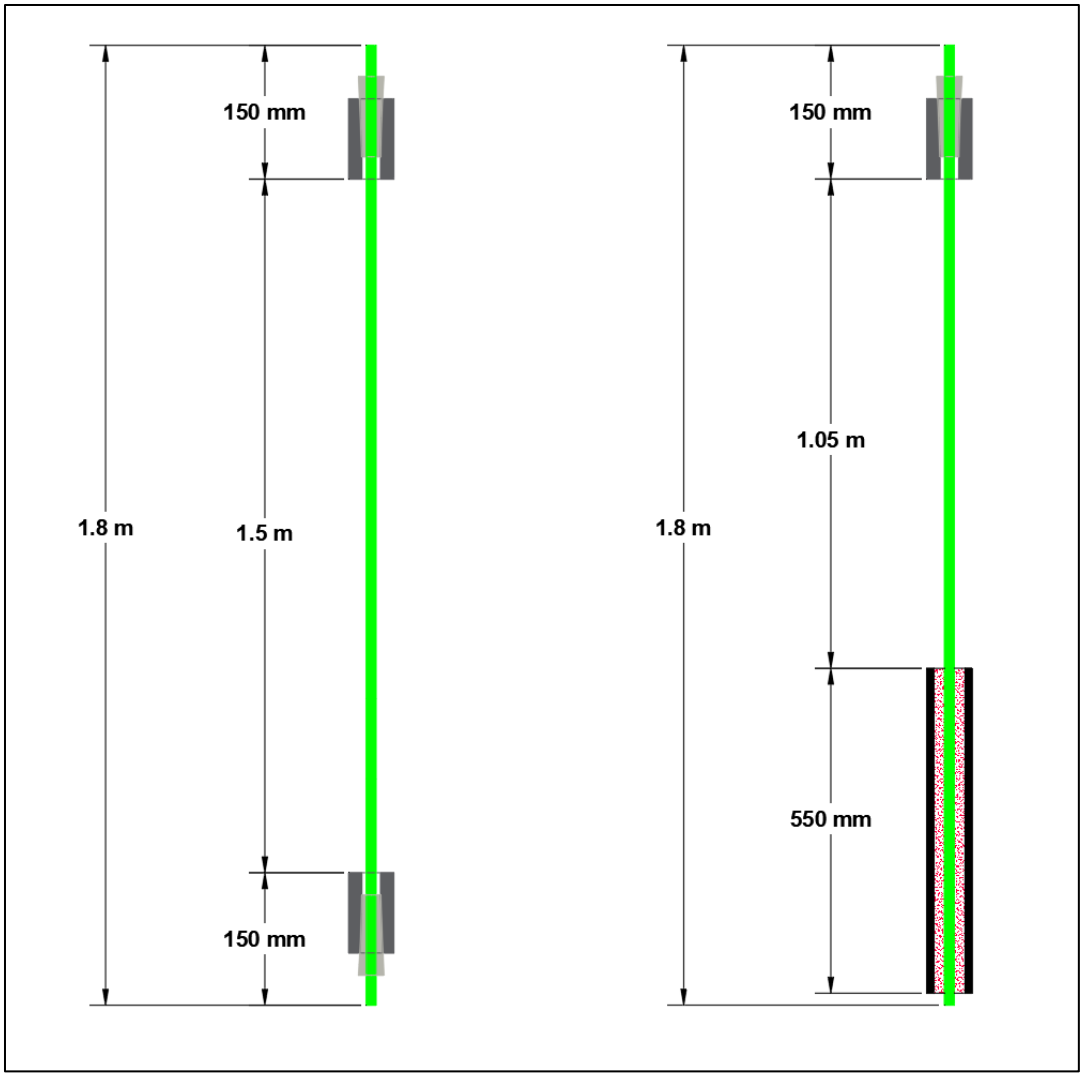

Figure 3-8. Preliminary Anchorage Static Test Specimens

The specimens were loaded based on a load-controlled stepwise loading protocol. The loading protocol was adapted from Rostasy 1998, and fib 1993. A load-controlled stepwise loading protocol was chosen for the movements of the anchorage system components to be observed during stages of applied and sustained loading. Table 3-7 presents the stepwise loading protocol that was implemented and Figure 3-9 presents the loading protocol graphically.

Table 3-7. CFRP Anchorage Test Loading Protocol

Load State	Load (kN)	Loading Rate (kN/min)	Load Step
20%	30	6	5 min Applied 5 min Sustained
40%	60	6	5 min Applied 5 min Sustained
60%	90	6	5 min Applied 5 min Sustained
70%	105	6	2.5 min Applied 60 min Sustained
100%	150	6	5-10 min Applied

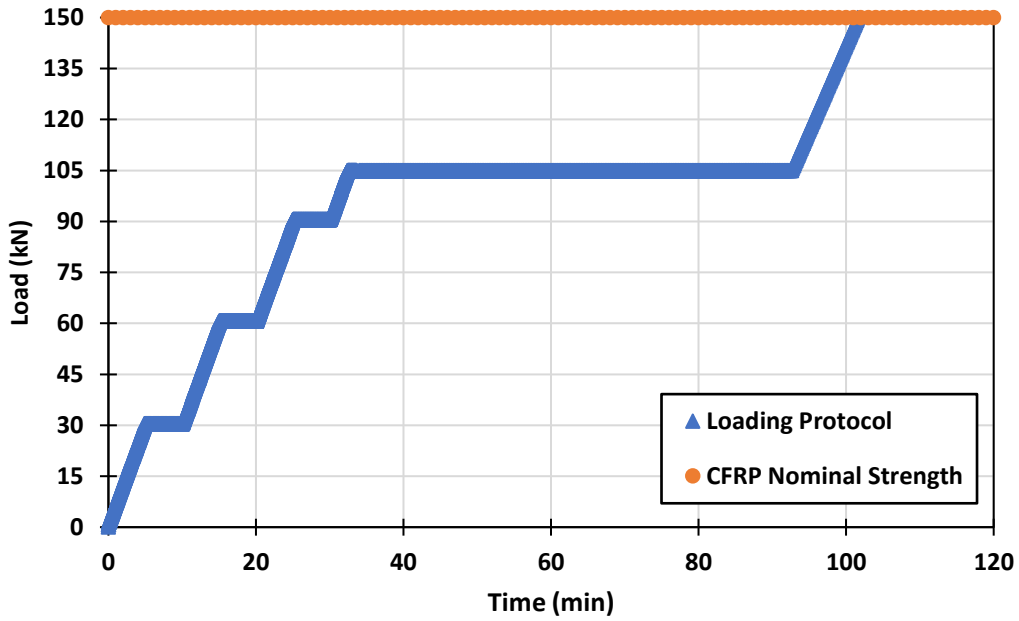

Figure 3-9. CFRP Anchorage Test Loading Protocol

The load-controlled stepwise loading protocol was adopted to capture the displacements of the anchorage components and as a better simulation of realistic periods of applied and sustained loading that bridge structures undergo. Thus, the load-controlled stepwise loading protocol was more advantageous than monotonic loading until failure. Linear potentiometers (LP) were placed on the top of the CFRP rod, the wedges, and the barrel to measure the draw-ins of each of the anchorage components as the tensile load increased. Figure 3-10 is a schematic portraying the placement of the LPs on the anchorage components to determine the draw-in measurements. "Δr", represents the draw-ins of the CFRP rod relative to the reference state at the beginning of the test. "Δw", represents the draw-ins of the wedges relative to the reference state at the beginning of the test. Component slippage is defined as the difference between the draw-ins of the CFRP rod and the wedges, | Δw - Δr |. The wedge seating distance, S, is the distance between the top surface of the wedges and the barrel. The wedge seating distance represents the placement of the wedges in the barrel which affects the performance of the anchors.

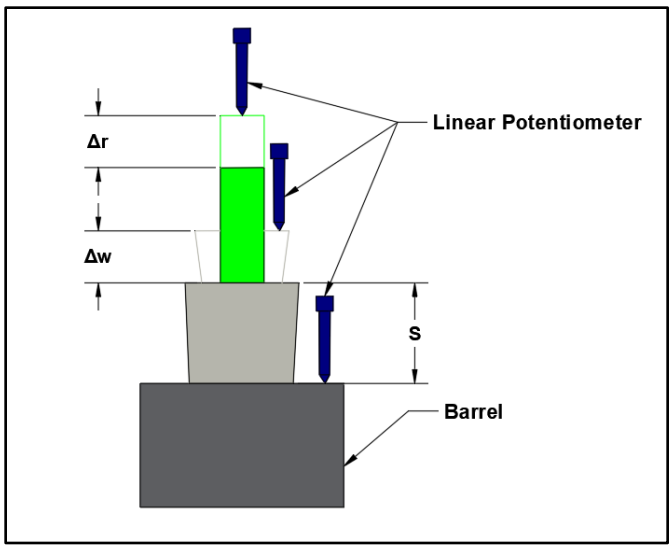

Figure 3-10. Anchorage Components Draw-in Measurement Schematic

3.3.2 Test Results and Discussion

Measurements obtained from the LPs on the anchorage components offered a better understanding of the behaviour of the CFRP rod and the split wedges in relation to each other and both in relation to the barrel. Both test specimens behaved similarly with respect to the performance of the mechanical anchorage system. Figure 3-11 presents the draw-ins of the CFRP rod and the split wedges graphically.

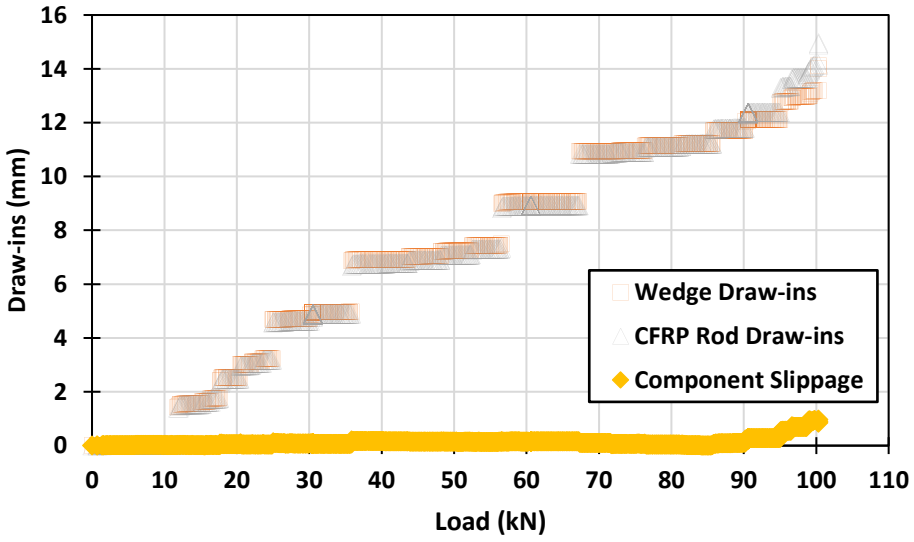

Figure 3-11. Preliminary Anchorage Components Draw-ins

The CFRP rod and wedges were drawing into the barrel gradually at a relatively early load as there was no pre-setting force applied to the system, hence early anchorage system slippage. Anchorage system slippage in this context is defined as the insertion displacement of the CFRP rod and the wedges together into the barrel. Additionally, the rate of draw-ins of the CFRP rod and the split wedges into the barrel were identical owing to the even distribution of pressure of the wedges on the rod from the uniform even spacing between the split wedges. Thus, there was no anchorage component slippage of the CFRP rod and the wedges with respect to each other. Anchorage component slippage in this context is defined as the difference in insertion displacement between the split wedges and the CFRP rod into the barrel. The displacement of the barrel was measured in relation to the anchorage component displacements and is portrayed graphically in Figure 3-12.

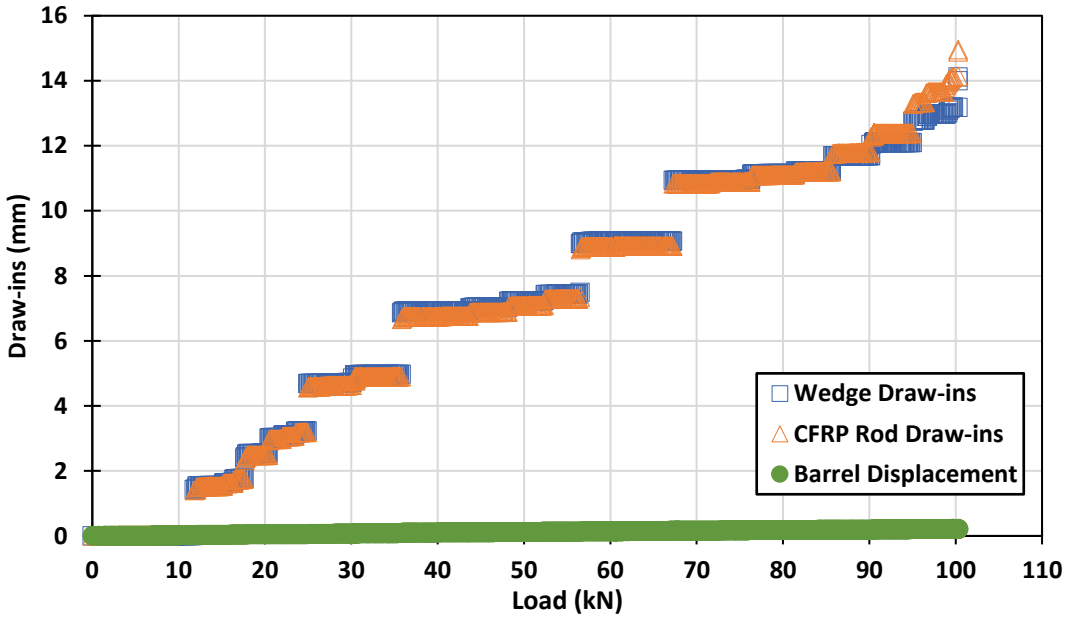

Figure 3-12. Preliminary Barrel Anchorage Component Displacement

The displacement of the conical barrel was null as expected for it was bearing on two steel plates bolted together within the universal Instron vertical testing machine as portrayed in Figure 3-10. Furthermore, the overall displacement of the preliminary anchorage specimens was recorded. Figure 3-13 presents the load-displacement curves of the split-split (S1) specimen and the split-potted (S2) specimen plotted together. Overall displacement is a summation of the draw-ins at each anchor end plus the elongation of the CFRP rod as the load increases. CFRP materials are

linear-elastic in nature, therefore Hooke's law was used to verify the elongation with the increase of load. In the loose natural state of the anchor specimens, there was excessive slippage observed for both specimens. Additionally, less overall displacement was observed with the second specimen (S2) owing to the epoxy potted anchor on the dead end which observes no movement.

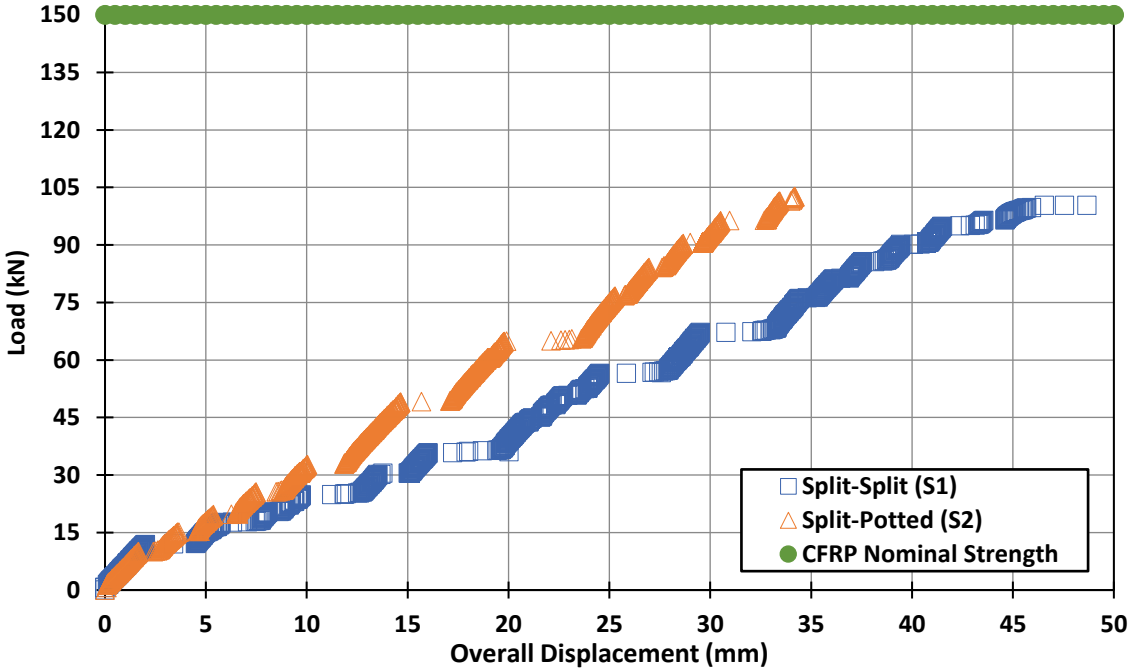

Figure 3-13. Load-Displacement Curve for Preliminary Anchorage Tests

The overall load results of the preliminary anchorage proof of concept tests were promising to permit the continuation of the proposed anchorage design and geometric details. The proposed anchorage system was a good preliminary candidate worthwhile pursuing static tests. Table 3-8 presents a summary of the preliminary anchorage proof of concept test results.

Table 3-8. Preliminary Anchorage CFRP Proof of Concept Test Results

Specimen ID	Load (kN)	Failure Mode	System Slippage	Efficacy (%)
S1	100.3	Pinching failure near the anchor	Around 10 kN	65
S2	102.7	Pinching failure near the anchor	Around 15 kN	66

The failure mode of pinching shear failure near the anchor is not ideal attributed to the anchorage effect of the wedges gripping the orthotropic in nature CFRP rod. However, knowing the limitations of the anchor, it could still be used to meet the goals of this research project. Figure 3-14 presents a closeup of the CFRP rod failure portraying the aftermath of the wedge grip effect on the CFRP rod.

Figure 3-14. Pinching Shear CFRP Failure Mode

The experimental preliminary anchorage proof of concept tests yielded several learned lessons. The following points indicate the steps that were undertaken to slightly improve the anchorage design before conducting anchorage static tests:

- Pre-setting the wedges to a certain load to activate the system, increase the contact pressure around the CFRP rod, reduce system slippage and overcome wedge seating losses rather than have loose wedges with no pre-setting.
- Arranging the three split wedges evenly around the CFRP Rod to ensure a uniformly distributed contact pressure on the CFRP rod.
- Application of metal-free anti-seize lubricant on the outer surface of the aluminum wedges to facilitate better insertion into the barrel and reduce any potential metal galling.

- Rounding off the tips of the wedges to reduce any sharp corners to reduce stress concentrators in the region of high shear and tensile stress.

The above design improvements would improve the proposed anchor but we expect the ultimate failure to be similar in nature to the conducted preliminary proof of concept tests.

3.4. Mechanical Anchorage Static Tests

Based on the results and learned lessons of the preliminary anchorage proof of concept tests, the design of the anchors was slightly improved. The anchors would be pre-set, a plastic spacer disc was machined to ensure an even arrangement of the three split wedges, and the tips of the wedges were rounded off. Mechanical anchorage static tests were conducted to evaluate the short-term performance of the proposed CFRP anchorage system under short-term applied and sustained loads. The number of specimens, test specimen dimensions, loading protocol, and loading rate for this round of anchorage tests was based on the previous acceptance criteria we had adopted as mentioned in the preliminary anchorage test section. The overall capacity and efficacy of the anchors were determined in addition to the draw-in measurements obtained of the CFRP rod and the split aluminum wedges. This round of testing was implemented to confirm a safe jacking force to post-tension #3 CFRP rods that are to be utilized in the PT bridge cantilever rehabilitation experimental program of this research project.

3.4.1 Test Matrix and Fabrication

The main objectives of the mechanical anchorage static tests were as follows:

- Determine the overall capacity and efficiency of the anchor against the nominal strength of the #3 CFRP rod.
- Determine the max safe permissible jacking force for the #3 CFRP rod.

Five test specimens were prepared for experimental mechanical anchorage static testing. Two distinctive pre-setting loads were selected for the anchorage specimens. The anchors were pre-set one anchor at a time to the specified load vertically using an Instron machine. Three anchor test specimens were pre-set at a load of 80 kN, and two specimens were pre-set at a load of 100 kN. The selection of the two pre-setting loads was based on literature research and primarily what was advantageous to meet the objectives of the research project. All five test specimens were

1.8 m in length utilizing split wedge and barrel anchors for both the live and dead ends. The same load-controlled stepwise loading protocol was applied as mentioned previously. A schematic of the fabrication of the specimens is equivalent to the preliminary specimen, S1 in Figure 3-7. Table 3-9 presents the observed test matrix for the anchorage static tests.

Table 3-9. Anchor Static Test Matrix

Specimen ID	**Material**	**Anchor Type**	**Pre-Setting Load (kN)**	**Specimen Length (m)**
S1	#3 CFRP Rod	Split Wedge & Barrel	80	1.8
S2	#3 CFRP Rod	Split Wedge & Barrel	80	1.8
S3	#3 CFRP Rod	Split Wedge & Barrel	80	1.8
S4	#3 CFRP Rod	Split Wedge & Barrel	100	1.8
S5	#3 CFRP Rod	Split Wedge & Barrel	100	1.8

Linear potentiometers were placed on the top of the CFRP rod, and the wedges were to measure the draw-ins of each of the anchorage components as the tensile load increased. The performance of the individual components was critical given that pre-setting was applied to the anchors to reduce overall anchorage system slippage to a certain load. Given the CFRP rod's orthotropic nature, the pre-setting load was optimized to balance between the necessary pre-setting that reduced system slippage while not inducing premature failure on the CFRP rod due to the imparted compression force.

3.4.2 Test Results and Discussion

The draw-in measurements of the CFRP rod and the split wedges are presented for just the top anchor for each specimen as both the top and bottom behaved identically. Additionally, the draw-in measurements are presented for one respective test specimen from each selected pre-setting load. The graphs for all five test specimens are presented in Appendix A for reference. Figure 3-15 presents the draw-ins of the CFRP rod and the split wedges graphically for specimen T1 which underwent a pre-setting load of 80 kN.

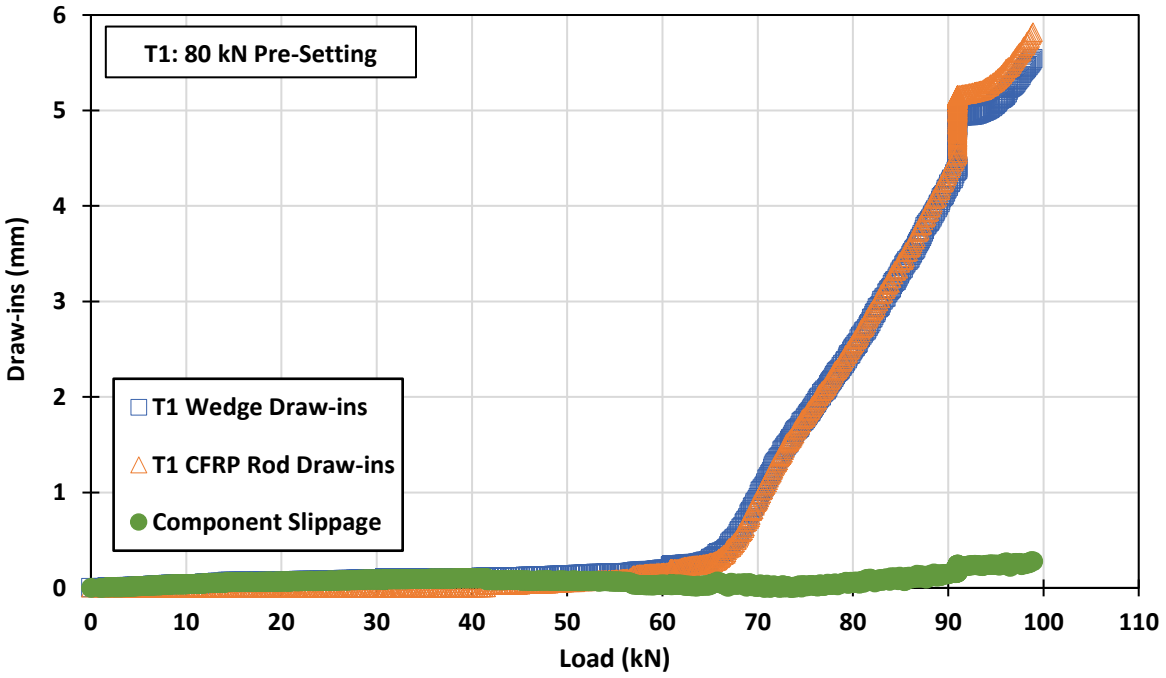

Figure 3-15. Specimen T1 Draw-ins

Pre-setting the anchor to a pre-setting load of 80 kN resulted in no anchorage system slippage until after 60 kN. Additionally, there was near zero component slippage between the wedges and the CFRP rod. The overall capacity of specimen T1 was 98.9 kN against a nominal strength of 154 kN, thus an overall efficiency of 64.3%. Pre-setting the anchor to 100 kN was implemented to observe whether a slightly higher pre-setting load (transverse compression force) would delay anchorage system slippage. Figure 3-16 presents the draw-ins of the CFRP rod and the split wedges graphically for specimen T5 that underwent a pre-setting load of 100 kN.

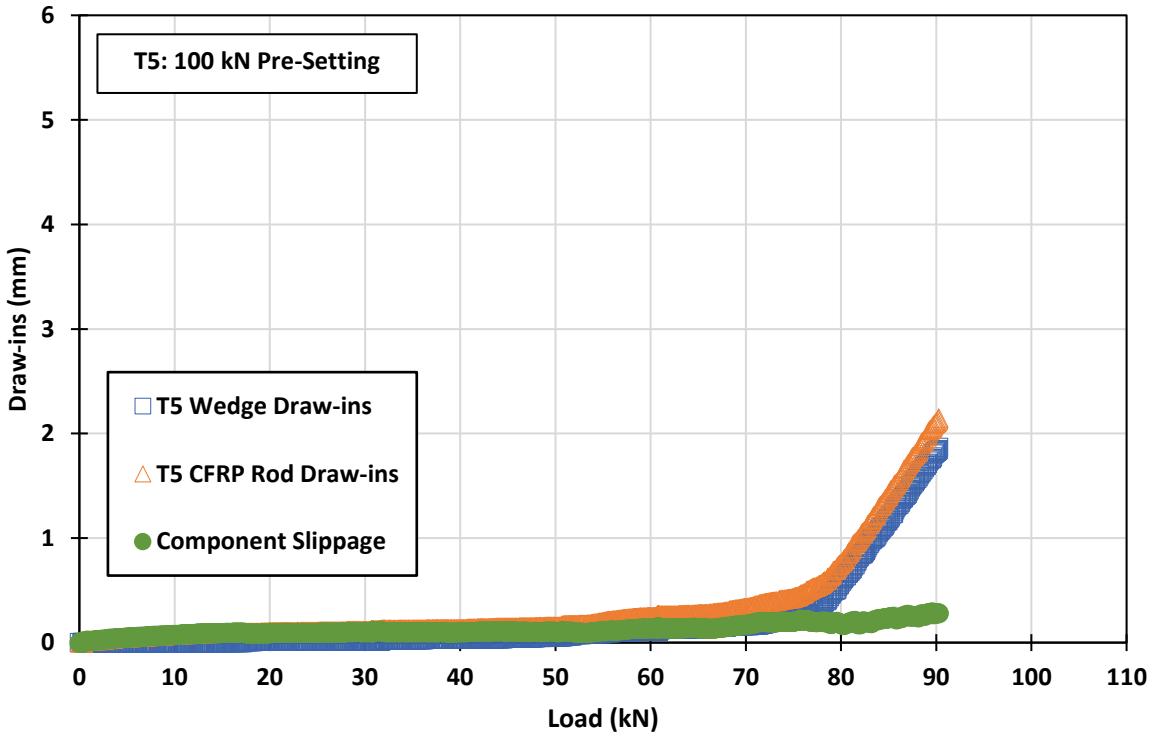

Figure 3-16. Specimen T5 Draw-ins

Pre-setting the anchor to a pre-setting load of 100 kN resulted in no anchorage system slippage until after 70 kN. Additionally, there was near zero component slippage between the wedges and CFRP rod until about 70 kN. Furthermore, the draw-ins were reduced owing to the increased anchor pre-setting force. However, the increased anchor pre-setting force yielded a reduction in overall capacity. The overall capacity of specimen T5 was 90.3 kN against a nominal strength of 154 kN, thus an overall efficiency of 58.7%. In contrast with the 80 kN pre-set specimen, the overall capacity of the anchorage was further reduced owing to the high pre-setting load as the induced transverse compression from pre-setting was too high for the

CFRP rod to bear and resulted in premature failure. The overall displacement of each anchor specimen against the increase of tensile load of the anchorage system was recorded for all pre-set anchors. Figure 3-17 presents the load-displacement curve for the pre-set anchors.

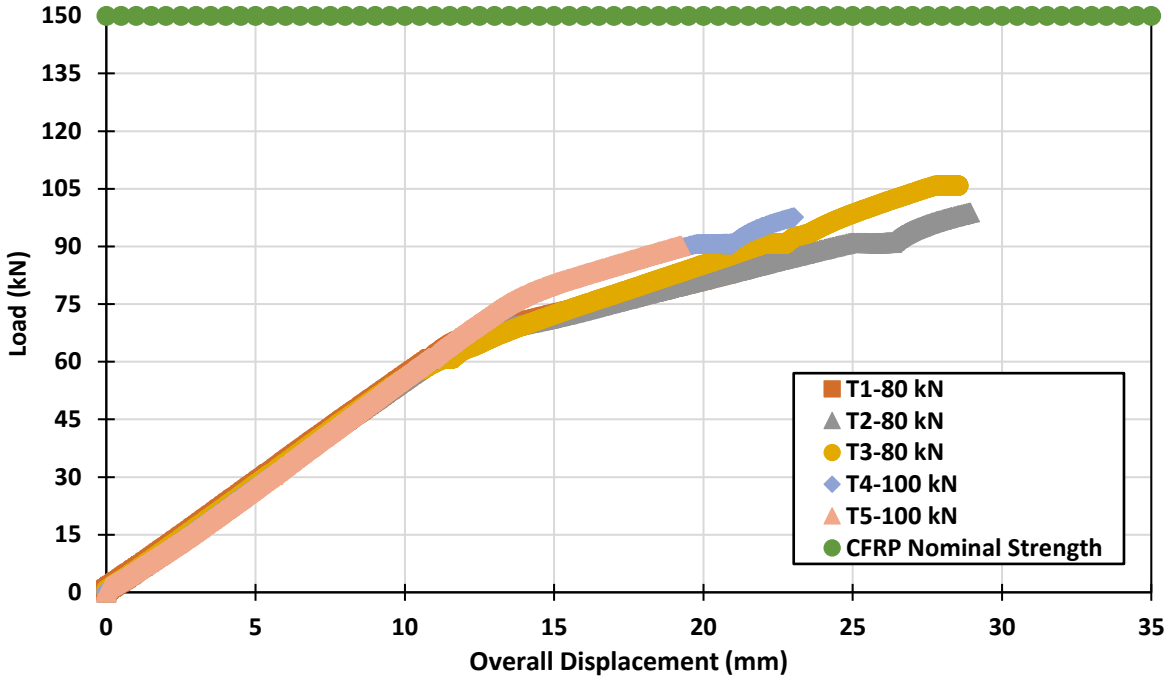

Figure 3-17. Load Displacement Curve for Pre-Set Anchors

The two 100 kN specimens underwent relatively less machine displacement at the same tensile load compared with their three 80 kN anchor specimen counterparts. However, the 80 kN anchor specimens attained a higher overall tensile load due to the smaller compressive pre-setting load. Thus, pre-setting to 80 kN was considered a better pre-setting load for this anchorage design. Figure 3-18 presents the load-displacement curve comparison between the pre-set anchors and the preliminary anchorage proof of concept specimen. As anticipated, pre-setting the anchors was necessitated as it reduced anchorage system slippage and reduced the machine displacement when attaining higher tensile loads. Our proposed mechanical anchor would still be advantageous compared to steel strand counterparts, as even steel-strand PT systems require pre-setting to reduce and/or eliminate detrimental slippage.

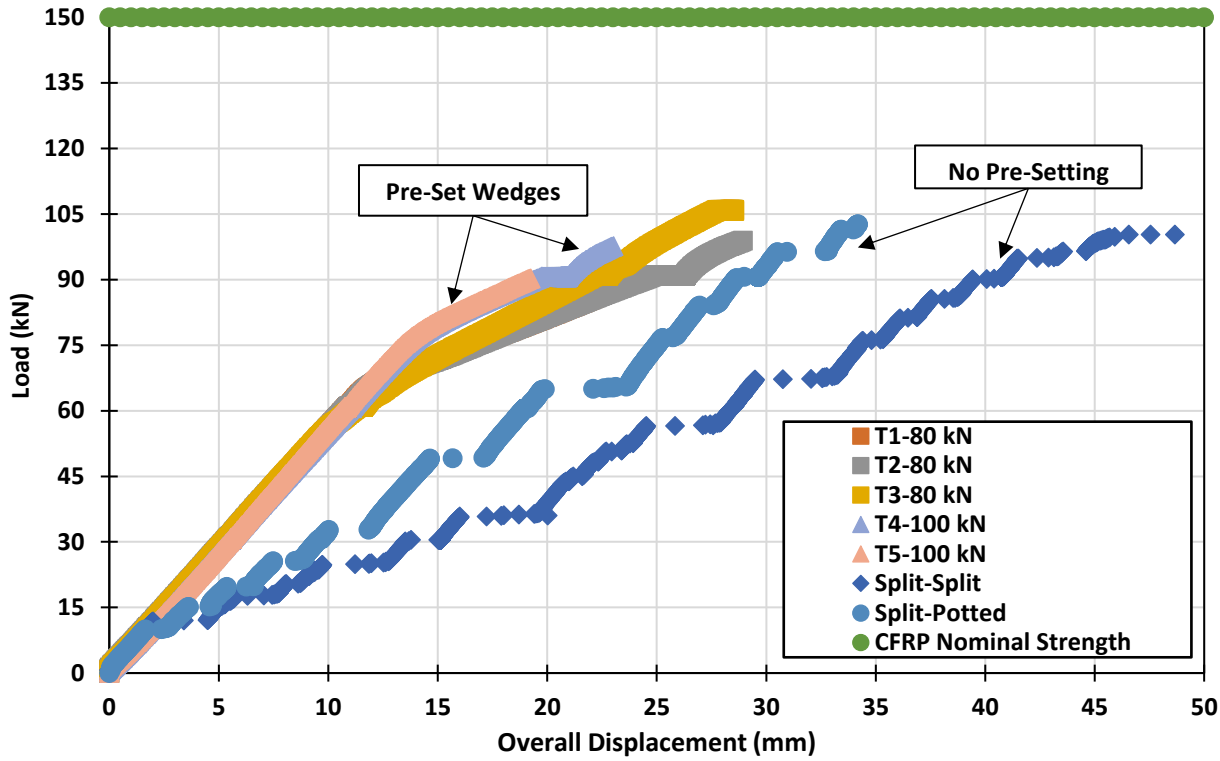

Figure 3-18. Anchorage Load Displacement Curve Summary

Table 3-10 presents the overall system capacity of the CFRP anchorage system for each test specimen, the load level where slippage was observed, and the efficacy of the anchorage system.

Table 3-10. CFRP Anchor Static Test Results

Specimen	Pre-Setting Load (kN)	Load (kN)	Observed Slippage	Efficacy (%)
S1	80	98.9	After 60 kN	64.3
S2	80	97.7	After 60 kN	63.5
S3	80	105.9	After 60 kN	68.9
S4	100	87.4	After 70 kN	56.8
S5	100	90.3	After 70 kN	58.7

From the obtained experimental results of the anchorage static tests, the proposed CFRP anchor was adopted to be implemented in the PT bridge cantilever experimental program. The pre-setting load for the anchor would be set to 80 kN and the maximum effective jacking force for the #3 CFRP rod would be set to 50 kN.

3.5 Final CFRP Anchorage Design

Based on the results of the preliminary proof of concept and the anchorage static tests that were conducted, the proposed split wedge and barrel CFRP mechanical anchorage system will be utilized for the strengthening of a half-scale post-tensioned concrete bridge cantilever wing specimen exhibiting deterioration in the steel PT. Unlike a static test, when jacking the CFRP rod against the steel bearing plate that was the medium to transfer the PT force to the concrete, a gap would be present between the loading end of the barrel and the bearing plate. To account for this difference/gap, we proceeded to thread the loading end of the barrels. Threading of the loading end of the barrels would allow for a commercial hex nut to thread onto the barrel to account for this gap. Additionally, tightening the hex nut against the steel bearing plate would facilitate the locking of the jacking force being transferred to the bridge cantilever concrete specimens from the PT CFRP rod. After barrel threading, the anchor was ready to be used to jack the selected #3 CFRP rods. Table 3-11 presents the materials for the finalized CFRP anchorage design.

Table 3-11. Final CFRP Anchorage Materials

Anchorage Component	Material
Barrel	316 Stainless Steel
Wedges	6061 Aluminum
Spacer Disc	Plastic
Hex Nut	316 Stainless Steel

A lubricant was used between the stainless-steel barrel and the aluminum wedges to allow for easier insertion of the wedges into the barrel when pre-setting. A metal anti-seize lubricant was used between the stainless-steel barrel threads and the hex nut threads to avoid any galling when tightening the hex nut to lock the PT force against the bearing plate.

The final proposed CFRP anchorage system features the following:

- 316 Stainless Steel Barrel.
- Three Split 6061 Aluminum Wedges.
- No sleeves or adhesives, pure frictional resistance.
- A longitudinal circular profile with a circular radius of 1650 mm was used for the inner conical hole of the barrel and the outer aluminum wedge core.
- Radial Plastic Spacer Disc.
- Fine Barrel Threading with 25 mm Thick 316 Stainless Steel Hex Nut at the loading end of the barrel.
- Pre-set live & dead-end anchors.

Figure 3-19 presents the final in-house developed and machined CFRP anchor.

Figure 3-19. Final Machined CFRP Anchor

Figure 3-20 presents the final CFRP anchorage system. The system is comprised of live and dead anchors bearing on steel bearing plates that would bear on the PT bridge cantilever concrete specimen. The stressing anchor (anchor #3) was not shown for clarity. A third anchor was required as is standard for post-tensioning behind the hydraulic cylinder to stress the CFRP rod. No pre-setting load was applied to the stressing anchor. The wedges of the stressing anchor were situated and tapped into place in the barrel by hand.

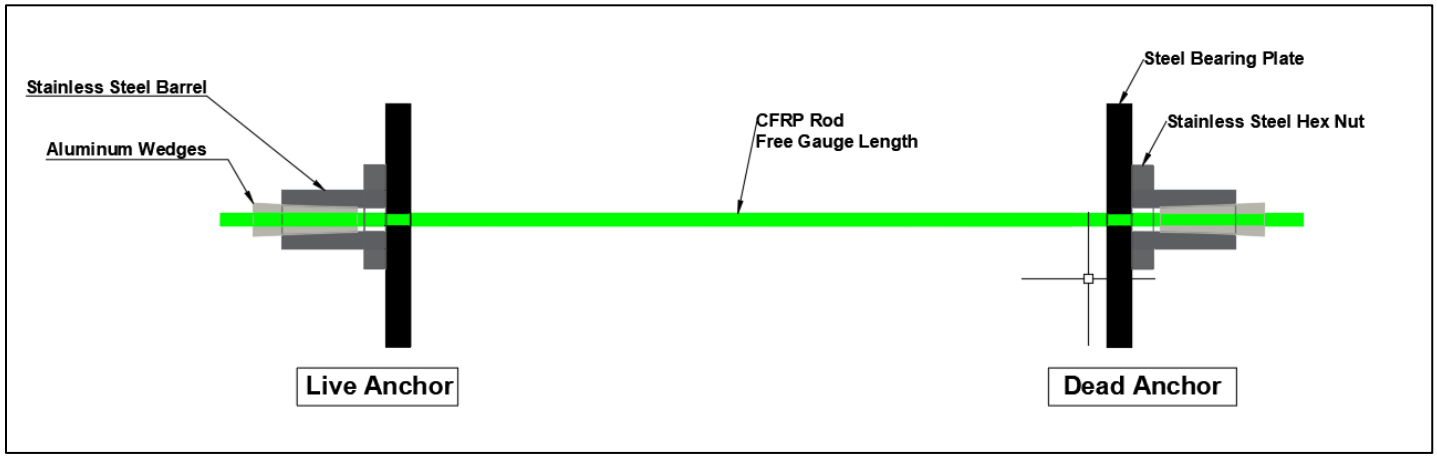

Figure 3-20. PT CFRP Anchorage System

The above system was used as permanent anchorage to rehabilitate a half-scale PT bridge cantilever wing slab presented in the following chapter.

CHAPTER 4 BRIDGE CANTILEVER EXPERIMENTAL PROGRAM

In the following stage of the research experimental program, the in-house developed CFRP anchorage system was implemented into PT concrete bridge specimen. This stage entailed fabricating scaled-down bridge cantilever specimens based on an existing post-tensioned concrete flyover in the Province of Nova Scotia's highway bridge network. The bridge structure under consideration is an approximately 240 m long, seven-span post-tensioned solid box girder with lengthy cantilever wings. The width of the bridge structure is 10.8 m, 9.9 m from curb to curb, carrying two lanes of traffic in one direction. The cantilever wing measures 3.6 m in length from the top cantilever root to the free end. The deck depth of the cantilever wing varies from 225 mm at the free end to 450 mm at the top root. Transverse 32 mm PT steel bars spaced 600 mm on centre encased in grouted 50 mm corrugated metal ducts serve as the primary structural reinforcement resisting the vehicular traffic loads imparted on the cantilever wings. Figure 4-1 presents a transverse cross-section of the bridge structure.

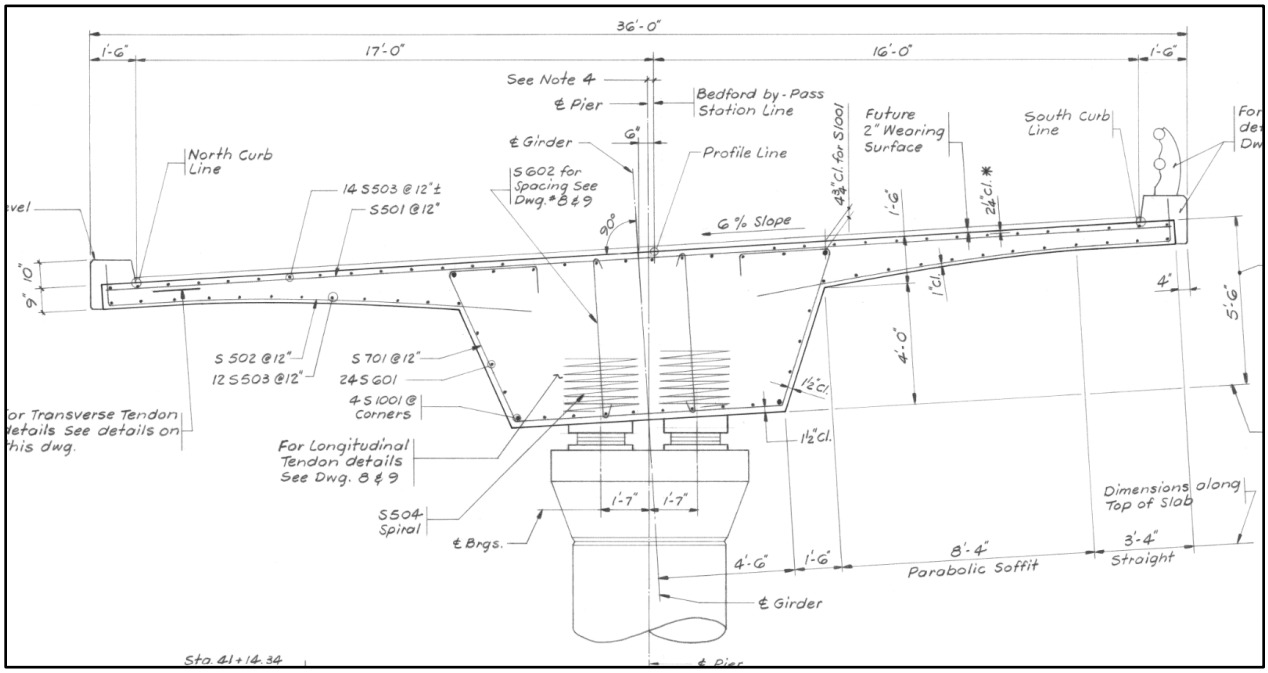

Figure 4-1. Bridge Structure Under Consideration Transverse Cross-Section

During routine maintenance scheduled for the under-consideration bridge structure in 2020, deteriorated transverse PT steel bars were unraveled. The bridge structure underwent emergency rehabilitation which included the implementation of mild (non-prestressed) reinforcement at the

time to safely reopen the bridge to carry vehicular traffic loads at the ultimate limit state (ULS). The concern with mild (non-prestressed) reinforcement in this situation, is there is no reintroduction of the lost pre-compression force that was transferred into the concrete during standard post-tensioning operations. Due to the loss of PT force from the deteriorated transverse steel bars, there is a concern concerning the serviceability limit state (SLS) of the bridge structure. The loss of the pre-compression force which squeezes the concrete resulting in an upward camber among other benefits has been lost, and the cantilever wing will deflect more under service. Therefore, research into the feasibility of using post-tensioned CFRP rods near the surface mounted on the top slab was proposed as a possible rehabilitation strategy. The intent was to rehabilitate the lost transverse steel PT force to control deflections and the sag of the bridge at the free end of the cantilevers. A CFRP anchor was developed as presented in Chapter 3 of this paper to jack a #3 CFRP rod used for the rehabilitation of a scaled-down bridge cantilever specimen. Two half-scale bridge cantilever wing specimens were fabricated for this stage of the research experimental program. One half-scale specimen served as the control. The second served as a specimen that underwent simulated damage before the application of the proposed rehabilitation methodology. The presentation of the performance and behavior of the post-tensioned concrete bridge cantilever specimen is detailed in the following sections of this chapter. The following sections include the design, materials, fabrication, post-tensioning, and testing of the half-scale bridge cantilever specimens.

4.1. Bridge Cantilever Materials

The materials utilized for this stage of the experimental research were comprised of emulating equivalent half-scale conditions from the existing bridge structure by utilizing the same manufacturers and similar strength materials where possible. The primary materials used for this experimental program stage are but are not limited to the following:

- 15 mm High Strength Prestressing Steel Bars.
- 32 mm Corrugated Metal Spiro Ducts.
- Unidirectional No.3 (10 mm) CFRP Rods.
- 35 MPa DOT Ready-Mix Concrete.
- In-House Machined & Developed Split Wedge & Barrel Mechanical Anchor.
- 10M Mild Steel Rebar.

Table 4-1 presents the material design properties of the various reinforcement used in the post-tensioned bridge cantilever specimen as obtained from the respective manufacturers.

Table 4-1. Reinforcement Material Design Properties

Material	Nominal Diameter (mm)	Cross Section Area (mm2)	Yield Strength (MPa)	Ultimate Strength (MPa)	Elastic Modulus (GPa)
Prestressing Steel Bar	15	177	880	1100	205
No.3 CFRP Rod	10	71.26	N.A*	2172	124
10M Steel	11.3	100	400	N.A*	200

*Not Applicable

The high-strength steel bars and associated corrugated metal ducts were purchased from the same manufacturer, Dywidag in the United States. The CFRP rods were purchased from Aslan/Geotree suppliers in the United States. The rebar, lumber, and plywood were all purchased locally in Nova Scotia. The concrete was also from a local ready-mix supplier. Based on the original drawings, at the time, the under-consideration bridge deck was poured with 5000 psi grade (35 MPa) concrete. Therefore, the selected ready-mix concrete for this experimental program was a 35 MPa grade concrete with a 10 mm nominal coarse aggregate size. It is common practice for the Nova Scotia DOT to use 35 MPa grade-10 mm aggregate stone for all their bridge rehabilitation and maintenance projects. 35 MPa is a very common standard performance grade of concrete. Additionally, the smaller stone is preferred due to the limited concrete cover predominantly present in old bridge structures. Table 4-2 presents the specifications the ready-mix concrete conformed to as per the Nova Scotia Transportation & Infrastructure Renewal (NSTIR) January 2021 Standard Specification manual, specifically Division 5 Section 7 (Cast in Place Concrete), and Division 5 Section 13 (Concrete Restoration-Bridge Structures).

Table 4-2. Ready-Mix Concrete Specifications

Structural Requirement	Value
f'c @ 28 Days (MPa)	35
Maximum W/C Ratio	0.40
Minimum Cementitious Content (kg/m3)	415
CSA Exposure Class	C-1
Nominal Maximum Aggregate Size (mm)	10
Maximum Fly Ash Replacement (%)	25
Plastic Air Content (%)	6 TO 9
Slump Range (mm)	80 +/- 20

4.2. Bridge Cantilever Design

The bridge cantilever design was a half-scale model of the transverse cross-section of the under-consideration bridge structure. Scaling down of the existing bridge was only necessitated for one cantilever wing. For various laboratory logistical purposes, the experimental specimen cantilever wings were capped at 900 mm in width. The total length of the specimens was 3.0 m. The experimental cantilever wing measured 1.75 m in length from the top cantilever root to the free end. The slab depth of the cantilever wing varied from 150 mm at the free end to 225 mm at the top root. 15 mm PT steel bars were utilized and spaced 300 mm on centre encased in grouted 32 mm corrugated metal ducts. Thus, three steel tendons were the primary structural reinforcement. Figure 4-2 presents a transverse cross-section of the experimental cantilever wing design.

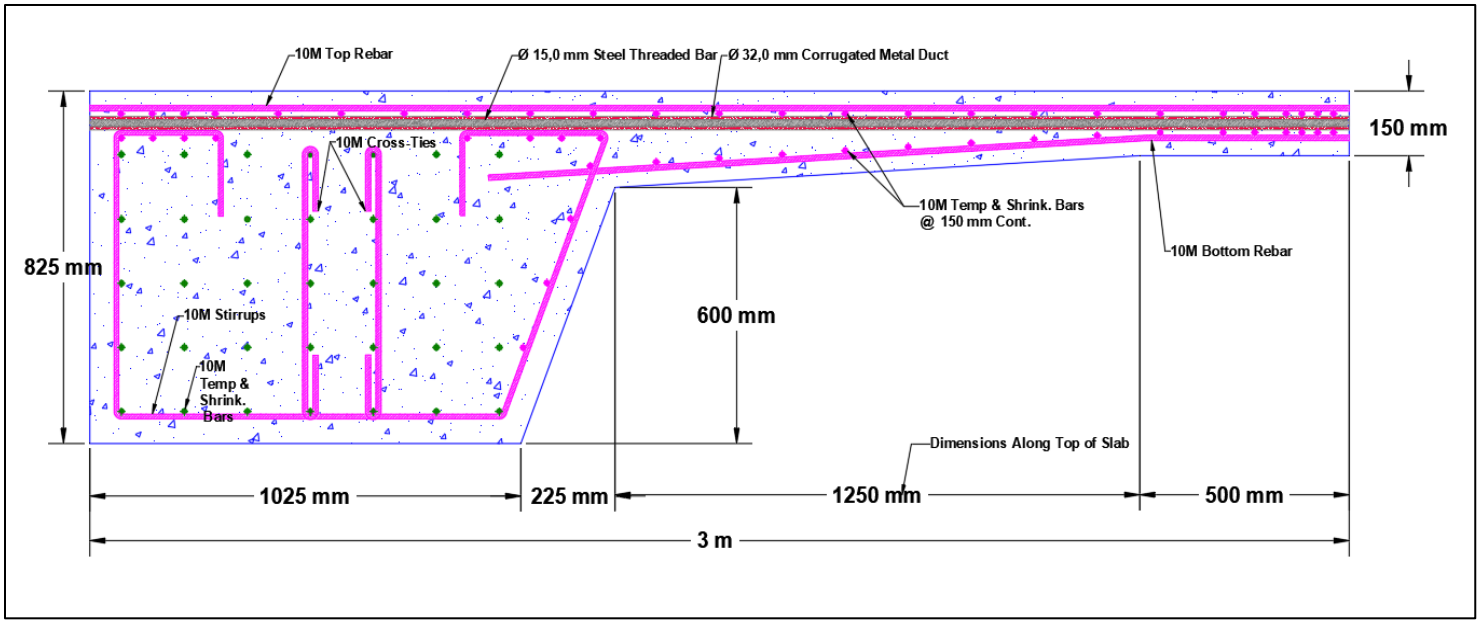

Figure 4-2. Experimental Bridge Cantilever Wing Design

Two experimental bridge cantilever wing specimens were cast based on the above design schematic. The first specimen, S1 served as the control, emulating a half-scale full structural capacity condition. The second specimen, S2 served as the rehabilitation test, emulating simulated damage conditions to weaken the structural capacity followed by the proposed PT CFRP rehabilitation methodology. The main objective was to witness the feasibility of the NSM PT CFRP rehabilitation methodology and to observe if it was able to rehabilitate the structural capacity that has been lost. Table 4-3 presents the system description of the two experimental cantilever wing specimens.

Table 4-3. Experimental Bridge Cantilever Specimen Description

Specimen ID	Specimen Description
S1-Control	Full Structural Capacity Conditions
S2-Rehabilitation	Simulated Damage Conditions with PT CFRP Rehabilitation

The control specimen, specimen S1, simulates existing full capacity conditions, i.e., existing steel post-tensioning with no deterioration. The rehabilitation specimen, S2, simulates damage conditions, i.e., a degree of deterioration to the steel post-tensioning which is characterized by the loss of one steel tendon in the system and the incorporation of two NSM PT CFRP rods aiming to rehabilitate the capacity of the cantilever. The high-strength steel bars and the CFRP rods each respectively have a unique anchorage system which is defined in Table 4-4.

Table 4-4. Bridge Cantilever Specimen Anchorage Systems

Material	**Anchorage System**
High Strength Prestressing Steel Bar	Bearing Plate with Full Load Steel Hex Nut System
CFRP Rod	Bearing Plate with Split Wedge & Barrel System

The prestressing steel bar's anchorage system was sourced from the manufacturer, Dywidag, as it was a commercial product. However, the CFRP anchorage system had to be developed and machined in-house for no commercial systems exist as indicated before. Specimen S1 included only steel post-tensioning. Specimen S2 included steel post-tensioning and two CFRP tendons. Figure 4-3 presents the prestressing steel anchorage system comprised of the bearing plate and hex nut. Figure 4-4 presents the CFRP anchorage system comprised of the split wedge and barrel system.

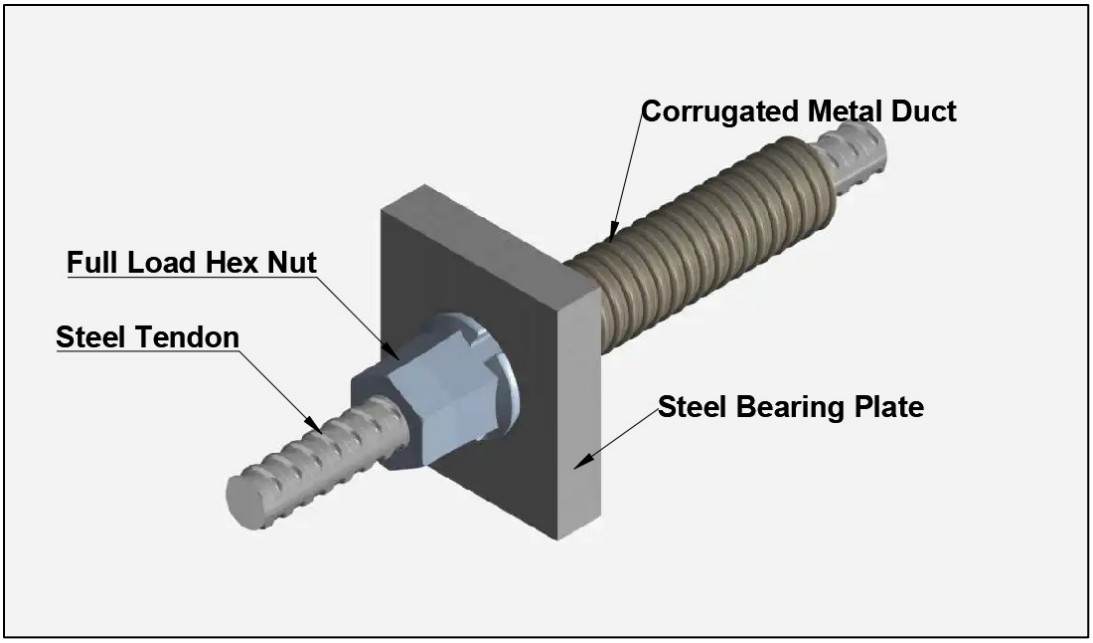

Figure 4-3. Steel Tendon Anchorage System (Modified from Dywidag 2022)

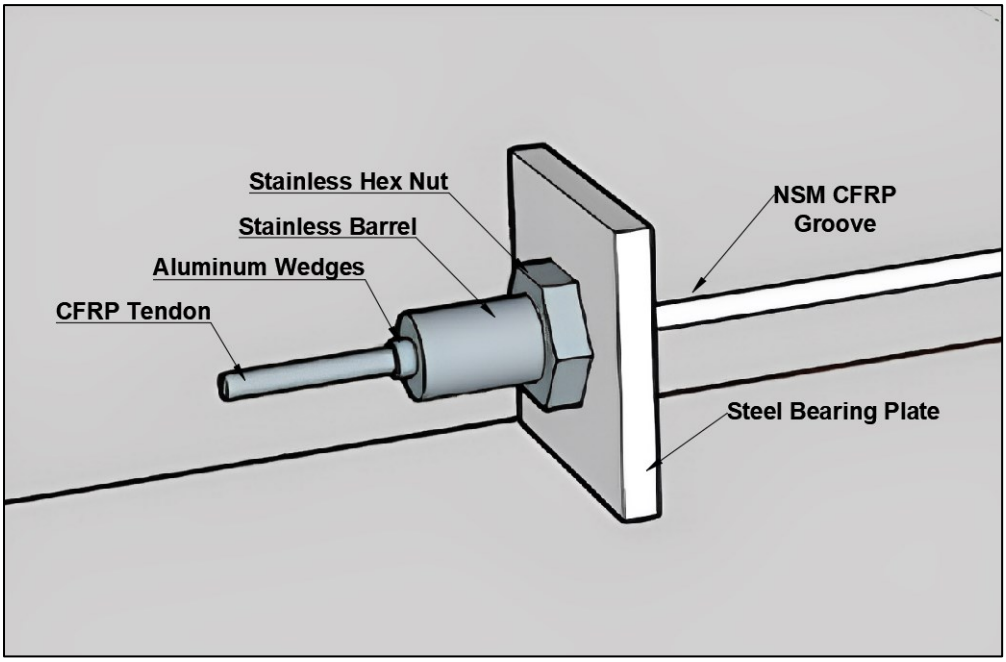

Figure 4-4. CFRP Tendon Anchorage System

The high-strength steel bar is threaded along its length, therefore, gripping and jacking the bar is simple. A steel bearing plate is needed and a hex nut threads onto the bar and locks the load. On the other hand, a CFRP rod is not threaded which poses a challenge for gripping and jacking the rod. Therefore, an in-house anchor had to be developed and machined.

4.3. Bridge Cantilever Specimen Test Matrix & Fabrication

The control and rehabilitation bridge cantilever bridge specimens were fabricated and framed in a structural laboratory using 19 mm structural plywood and 2 x 4 lumber. Two high-strength steel bars with associated washers and hex nuts were utilized per specimen as a formwork tie-rod system to resist the high pressure imparted on the forms when casting the fresh concrete and until the concrete cures. Figure 4-5 presents the fabrication of the bridge specimens in the laboratory.

Figure 4-5. Bridge Cantilever Specimen Fabrication

Various parameters were kept constant within the experimental program for the control and rehabilitation PT bridge cantilever specimens which are portrayed in Table 4-5.

Table 4-5. Fixed Experimental Parameters

Fixed Variables	Variable Metric
Anchorage System	Permanent Mechanical Anchorage
Steel Bar Tendon Spacing	300 mm c/c Spacing
CFRP Size & Geometry	#3 (10 mm) CFRP Rod
NSM Groove	35 mm Width x 47 mm Depth

Firstly, the anchorage systems for the steel prestressing bars and the CFRP rods respectively were the same for both bridge cantilever specimens. Secondly, the spacing between the prestressing steel bars was fixed at a spacing of 300 mm c/c. The c/c spacing between the prestressing steel bars was selected as half the spacing from the existing 600 mm transverse tendon spacing on the existing bridge structure. Thirdly, the rehabilitation methodology was fixed to the utilization of #3 (10 mm) CFRP rods for post-tensioning in near-surface-mounted grooves. No dissimilar rod sizes, CFRP strips, or fabrics were used. Fourthly, the NSM groove dimensions were fixed. The NSM groove dimensions adhere to the minimum dimensions specified by the ACI 440.2-17 specification and the manufacturer's recommendations. The CSA S6-19 bridge code provides NSM grooves recommendations for the rehabilitation of timber beams with GFRP, however, no mention of NSM grooves in concrete. Furthermore, the groove dimensions of 35 mm x 47 mm were specified as-is for constructability purposes. In both specimens, three corrugated metal ducts were incorporated and spaced at a fixed 300 mm c/c spacing facilitating the voids necessary for bonded post-tensioning. The control specimen, specimen S1, which simulated existing full capacity conditions has three ducts with three high-strength steel bars: One steel bar running down the centre of each duct. The rehabilitation specimen, specimen S2, which simulated damage conditions has three ducts but only two high-strength steel bars. No high-

strength steel bar was placed in the centre duct. The steel bar in the second (central) duct is eliminated to represent an equivalent loss of structural capacity emulating a snapped tendon in the field. The incorporation of two NSM CFRP rods serves to be the proposed rehabilitation strategy for the cantilever section. Table 4-6 presents the steel tendon and CFRP tendon layout, in addition to the target transfer forces for each bridge cantilever specimen.

Table 4-6. Bridge Cantilever Specimen Tendon Schedule

Specimen ID	**Bonded Steel Tendon Layout**	**Steel Target Transfer Force (kN)**	**CFRP Tendon Layout**	**CFRP Target Transfer Force (kN)**
S1-Control	3 Ducts 3 Threaded Bars	50 - 100 - 50	0 Rods	N.A*
S2-Rehabilitation	3 Ducts & 2 Threaded Bars	50 - N.A - 50	2 Rods	50 EACH

*Not Applicable

The target transfer forces for the steel tendons were selected to emulate varied post-tensioning forces possibly exhibited on the real bride structure. The steel tendons were not stressed to the full capacity threshold as per the CSA S6-19 bridge code owing to the limiting jacking force that could be applied on the CFRP rods. Based on the anchorage experimental program test results previously presented in Chapter 3, the maximum safe jacking force the CFRP rods could withstand was 50 kN. The anchorage effect on the CFRP rods dictated the max effective PT force. Therefore, for the control specimen, the central steel tendon was jacked to a force of 100 kN. Consequently, for the rehabilitation specimen, simulated damage conditions, denoted as the loss of one steel tendon, resulted in the loss of 100 kN of PT force in the system. Thus, the proposed rehabilitation strategy consisted of two CFRP rods at 50 kN each within the influence zone of the central tendon. In theory, the rehabilitation proposal would be restoring the lost 100 kN from the one 15mm steel tendon by means of two 10 mm CFRP rods near-surface mounted in grooves with a total force of

100 kN. Figure 4-6 presents the free end (jacking end) of the control specimen and Figure 4-7 presents the free end (jacking end) of the rehabilitation specimen.

Figure 4-6. Control Specimen Jacking End

Figure 4-7. Rehabilitation Specimen Jacking End

The structural behaviour of a concrete cantilever slab under any load bends the cantilever downwards by creating a convexity upwards. Thus, the main reinforcement is required to be within the top fibres which experience tension. The major advantage of a bridge cantilever wing is the bridge top slab is easily accessible. Therefore, for rehabilitation, near-surface mounting of reinforcement in grooves is quite feasible and realistic. However, even though the top slab is easily accessible, there is currently minimal guidance and limited NSM CFRP detailing requirements available. FRP manufacturers recommend minimum dimensions of NSM grooves but with little specific detailing. In this application, we proposed our own CFRP reinforcement detailing. The only pertinent clause in the CHBDC on NSM rehabilitation is as follows. The CSA S6-19 bridge code about the rehabilitation of existing concrete structures with FRP stipulates the following: "Clause 16.12 applies to existing concrete structures that have an f'c of less than or equal to 50 MPa and are strengthened with FRP comprising externally bonded system or NSMR. If the concrete cover is less than 20 mm, NSMR shall not be used." For our rehabilitation strategy, we proposed the CFRP rod be placed at a depth of 32 mm on centre in a 35 mm by 47 mm NSM groove. As indicated in the literature review section of this document in Chapter 2, smaller NSM grooves have resulted in bond slip failure of the FRP reinforcement and the splitting of the groove grout which is an undesirable failure mode. Thus, our FRP NSM detailing proposal delivers on the following:

- Avoids FRP reinforcement bond-related failure.
- Meets CSA S6-19 concrete cover requirements for NSMR.
- Constructability and Feasibility.

The width of the NSM groove was selected to match the nominal dimension of a 2 x 4 piece of lumber. The depth of the NSM groove was selected based on the theoretical concrete cover typically observed in old concrete bridges in Nova Scotia. The depth on centre to the CFRP rod was selected to ensure adequate coverage of grout encasing the reinforcement within the groove. Figure 4-8 presents a schematic of our proposed CFRP rod NSM groove detailing that was implemented for the rehabilitation bridge cantilever specimen.

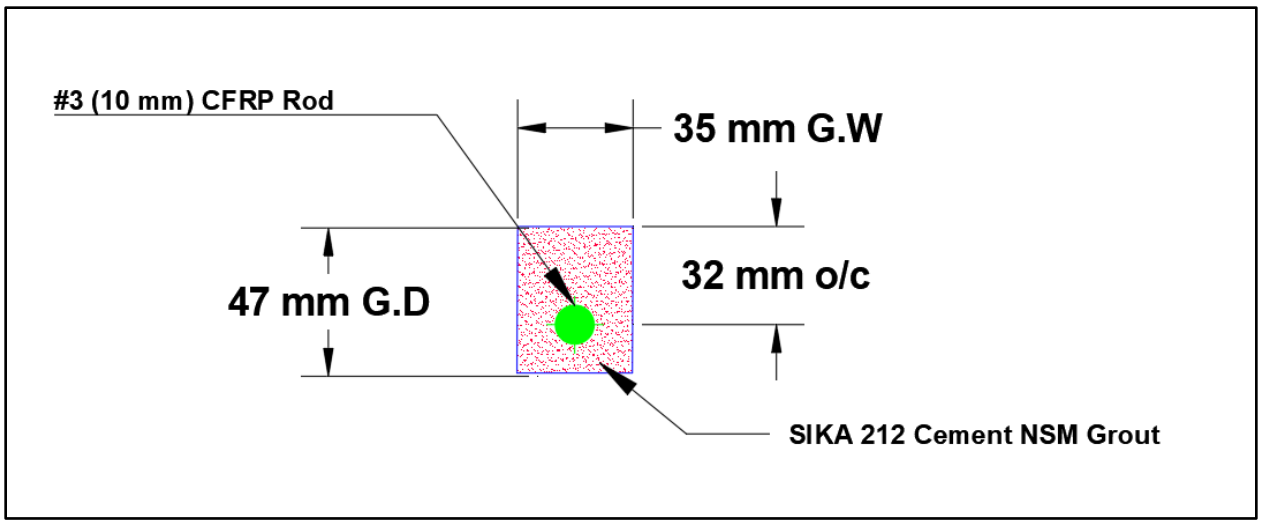

Figure 4-8. CFRP NSM Groove Detail

A cement-based grout was selected as the proposed rehabilitation strategy is comprised of a bonded PT system. A bonded PT system allows for the tendon to be bonded with the concrete where primary reliance is not just on the anchorage ends. The grout locks the CFRP force along the length of the groove and strain compatibility is established with the existing concrete substrate. SIKA 212 grout was chosen as a common in-expensive construction cement-based grout as the matrix to fill the NSM grooves. When casting the cement grout into the NSM grooves, no bonding agent was applied to the grooves and the grooves were not sand-blasted or pre-wet. The above conditions simulated a worst-case bond scenario between the CFRP and the concrete substrate where a contractor avoids or forgets to properly prepare a concrete substrate as is sometimes the case in the field.

4.4. Bridge Cantilever Specimen Post-Tensioning

The control and the rehabilitation bridge cantilever specimens were post-tensioned to the jacking forces specified in the tendon schedule in Table 4-6. After the concrete had reached sufficient strength, the tendons were jacked to the specified stress. Stressing of the tendons was completed employing 300 kN hollow hydraulic cylinders bearing against a steel bearing plate. In preparation for post-tensioning, the hydraulic cylinders were calibrated to the specified jacking forces. Calibration of the hydraulic cylinders and pump/transducer system was completed using a 2 MN Instron machine. Load cells were attached on the top of the extended pistons of the hydraulic

cylinders that were bearing on the vertical Instron machine head. At each load increment, the force between the pump/transducer system and the hydraulic cylinder load cells was calibrated with the aid of a data acquisition system. Stressing records and respective post-tensioning protocols were established for each bridge cantilever specimen. Symmetry while jacking was maintained with the prescribed post-tensioned protocol. For the control specimen, the following stressing protocol was adhered to:

1- Stress the two outer steel tendons together first (double pull).

2- Stress the central steel tendon individually subsequently (single pull).

The stressing records for the control specimen, both the steel tendon double pull and the steel tendon single pull are detailed and presented in Appendix B.1 and Appendix B.2 respectively. For the CFRP rehabilitation specimen, the following stressing protocol was adhered to:

1- Stress the two outer steel tendons together first (double pull).

2- Stress the two CFRP rods together subsequently (double pull).

The stressing records for the rehabilitation specimen, both the steel tendon double pull and the CFRP tendon double pull are detailed and presented in Appendix B.3 and Appendix B.4 respectively. Stressing operations occurred in five load increments (20% at a time) per pull until the final stressing force was achieved. During the stressing operations, tendon elongation and pump pressure were measured as primary means of force transfer confirmation. Identical to in-situ field measurement of tendon elongation operations, laboratory measurements serve as confirmation that the required force had been transferred to the tendon. Additionally, strain gauges were placed on both the steel tendons and the CFRP tendons as secondary means of force transfer confirmation. As the physical properties of the tendons, the tendon profile, the length of the tendon, and the force that is to be applied are all known, the theoretical elongation and theoretical strain of the tendon can be calculated. Micro-Strain readings were recorded at the following times during the stressing operations:

- At each load increment
- At the specified jacking force
- At pump stabilization
- At tightening of the hex nut

- At pump release
- At 60 minutes after release
- At 24 hours after release
- Re-Tension if necessary

There are losses in any system, and pumps are never 100% efficient, therefore these losses had to be accounted for. PT system losses were accounted for by jacking a little higher than the specified stressing force. Strain readings after the release of the pump confirmed the predicted losses and once the force was below the required minimum threshold, it was simply re-tensioned. As long as the steel tendon ducts and the NSM grooves were not grouted, the tendons could be re-tensioned to the necessary threshold. Moreover, the tendons could be de-tensioned if any errors during stressing operations were encountered and a re-do is required. Figure 4-9 presents a schematic of the control specimen PT operations, and Figure 4-10 presents a schematic of the CFRP rehabilitation PT operations.

Figure 4-9. Control Specimen Post-Tensioning Operations

Figure 4-10. Rehabilitation Specimen Post-Tensioning Operations

After the final jacking force for all tendons was locked and transferred to the concrete, the steel tendon ducts and the CFRP NSM grooves were grouted respectively. SIKA 300 PT was utilized as a specialized matrix to grout the corrugated metal ducts and SIKA 212 was utilized to grout the NSM grooves.

4.5. Bridge Cantilever Instrumentation & Test Setup

The bridge cantilever specimens were tested under simulated service and ultimate loads utilizing a 1 mega-newton actuator pushing down as a point simulated truck wheel load distributed by a 250 mm wide x 500 mm long x 25 mm thick steel plate. The centreline of the load was 500 mm from

the free end of the cantilever and 450 mm from the edges respectively. The centreline of the test point load emulates an estimated realistic location of wheel loads on the in-situ existing bridge structure and the location of cantilever geometry change to observe maximum load effects. A 12.5 mm thick neoprene rubber pad was placed under the loading steel plate. Both specimens at the fixed cantilever end were anchored to the ground. Anchoring the specimens to the laboratory concrete floor was completed employing a 1.5 m long by 162.5 mm wide by 0.90 m deep steel I-beam and two 50 mm diameter threaded bolts and associated washers and nuts. The I-beam was bearing on two, 200 mm x 200 mm x 25 mm thick steel plates. Similarly, a 12.5 mm thick neoprene rubber pad was placed under each steel plate. Figure 4-11 presents the test setup of the specimens in the lab under the loading actuator frame.

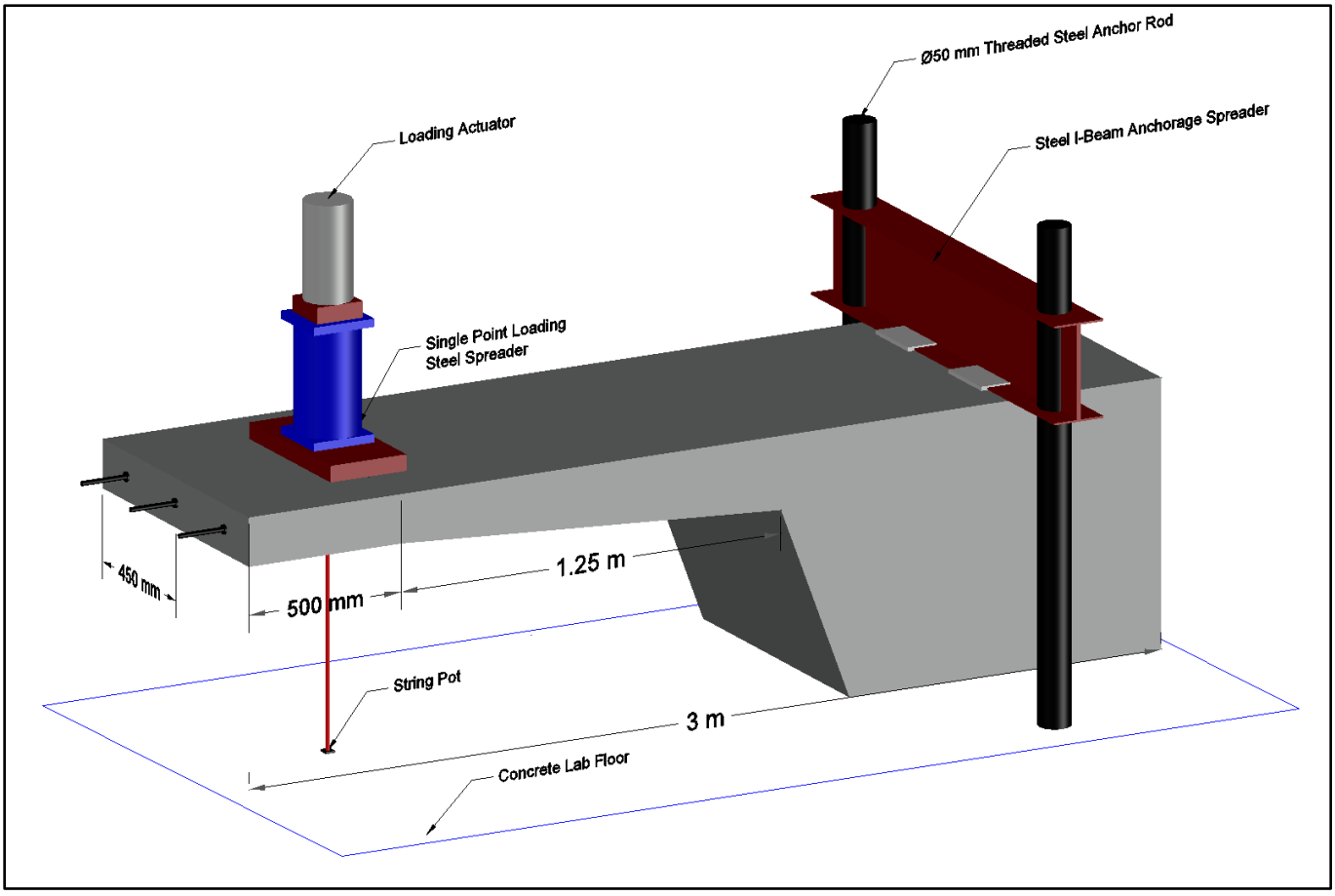

Figure 4-11. Bridge Cantilever Specimen Test Setup

Various instrumentation and sensors were set up on the bridge cantilever specimens to obtain the necessary experimental data. For both specimens the following instrumentation was placed:

- Strain Gauges on the CFRP Tendons (Applicable only to Rehab Specimen)
- Strain Gauges on the Steel Tendons
- Single string potentiometer directly underneath the load
- Two LPs at 250 mm from the cantilever free end and 150 mm respectively from the width ends to witness if the specimen twists when loading
- Three LPs spaced at 375 mm increments in between the string pot and the cantilever root on the cantilever soffit
- One LP at the box girder rear end to record specimen uplift when loading

Figure 4-12 presents the sensory instrumentation layout for the bridge cantilever specimens.

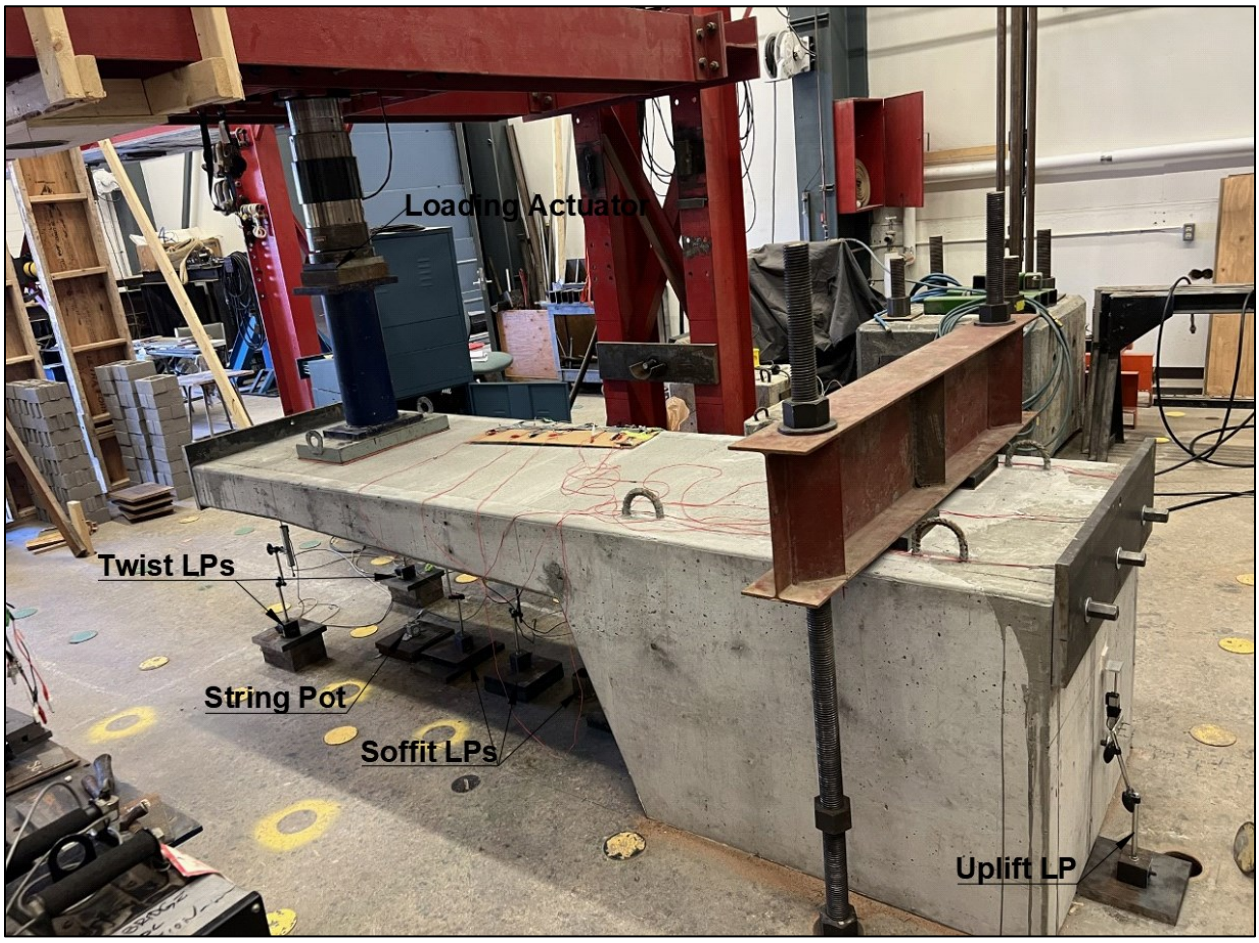

Figure 4-12. Bridge Cantilever Specimen Instrumentation Layout

4.6. Bridge Cantilever Loading Protocol

The control and rehabilitation bridge cantilever specimens were both statically loaded under a specified 2.5 mm/min displacement-controlled loading protocol. Both specimens were tested under simulated service and ultimate conditions. Simulated service conditions for the bridge specimens were established by referring to the CSA S6-19 bridge code specifically clause 8.8.4.6 (prestressed concrete stress limitations) as follows:

1- At the serviceability limit states,
   i. Compression due to dead load plus effective prestress after all losses: 0.45 f'c;
   ii. Compression due to SLS Combination 1: 0.60 f'c;
   iii. If the tension in the concrete exceeds fcr, Clause 8.12 shall apply.

SLS combination 1 is presented as Equation 4-1 as per the CHDBC clause 3.5.1 (Load Factors and Load Combinations):

$$SLS\ Combination\ 1 = 1.00\ D.L + 0.90\ L.L \tag{4-1}$$

Where: D.L is the dead load

L.L is the live load

If the tension in the concrete exceeds fcr, clause 8.12 would apply. The CHDBC clause 8.12.3.4 (tensile stress limits for reinforcing steel) stipulates the following tensile stress limit under service: For Category A exposure: The lesser of 300 MPa or Equation 4-2:

$$\sqrt{\frac{1.6\ xf_{cr}\ xE_s}{a_b\ xd_b}} \tag{4-2}$$

Where: fcr is the cracking strength of concrete (MPa)

Es is the modulus of elasticity of reinforcing bars (MPa)

ab is 1.0 for uncoated bars

db is the nominal diameter of a bar (mm)

The above code clauses were set as the criteria to establish the serviceability limit state and the overall experimental loading protocol for the bridge cantilever specimens. The three SLS conditions were run for the control and the rehabilitation specimen to establish the magnitude of the simulated "service point load" that would be imparted 500 mm onto the system from the cantilever free end using a loading actuator. The simulated service load is represented by the point load loading actuator as the live load. The dead load is represented by the self-weight of the bridge cantilever specimens. Condition I requirements yields meeting Equations 4-3 for the control specimen and Equations 4-4 for the rehabilitation specimen.

$$fc = \frac{P_{ps}}{A_{Conc.}} + \frac{M_{Dead}}{S_{Conc}} < 0.45\, f'c \tag{4-3}$$

$$fc = \frac{P_{ps}}{A_{Conc.}} + \frac{P_{frp}}{A_{Conc.}} + \frac{M_{Dead}}{S_{Conc}} < 0.45\, f'c \tag{4-4}$$

Where: fc is compression stress in the concrete (MPa)

Pps is the effective prestressing force applied to the high-strength steel bars (N)

Pfrp is the effective prestressing force applied to the CFRP tendons (N)

Aconc. is the area of concrete that bears the prestressing force (mm2)

Mdead is the self-weight moment (N.mm)

Sconc. is the concrete section modulus (mm3)

f'c is the compressive strength of the concrete during loading (MPa)

Condition II requirements yield meeting Equations 4-5 for the control specimen and Equations 4-6 for the rehabilitation specimen.

$$fc = -\frac{P_{ps}}{A_{Trans.}} + \frac{M_{ps}\, x\, y_c}{I_{Crack}} - \frac{M_{Dead}\, x\, y_c}{I_{Crack}} - \frac{0.9\, x\, M_{Live}\, x\, D.L.A\, x\, y_c}{I_{Crack}} < 0.60\, f'c \tag{4-5}$$

$$fc = -\frac{P_{ps}}{A_{Trans.}} - \frac{P_{frp}}{A_{Trans}} + \frac{M_{ps}\ x\ y_c}{I_{Crack}} + \frac{M_{frp}\ x\ y_c}{I_{Crack}} - \frac{M_{Dead}\ x\ y_c}{I_{Crack}} - \frac{0.9\ x\ M_{Live}\ x\ D.L.A\ x\ y_c}{I_{Crack}} < 0.60\ f'c$$

(4-6)

Where: fc is compression stress in the concrete (MPa)

Pps is the effective prestressing force applied to the high-strength steel bars (N)

Pfrp is the effective prestressing force applied to the CFRP tendons (N)

Atrans. is the transformed area of concrete that bears the prestressing force (mm2)

Mps is the steel prestressing moment (N.mm)

Mfrp is the CFRP prestressing moment (N.mm)

yc is the distance to the cracked concrete section neutral axis (mm)

Icrack is the cracked transformed concrete moment of inertia (mm4)

Mdead is the self-weight moment (N.mm)

Mlive is the moment caused by the service point load (N.mm)

D.L.A is the dynamic load allowance

f'c is the compressive strength of the concrete during loading (MPa)

The dynamic load allowance was set to one for our scenario due to the inherently static nature of the experimental laboratory loading of the bridge cantilever specimens. Condition III requirements yield meeting Equations 4-7 for the control specimen and Equations 4-8 for the rehabilitation specimen.

$$\frac{f_s}{n_s} = -\frac{P_{ps}}{A_{Trans.}} - \frac{M_{ps}\ x\ y_s}{I_{Crack}} + \frac{M_{Dead}\ x\ y_s}{I_{Crack}} + \frac{0.9\ x\ M_{Live}\ x\ D.L.A\ x\ y_s}{I_{Crack}}$$

(4-7)

$$\frac{f_s}{n_s} = -\frac{P_{ps}}{A_{Trans.}} - \frac{P_{frp}}{A_{Trans.}} - \frac{M_p\ x\ y_s}{I_{Crack}} - \frac{M_{frp}\ x\ y_s}{I_{Crack}} + \frac{M_{Dead}\ x\ y_s}{I_{Crack}} + \frac{0.9\ x\ M_{Live}\ x\ D.L.A\ x\ y_s}{I_{Crack}}$$

(4-8)

Where: fs is the tensile stress limit for the reinforcing steel (MPa)

ns is the transformation factor

Pps is the effective prestressing force applied to the high-strength steel bars (N)

Pfrp is the effective prestressing force applied to the CFRP tendons (N)

Atrans. is the transformed area of concrete that bears the prestressing force (mm2)

Mps is the steel prestressing moment (N.mm)

Mfrp is the CFRP prestressing moment (N.mm)

ys is the distance to the level of the tensile reinforcement centroid (mm)

Icrack is the cracked transformed concrete moment of inertia (mm4)

Mdead is the self-weight moment (N.mm)

Mlive is the moment caused by the service point load (N.mm)

D.L.A is the dynamic load allowance

Although the specified compressive strength of the utilized ready-mix concrete was 35 MPa, that value had to be confirmed in the lab to refine the loading protocol. Uniaxial compression tests were conducted on cast 100 mm x 200 mm concrete cylinders before loading each specimen. Table 4-7 presents the results of the mechanical properties of the utilized ready-mix concrete.

Table 4-7. Ready-Mix Concrete Mechanical Properties

Specimen ID	Compressive Strength (MPa)	Cracking Strength (MPa)	Elastic Modulus (GPa)
S1-Control	39.8	2.5	27.2
S2-Rehabilitation	41.9	2.6	27.3

Based on all the above, Condition III was the governing condition for the limiting max magnitude of the service live load. Table 4-8 presents the max service live load for each specimen.

Table 4-8. Bridge Cantilever Specimen Max Service Live Load

Specimen ID	Service Live Load (kN)	Tensile Stress Limit (MPa)
S1-Control	67	267
S2-Rehabilitation	72	271

Therefore, a loading protocol was established after numerically running Equations 4-1 to 4-8. 65 kN was determined to be the service live load as an even whole conservative number. For both the control and rehabilitation specimens, there were ten conducted load steps in total, and are detailed as follows:

1. Load Step #1: 25 kN (Uncracked Moment Region).
2. Load Step #2: 35 kN (Onset of Cracking Region).
3. Load Step #3: 45 kN.
4. Load Step #4: 55 kN.
5. Break: 40 kN
6. Load Step #5: 65 kN

7. Load Step #6: 85 kN
8. Load Step #7: 100 kN
9. Load Step #8: 115 kN
10. Load Step #9: 140 kN
11. Load Step #10: Ultimate Destruction Stage

At each load stage, the specimens were loaded to the specified load step and then back to 0 kN. The bridge cantilevers were cycled five times statically per load stage up to the 85 kN load step. However, at the break stage, only two cycles were conducted. After the 85 kN load stage (post-service), the bridge cantilevers were cycled three times statically per load step until the ultimate destruction load stage. The detailed loading protocol and test observations at every load step for the control and the rehabilitation specimens are presented in Appendix C and Appendix D respectively.

4.7. Bridge Cantilever Test Results & Discussion

The following section presents the results of the bridge cantilever experimental specimens. The load-deflection curves at the theoretical serviceability limit state and ultimate will be presented. Additionally, the load-strain curves will be presented at the simulated service level. Due to the sensitive nature of the strain gauges and the fatigue overload on them, the load-strain curves at the ultimate will not be shown. Furthermore, the deflected shape of each bridge cantilever specimen is portrayed at simulated service (65 kN) and simulated post-service (85 kN). As the bridge cantilever specimens were a half-scale design of an existing bridge structure, there were no stirrups placed within the slabs to emulate the in-service bridge. To obtain and achieve meaningful test results, by design all premature failures (i.e., shear, bursting, splitting, localized compression crushing) were prevented. By design, a flexural failure, i.e., a concrete crushing failure mode was intended for both specimens to compare the behaviours of each system. The results of the control specimen are presented first before the rehabilitation specimen. A comparison between the two specimens and a discussion of the results is presented subsequently.

4.7.1. Control Specimen

The control specimen was loaded as per the loading protocol prescribed in section 4.6 of this document. At simulated service conditions, equivalent to a loading actuator point load magnitude

of 65 kN pushing on the system, the cantilever was deflecting approximately 6 mm underneath the load. At post-service, equivalent to a loading actuator point load magnitude of 85 kN pushing on the system, the cantilever was deflecting approximately 9.35 mm underneath the load. A post-service load is presented to demonstrate the cantilever being loaded past simulated service limits, simulating a heavier truckload as is common for in-service bridges today. Figures 4-13 and 4-14 portray the deflected shape of the control specimen under service (65 kN) and post-service (85 kN) loads respectively. As shown previously in Figure 4-11, the load was applied 1.25 m from the cantilever root.

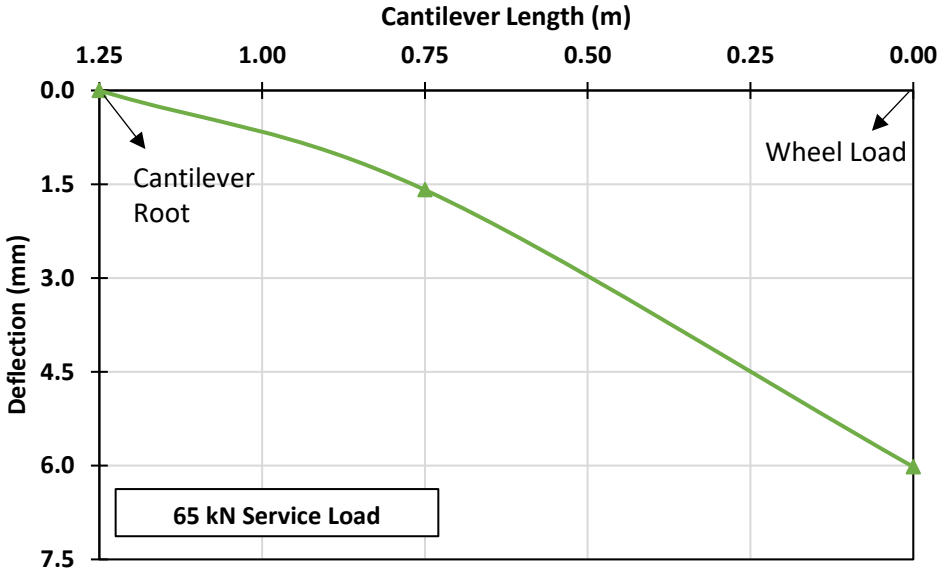

Figure 4-13. Control Specimen Service Load Deflected Shape

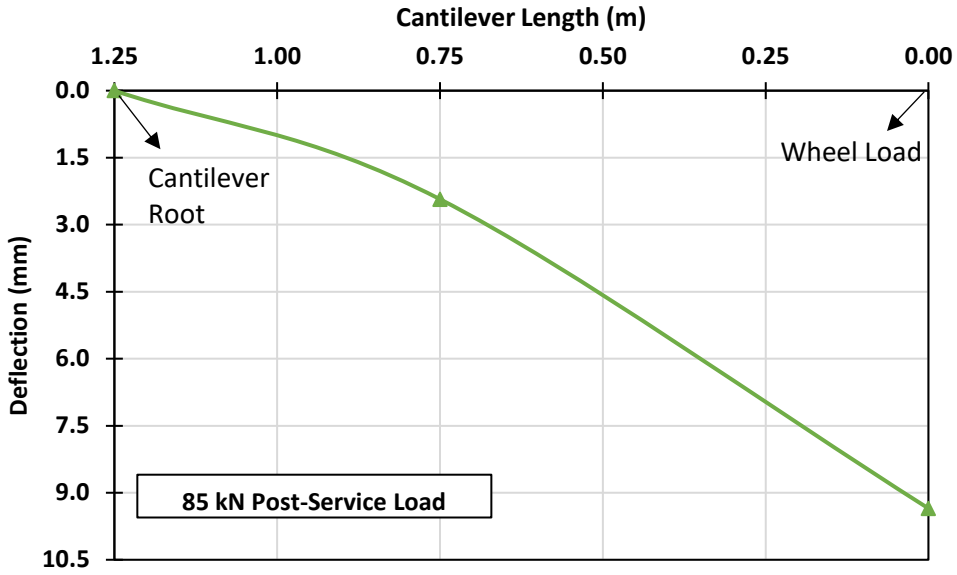

Figure 4-14. Control Specimen Post-Service Load Deflected Shape

The control specimen under service load and post-service load behaved as predicted. Under service (65 kN), top slab cracks were present in the tension region of the cantilever since the load was past the cracking stress limit of the concrete. By design, the PT bars were not stressed to the maximum limit for the reasons stated in previous sections. Cracks in the specimen would run across the width of the top slabs. The cracks were visible and measurable when the service load was held constant. The range of crack widths measured from 0.05 mm to 0.20 mm approximately. The location of the cracks was quite distinct in nature running at a certain defined spacing of approximately 150 mm on centre. Figure 4-15 presents the cracking pattern of the control specimen on the top slab. It is important to note that the image presents cracks at the ultimate on the top slab but the purpose of the figure is to exemplify the distinct spacing between the cracks and the overall cracking pattern.

Figure 4-15. Control Specimen Top Slab Cracking Pattern

When the cantilever specimen was unloaded back to zero, i.e., at end of the load cycle, the cracks closed up. Similarly, post-service (85 kN), top slab cracks were present in the tension region of the cantilever. However, unsurprisingly, more cracks were present, and the range of crack widths measured from 0.05 mm to 0.25 mm approximately. When the cantilever specimen was unloaded back to zero, i.e., at the end of the load cycle, the cracks closed up. The load-deflection curve and the steel tendon load-strain curve for the control specimen at the service load are portrayed in Figures 4-16 and 4-17 respectively.

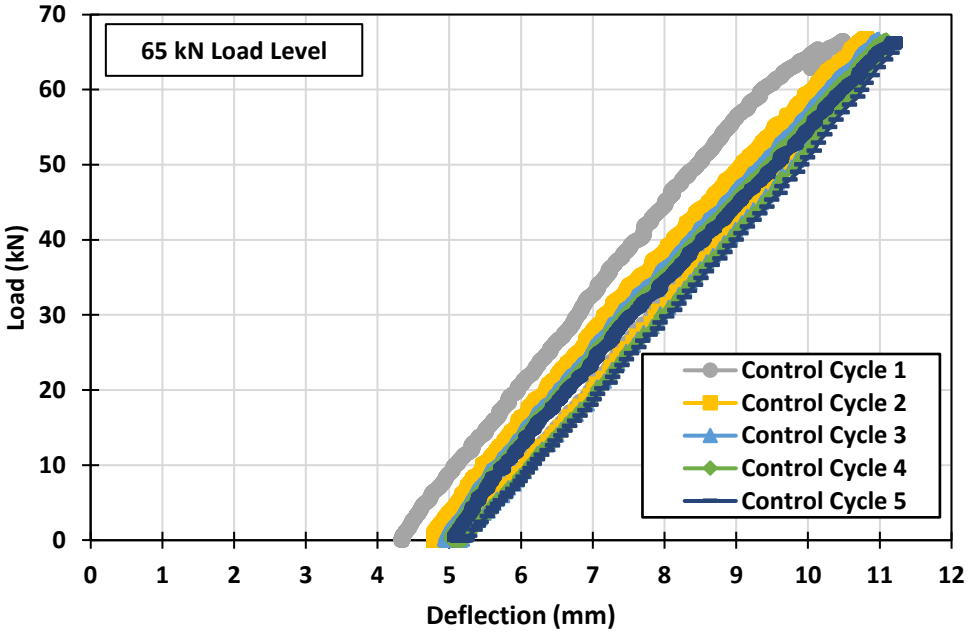

Figure 4-16. Control Specimen Service Load-Deflection Curve

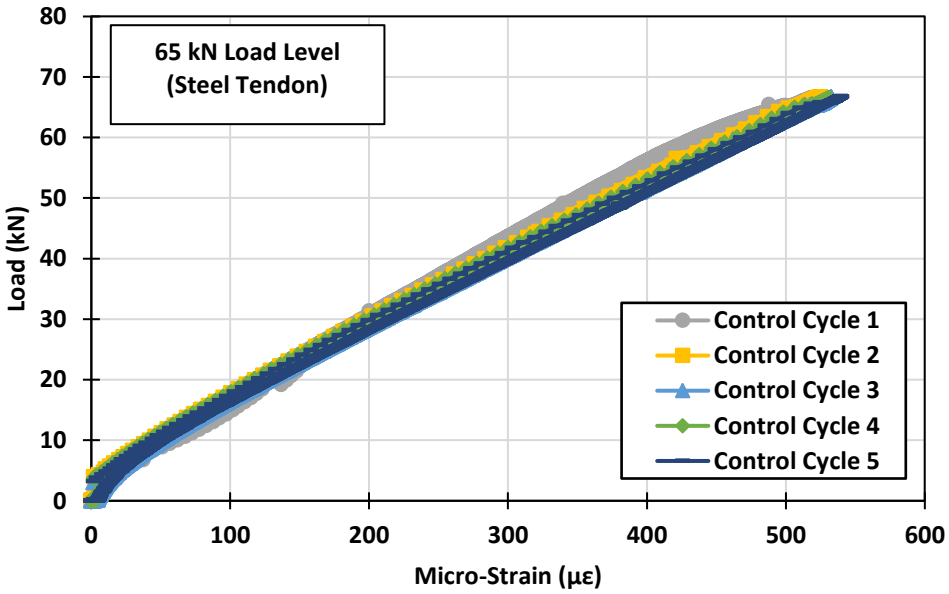

Figure 4-17. Control Specimen Service Steel Tendon Load-Strain Curve

Five static load cycles were selected as a reasonable and feasible number to observe the behaviour of the system at service and other load steps. The remainder of the load-deflection curves for each load step for the control specimen is presented in Appendix E for reference. The load-strain curve under service confirms the steel PT bars were not near the yielding point and were within service

limits. Important to note, the presented load-strain curve is purely the flexural strain during the test and does not include the applied prestressing strain. The ultimate failure of the control specimen was around a loading actuator point load magnitude of 150 kN. The primary mode of failure was a flexural bending moment failure, i.e., concrete crushing (compression region at the bottom) at the cantilever root. Tob slab cracks were measuring around 2.5-3.0 mm in width. The ultimate failure of the specimen was not too brittle or violent as near the ultimate load, there were signs of distress on the soffit side of the cantilever near the cantilever root indicating approaching failure. At 150 kN, the concrete in the compression region spalled and was considered crushed. Figure 4-18 presents the concrete crushing failure mode of the control specimen.

Figure 4-18. Control Specimen Ultimate Failure Concrete Crush

The primary mode of failure was a flexural failure; however, the loading actuator was kept on and running and continued to displace downward. As a result of the increased deformation, the specimen sheared which was expected. It is important to note that shear only occurred after a loss of system load-bearing capacity of the bridge cantilever specimen. Shear was considered a secondary mode of failure because of the increased deformation from the increased displacement of the actuator and not from any increased load-induced stress. The load-displacement curve of the control specimen at ultimate is portrayed in Figure 4-19.

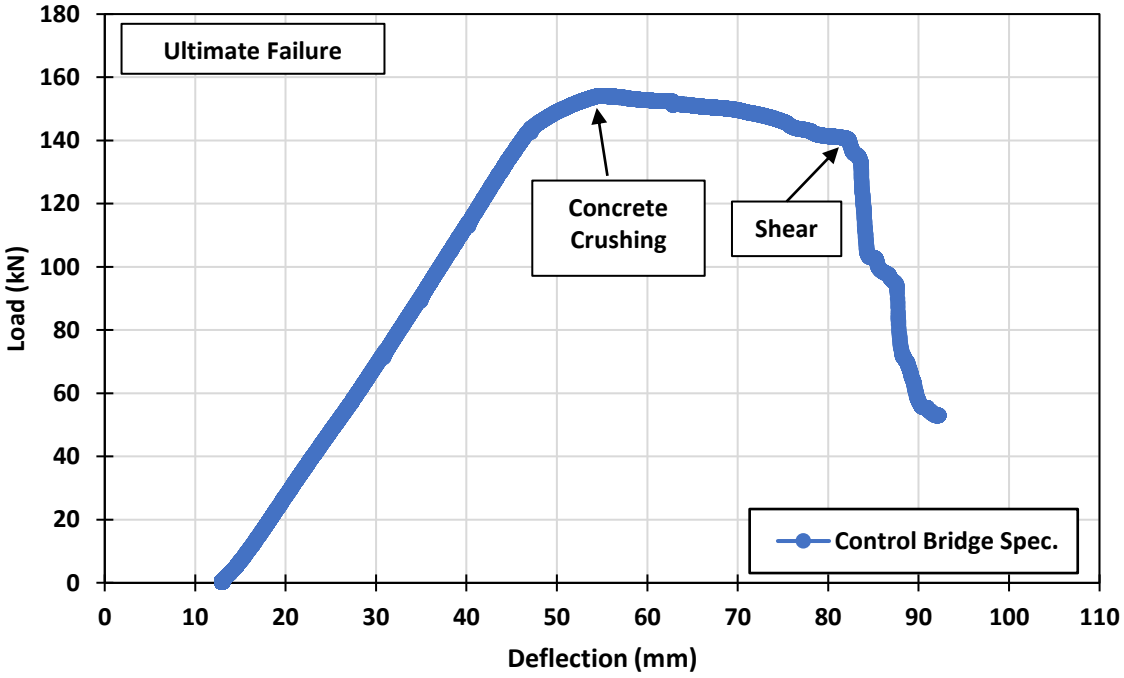

Figure 4-19. Control Specimen Ultimate Failure Load-Deflection Curve

4.7.2. CFRP Rehabilitation Specimen

The CFRP rehabilitation specimen was loaded as per the loading protocol prescribed in section 4.6 of this document. At service, equivalent to a loading actuator point load magnitude of 65 kN pushing on the system, the cantilever was deflecting approximately 4.99 mm underneath the load. At post-service, equivalent to a loading actuator point load magnitude of 85 kN pushing on the system, the cantilever was deflecting approximately 7.74 mm underneath the load. As mentioned earlier, the post-service load is presented to demonstrate the cantilever being loaded past service

limits, simulating a heavier truckload as is common for in-service bridges today. Figures 4-20 and 4-21 portray the deflected shape of the CFRP rehabilitation specimen under service (65 kN) and post-service (85 kN) loads respectively. As shown previously in Figure 4-11, the load was applied 1.25 m from the cantilever root.

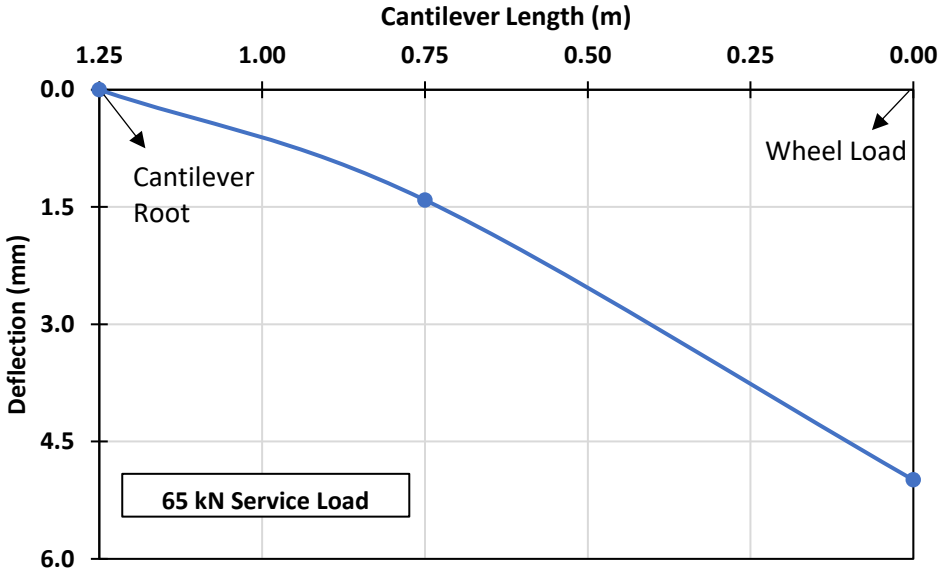

Figure 4-20. Rehabilitation Specimen Service Load Deflected Shape

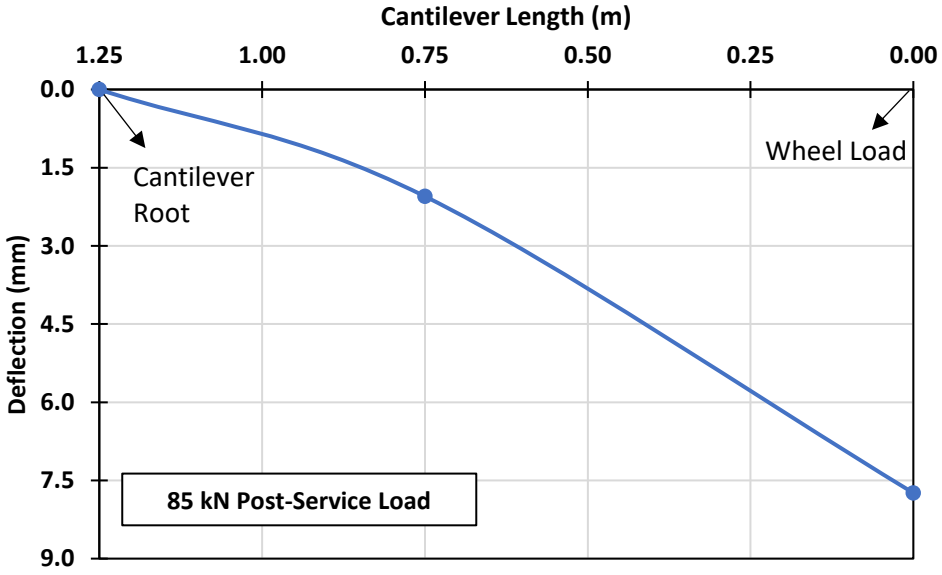

Figure 4-21. Rehabilitation Specimen Post-Service Load Deflected Shape

The CFRP rehabilitation specimen under service load and post-service load behaved as predicted. Under service (65 kN), top slab cracks were present in the tension region of the cantilever since the load was past the cracking stress limit of the concrete. By design, the PT bars were not stressed to the maximum limit for the reasons mentioned in previous sections. Cracks would run across the width of the top slabs. The cracks were visible and measurable when the service load was held constant but were smaller in size than the control. The range of crack widths measured from 0.05 mm to 0.10 mm approximately. The location of the cracks was identical to the control specimen; however, the cracking pattern was more pronounced. There was more map cracking and intertwining of cracks with the rehabilitation specimen. We describe the cracking pattern as a network of spider web cracks rather than just straight-defined cracks across the width of the specimen. Figure 4-22 presents the cracking pattern of the rehabilitation specimen on the top slab. It is important to note that the image presents cracks at the ultimate on the top slab, but the purpose of the figure is to exemplify the map cracking and intertwining crack pattern observed.

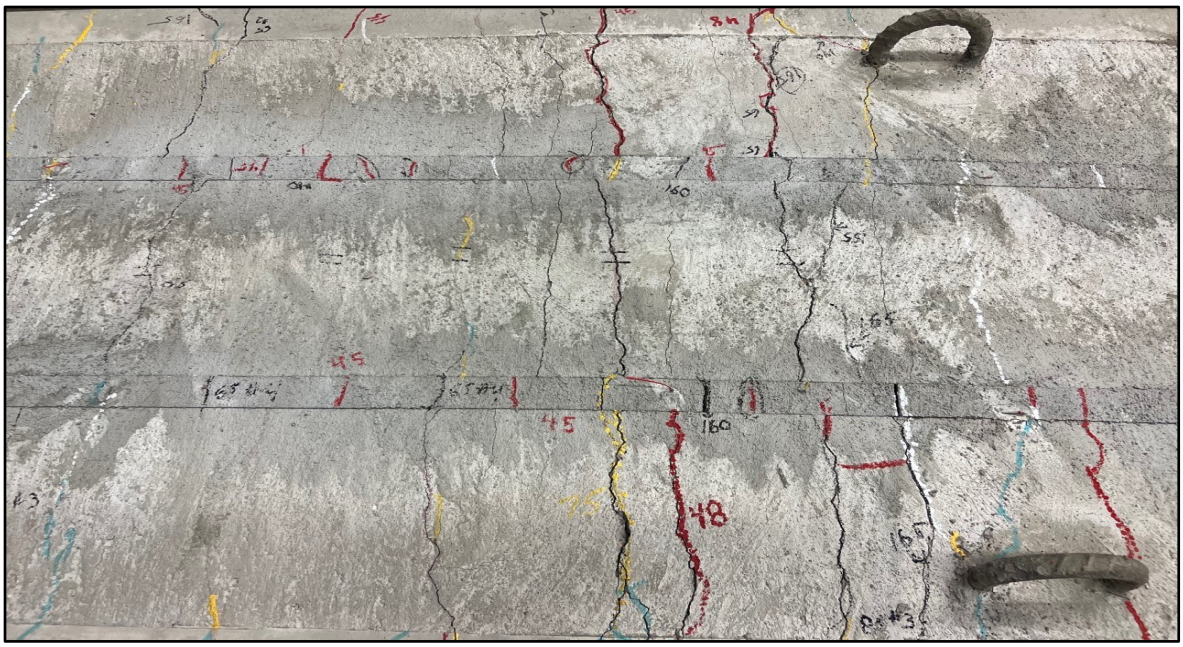

Figure 4-22. Rehabilitation Specimen Top Slab Cracking Pattern

The observed crack pattern can be owed to the bond transfer difference between CFRP and steel when the concrete cracks and the tensile stresses are transferred through bond to the bonded reinforcement. Major observations during service and post-service were that there was no indication of any splitting or major cracking of the cement grout in the NSM grooves. No bond

slip failure of the NSM CFRP was observed. The proposed NSM groove detailing proved successful. When the rehabilitation specimen was unloaded back to zero, i.e., at end of the load cycle, the cracks closed up. Similarly, at post-service (85 kN), top slab cracks were present in the tension region of the cantilever. However, unsurprisingly, more cracks were present, but the range of crack widths still measured from 0.05 mm to 0.10 mm. When the rehabilitation specimen was unloaded back to zero, i.e., at the end of the load cycle, the cracks closed up. The load-deflection curve for the rehabilitation specimen under service is portrayed in Figure 4-23. The load-strain curves for the steel tendon and the CFRP tendon in the rehabilitation specimen under service are portrayed in Figures 4-24 and 4-25 respectively.

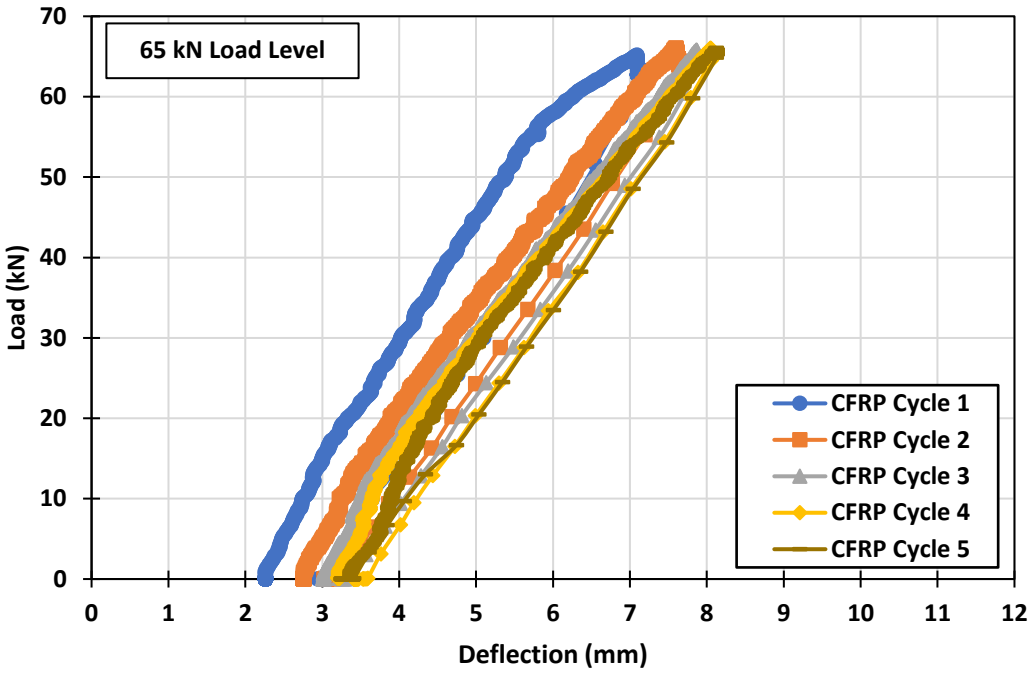

Figure 4-23. Rehabilitation Specimen Service Load-Deflection Curve

Five static load cycles were selected as a reasonable and feasible number to observe the behaviour of the system at service and other load steps. The remainder of the load-deflection curves for each load step for the rehabilitation specimen is presented in Appendix E for reference. In contrast with the control specimen, at service, the magnitude of deflection by the rehabilitation specimen is reduced at equivalent load levels.

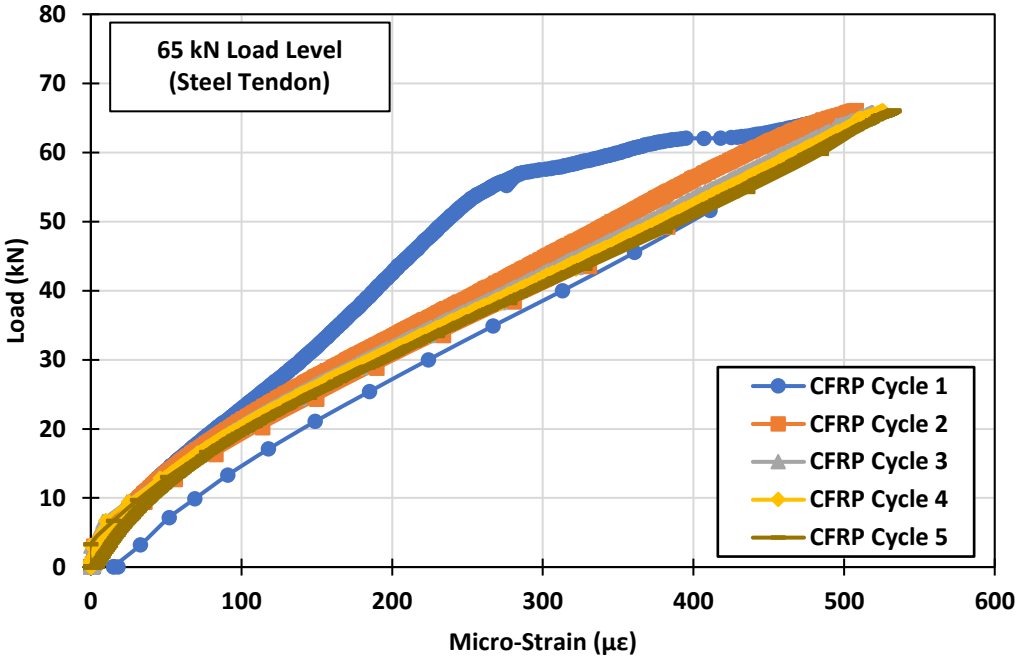

Figure 4-24. Rehabilitation Specimen Service Steel Tendon Load-Strain Curve

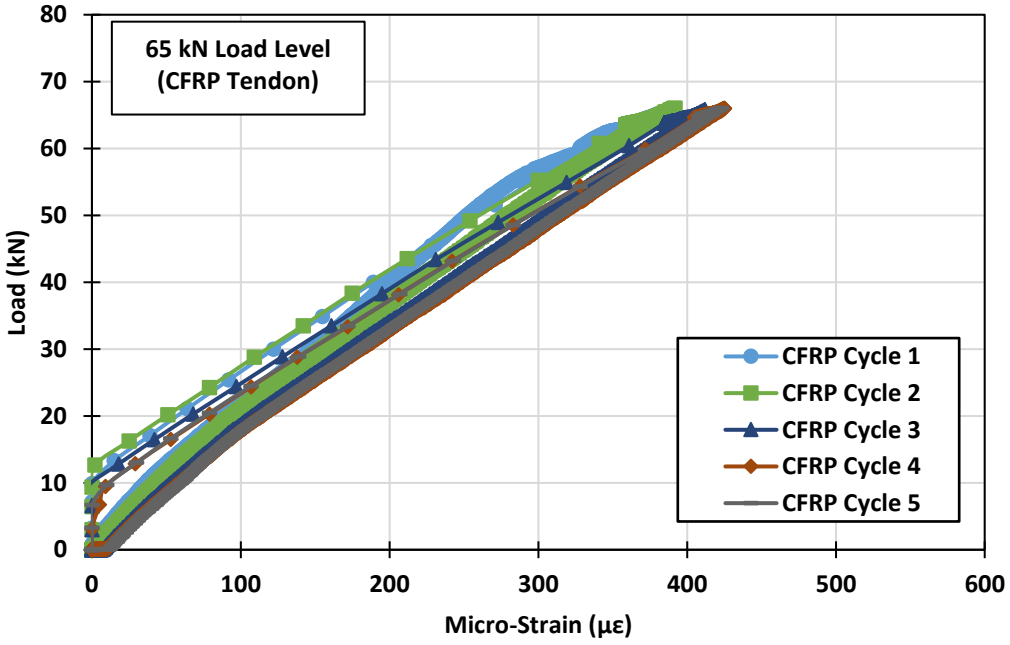

Figure 4-25. Rehabilitation Specimen Service CFRP Tendon Load-Strain Curve

The steel tendon load-strain curve under service conditions confirms the steel PT bars were not near the yielding point and were within serviceability limits. Similarly, the CFRP tendon load-strain curve under service conditions confirms the CFRP rods were not near the rupture point and were within serviceability limits. It is important to note that the presented load-strain curves are purely a representation of the flexural strain during the test and do not include the applied prestressing strain. The ultimate failure of the rehabilitation specimen was around a loading actuator point load magnitude of 160 kN. The primary mode of failure was a flexural bending moment failure, i.e., concrete crushing (compression region at the bottom) at the cantilever root. Tob slab cracks were measuring around 1.25-1.50 mm in width. The ultimate failure of the specimen was not too brittle or violent as near the ultimate load, there were signs of distress on the soffit side of the cantilever near the cantilever root indicating approaching failure. At 160 kN, the concrete in the compression region spalled and was considered crushed. As the load approached ultimate conditions, at about 155 kN, is when the onset of the cement grout splitting in the NSM grooves at the cantilever root was observed. There was minor uplift of the grout at the cantilever root at ultimate but overall, the grout was still intact within the groove and had no major debonding or slippage. As stated earlier, the proposed NSM detailing was a success. Figure 4-26 presents the concrete crushing failure mode of the control specimen.

Figure 4-26. Rehabilitation Specimen Ultimate Failure Concrete Crush

Even after the flexural failure, the loading actuator was kept on and running and continued to displace downward. Although concrete crushing occurred and the load was past the peak, the rehabilitation specimen was able to withstand sustained deflection post-ultimate without a significant drop in load. Figure 4-27 presents the load-deflection curve of the rehabilitation specimen at the ultimate.

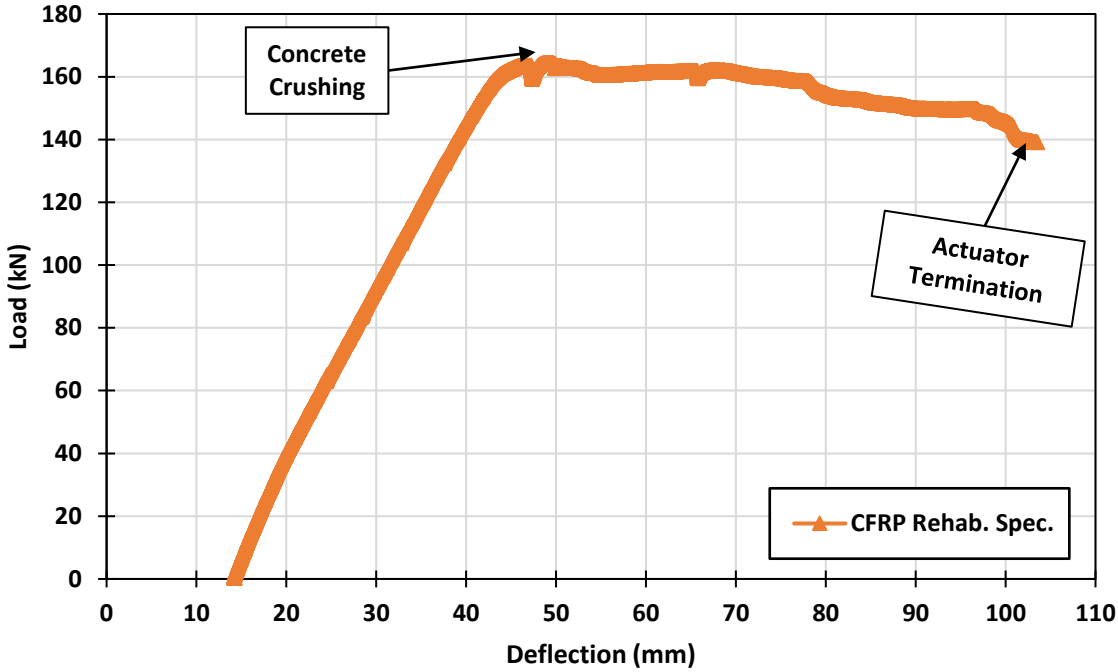

Figure 4-27. Rehabilitation Specimen Ultimate Failure Load-Deflection Curve

No shear was observed even after sustained deformation. The specimen would have ultimately sheared but the actuator was terminated after 100 mm of deflection as some test sensors' maximum stroke was 100 mm.

4.7.3. Bridge Cantilever System Test Result Summary

The control and rehabilitation bridge cantilever specimens both experienced flexural failure modes with concrete crushing occurring at the root of the cantilever. The control specimen cantilever had an ultimate moment capacity of 187.5 kN.m (P=150 kN). Whereas the CFRP rehabilitation specimen had an ultimate moment capacity of 200 kN.m (P=160 kN). The rehabilitation specimen restored/rehabilitated the load capacity of the lost 15 mm-100 kN PT steel tendon with the utilized

two 10 mm-100 kN total prestressed CFRP tendons. Although the modulus of the CFRP tendons at 124 GPa is less than the steel tendons at 200 GPa, the NSM placement of the CFRP tendons facilitated a slightly larger lever arm for moment resistance. The rehabilitation specimen at all load levels experienced less deflection than the control. Figures 4-28 and 4-29 portray the deflected shape of the control versus the rehabilitation specimen at service (65 kN) and post-service (85 kN).

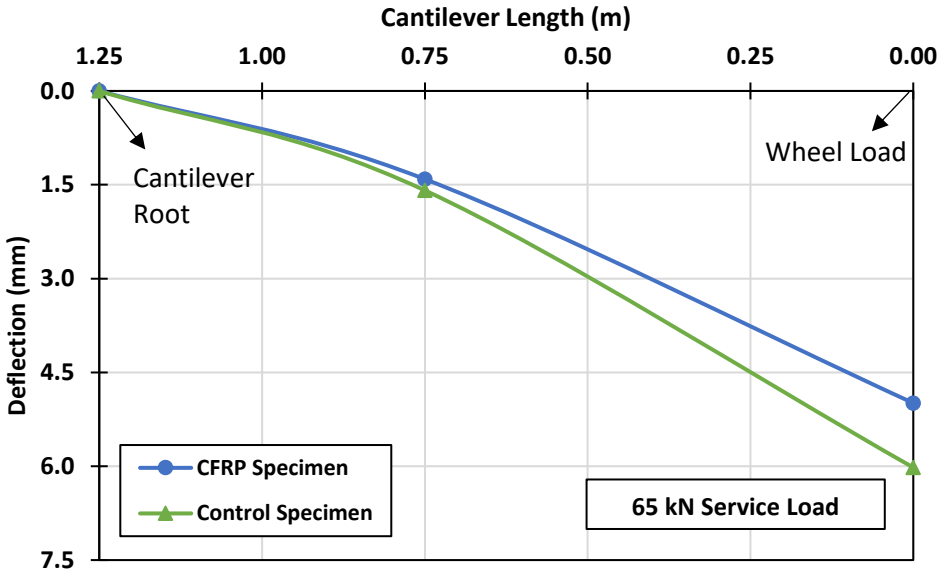

Figure 4-28. Experimental Specimen Service Load Deflected Shape

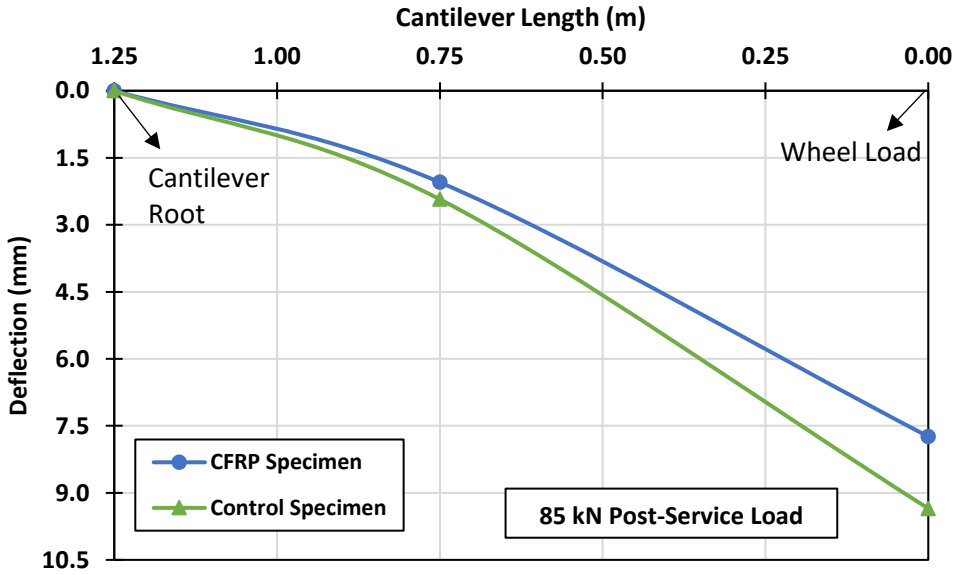

Figure 4-29. Experimental Specimen Post-Service Load Deflected Shape

The rehabilitation specimen served its purpose in rehabilitating structural deterioration within a bridge cantilever system. The rehabilitation specimen was able to achieve a slightly higher load and post-ultimate it sustained more deflection and did experience a significant drop in load. Figure 4-30 presents the contrast between the control and the rehabilitation specimens' load-deflection curves at the ultimate.

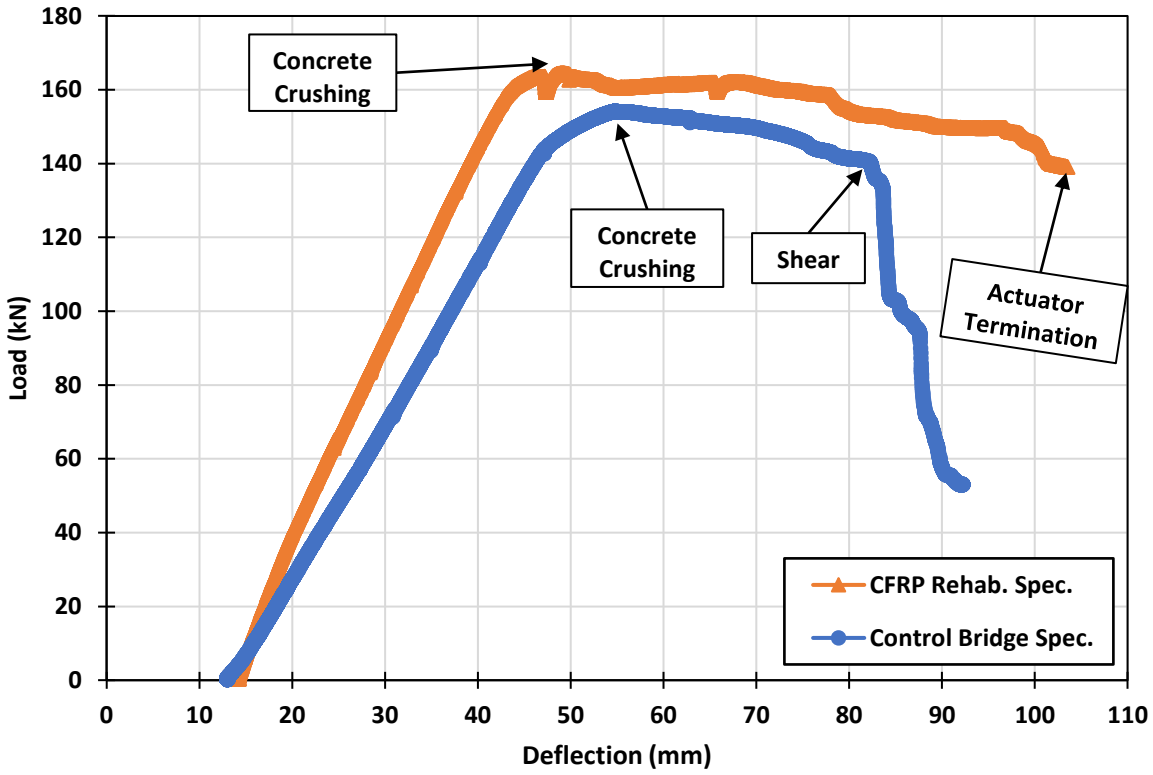

Figure 4-30. Experimental Specimen Ultimate Load-Deflection Curve

During the entirety of the loading process of the experimental rehabilitation specimen, there was no slippage or movement observed/measured on the PT CFRP permanent mechanical anchors. Furthermore, there was a good bond between the CFRP tendons and the concrete substrate when bonded in the NSM grooves. Figure 4-31 presents the control and rehabilitation specimen top slab side by side after test completion for reference.

Figure 4-31. Bridge Cantilever Specimens Top Slab Side by Side Photo

CHAPTER 5 ANALYTICAL STUDY

An analytical study was conducted to validate and substantiate the experimental results of the bridge cantilever experimental program. Additionally, the analytical study facilitated a parametric study to be performed to apply the proposed PT CFRP rehabilitation methodology to a real-life bridge that exhibits deteriorated transverse PT steel tendons within its cantilever wings. In the following sections, a numerical model is presented to predict the ultimate flexural capacity of the experimental bridge cantilever sections and predict the deflection of the bridge cantilever sections at simulated service conditions. The analytical model was verified against the experimental test data for ultimate flexural capacity and deflection at simulated service. Good predictability was observed between the theoretical analytical calculations and the observed experimental test data for the test/model ratio was near one. The number of tested bridge specimens was sufficient due to the sound predictability of the analytical model. After model verification, a parametric study was conducted applying the analytical model to a small representative section of the existing under consideration bridge structure that this research was based on. The total length of the existing bridge is 240 m; therefore a 3 m section of the existing in-situ bridge cantilever wing was utilized as a representative section for the parametric study. The selection of the representative 3.0 m strip was similar in essence to the selection of a unit strip of slab cut out in a one-way concrete slab for purposes of analysis and design. The verified model was used to estimate the flexural capacity of the parametric study section and the deflection at simulated service. The parametric study involved three stages. The first stage entailed the nominal exiting as the built capacity of the section that exhibits no damage. The second stage entailed the damage capacity of the section simulated by a deterioration of a transverse steel tendon in the system. The third stage entailed the capacity of the section after the proposed PT CFRP methodology was implemented to try and restore lost structural capacity. For all three stages, the associated deflection of the section at service was calculated as well.

5.1. Description of Model

The analytical model is divided into two main components. The first component deals with predicting the ultimate flexural capacity of the bridge cantilever sections. The second component deals with predicting the deflection of the cantilever sections under service. Mathematical equations were used to predict the ultimate flexural capacity and the deflection under service based

on meeting the conditions of equilibrium, compatibility of strains, and conducting a cross-sectional analysis. For calculating the ultimate flexural capacity (component one), in addition to the conditions of equilibrium and compatibility of strain, the following assumptions as adapted from the CSA S6-19 bridge code were applied:

- Strain in the concrete is assumed to vary linearly over the depth of the section.
- Strain changes in the bonded reinforcement are assumed to be equal to strain changes in the surrounding concrete.
- The maximum usable strain at the extreme concrete compression fibre is assumed to be 0.0035 unless a higher value of strain can be justified. In the latter case, a strain compatibility analysis shall be used.
- The tensile strength of the concrete shall be neglected in the calculation of the flexural resistance.
- An equivalent rectangular concrete stress distribution is used as the relationship between concrete strain and concrete compressive stress.

At ultimate, the compressive stress distribution of concrete is known to be non-linear in nature. However, the utilization of an equivalent rectangular stress distribution simplifies the analysis. The equivalent concrete stress block provides an approximated concrete stress distribution as a rectangle with applicable empirical factors, $\alpha 1$, and $\beta 1$. Consequently, a cross-sectional analysis can now be performed to predict the flexural capacity of the section. For calculating the deflection under service (component two), in addition to meeting the conditions of equilibrium and compatibility of strain, the following assumptions as adapted from the CSA S6-19 bridge code were applied:

- Linear triangular concrete stress distribution is used as the relationship between concrete strain and the concrete compressive stress up to the peak linear limit.
- Stress in the concrete is assumed to be directly proportional to strain.
- Strain in the concrete is assumed to vary linearly over the depth of the section.
- Strain changes in the bonded reinforcement are assumed to be equal to the strain changes in the surrounding concrete.
- The transformed area of bonded reinforcement is included in the calculation of section properties.

Concrete is not linear-elastic in nature but looking at the stress-strain curve for concrete, some assumptions can be made to simplify the analysis to predict the service deflection. Under service, the concrete has not reached the max peak stress. Hence, during service, the concrete can be assumed as linear until that point. Therefore, a linear triangular distribution can be assumed and used as the relationship between concrete strain and concrete compressive stress. For concrete that is past the max peak stress a non-linear distribution for the compressive concrete stress would be required which is outside the scope of this project. Based on uniaxial compression tests conducted on concrete cylinders presented earlier in Table 4-7, the concrete compressive strengths were 39.8 MPa and 41.9 MPa for the control and rehabilitation specimens respectively. Therefore, the concrete compressive strength hovered around 40 MPa. Figure 5-1 presents the stress-strain relationship for different grades of concrete.

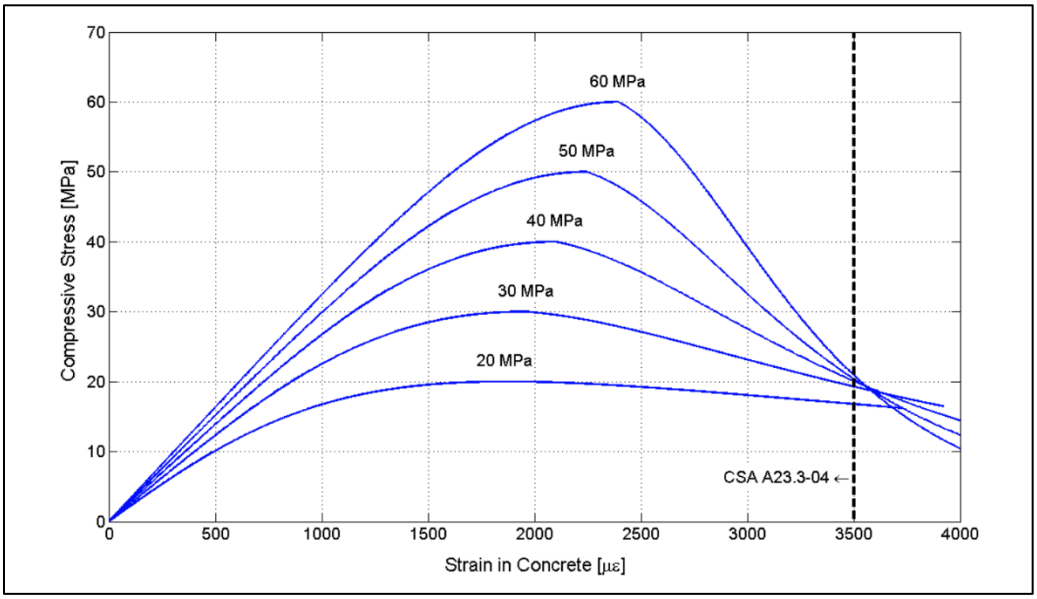

Figure 5-1. Stress-Strain Relationships for Concrete (Obtained from ISIS Design Manual 3)

The max peak stress for 40 MPa grade concrete is around a strain level of 2000 micro-strain and the stress distribution of concrete is linear up to approximately 1000 micro-strain (0.001). Under service, the concrete strain level is within this range and the utilization of a linear triangular distribution for the concrete compressive stress to predict deflection is permissible. The deflection of the bridge cantilever sections under service is determined by using the moment-area method. The moment area method uses the area of moment divided by the flexural rigidity (M/EI) diagram

of the cantilever section to determine the deflection along the cantilever. The flexural rigidity diagram also known as the curvature diagram is developed for the service load case through means of strain compatibility and conditions of equilibrium. The curvature diagram (M/EI) is obtained and then divided into simple geometric shapes. The deflection under the load is then obtained by applying the second moment-area theorem to the curvature diagram for the service load case.

5.1.1. Bridge Cantilever Specimen Flexural Capacity

A cross-sectional analysis based on the assumptions previously stated was conducted to determine the flexural capacity of each section. To meet the conditions of static equilibrium, the sum of the axial forces in the system is zero and the moment capacity of the section is the sum of the force moments about any reference point. Each bridge cantilever section had two static equations of equilibrium that had to be satisfied. Presented below are Equations 5-1, 5-2, 5-3, and 5-4, the equations of equilibrium for the control specimen and rehabilitation specimen respectively.

$$\Sigma Fx = 0: F_c + F_{s1} - F_{ps} - F_{s2} - F_{s3} = 0 \tag{5-1}$$

$$M_r = F_c \left[d_{s1} - \frac{a}{2}\right] + F_{s2}\, x\, [d_{s2} - d_{s1}] + F_{ps}\, x\, \left[d_{ps} - d_{s1}\right] + F_{s3}\, x\, [d_{s3} - d_{s1}] \tag{5-2}$$

$$\Sigma Fx = 0: F_c + F_{s1} - F_{ps} - F_{s2} - F_{s3} - F_{frp} = 0 \tag{5-3}$$

$$M_r = F_c \left[d_{s1} - \frac{a}{2}\right] + F_{s2}\, x\, [d_{s2} - d_{s1}] + F_{ps}\, x\, \left[d_{ps} - d_{s1}\right] + F_{s3}\, x\, [d_{s3} - d_{s1}] + F_{frp}\, x\, \left[d_{frp} - d_1\right] \tag{5-4}$$

Where: Fx is the axial force in the system (kN)

Fc is the compressive concrete force applied through its centroid (kN)

Fs1 is the steel reinforcing bar in compression force (kN)

Fps is the prestressing steel tendon force (kN)

Fs2 is the steel reinforcing bar layer #1 in tension force (kN)

Fs3 is the steel reinforcing bar layer #2 in tension force (kN)

Ffrp is the CFRP tendon force (kN)

Mr is the moment resistance of the section (kN.m)

ds1 is the distance from the compression fibre to the compression steel (mm)

ds2 is the distance from the compression fibre to the first tension steel (mm)

ds3 is the distance from the compression fibre to the second tension steel (mm)

dps is the distance from the compression fibre to the steel tendons (mm)

dfrp is the distance from the compression fibre to the CFRP tendons (mm)

Figures 5-2 and 5-3 portray the cross-sectional analysis for each concrete cantilever section pertaining to how the strain compatibility and conditions of equilibrium are met. The forces and location of the forces in each system are present in the visual figures.

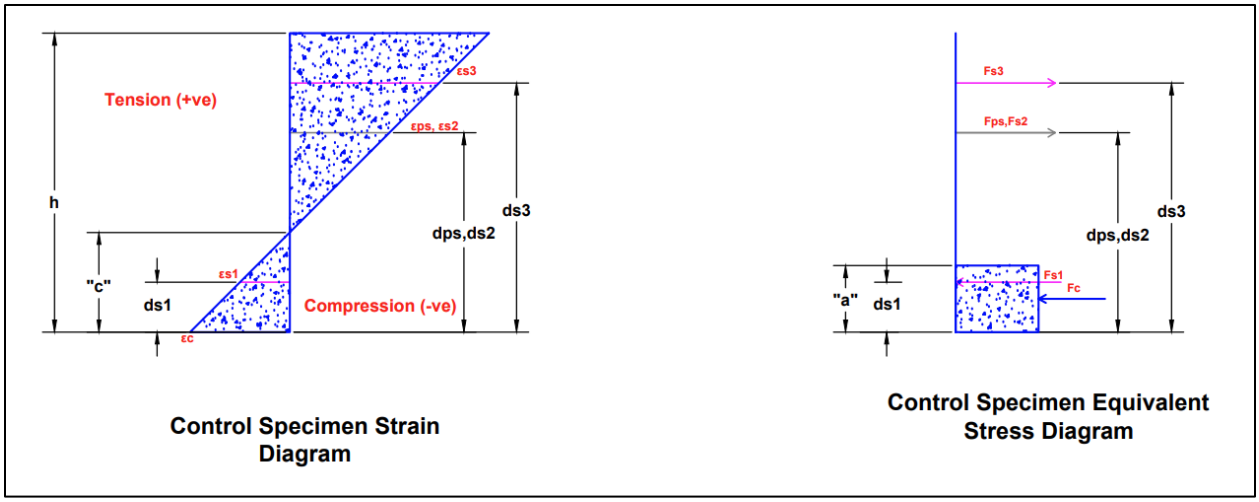

Figure 5-2. Control Specimen Cross-Sectional Analysis

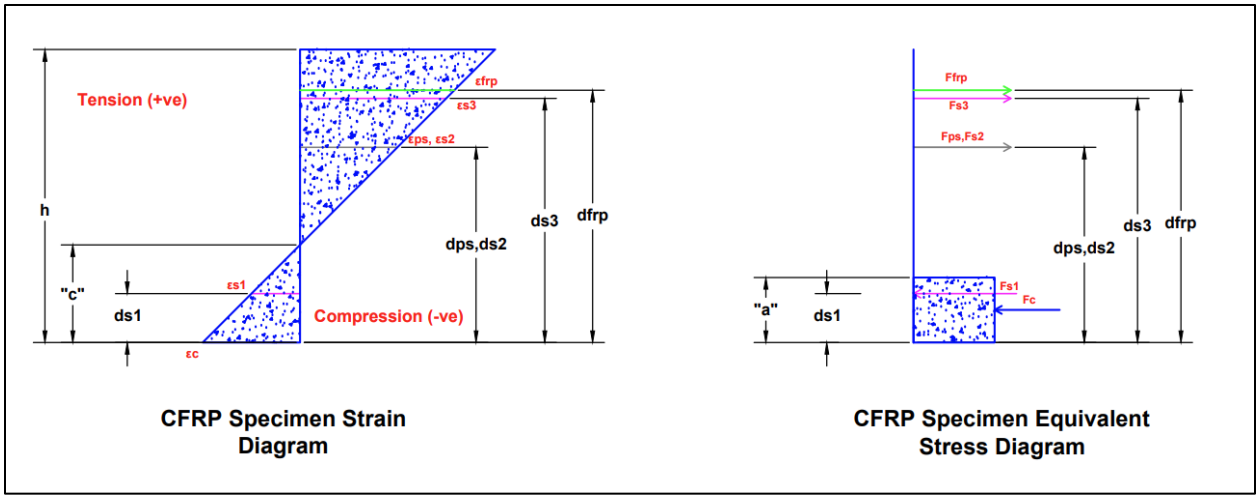

Figure 5-3. Rehabilitation Specimen Cross-Sectional Analysis

The material properties presented earlier in Chapters 3 and 4 of this document were used for the analysis in Equations 5-1 to 5-4 to determine the ultimate flexural capacity of the concrete cantilever sections. Initially for the analysis, the maximum usable strain at the extreme concrete compression fibre was assumed to be 0.0035 nominally as set by the code. The empirical factors of $\alpha 1$ and $\beta 1$ used in the equivalent concrete stress distribution have been calibrated per the CSA code for a maximum concrete stain of 0.0035. Satisfying equilibrium and conditions of strain compatibility, the model predicted a moment capacity of 173 kN.m for the control specimen and 179 kN.m for the rehabilitation specimen respectively. Based on where the load was being applied, the moment capacities correspond to a theoretical loading actuator magnitude of 138 kN and 143 kN respectively. The model flexural capacity prediction is compared with the experimental data for verification. Table 5-1 presents the comparison of the nominal ultimate flexural capacity of the bridge cantilever specimens between the model and the experimental data.

Table 5-1. Nominal Ultimate Flexural Capacity

Specimen ID	M_Exp (kN.m)	M_Model (kN.m)	P_Exp (kN)	P_Model (kN)	Test / Model	εcu
S1-Control	188	173	150	138	1.09	0.0035
S2-Rehabilitation	200	179	160	143	1.12	0.0035

The comparison with the experimental data yields that the model underpredicts the ultimate flexural capacity of each of the specimens, i.e., conservative. From a nominal design perspective, the model has a safety margin built in when the ultimate strain is capped. A test/model number over one is ideal. The specimens were a bit stronger than predicted. However, to make sense of the source of this difference, the assumptions made were reviewed. One main design assumption was limiting the maximum usable strain at the extreme concrete compression fibre to 0.0035. This value is a requirement for design but for our scenario we could find the true extreme concrete compression fibre strain as strain gauges were placed on two different reinforcement levels. We had strain values at the CFRP tendon level and the steel tendon level and through similar triangles, we could obtain the strain magnitude at the extreme concrete compression fibre. From strain compatibility, Equations 5-5 and 5-6 were formed as shown below.

$$c = \frac{(\varepsilon_{frp}\ x\ d_{ps}) - (\varepsilon_{ps}\ x\ d_{frp})}{(\varepsilon_{frp} - \varepsilon_{ps})} \tag{5-5}$$

$$\varepsilon_c = \varepsilon_{frp}\ x\ \left(\frac{c}{d_{frp} - c}\right) \tag{5-6}$$

Where: c is the concrete section neutral axis (mm)

dps is the distance from the compression fibre to the steel tendons (mm)

dfrp is the distance from the compression fibre to the CFRP tendons (mm)

εc is the compressive concrete strain

εps is the steel tendon strain

εc is the CFRP tendon strain

From the experimental strain values inputted into Equations 5-5 and 5-6, strain compatibility yielded an extreme concrete compression fibre of 0.005. Obtaining a slightly higher test value is

reasonable compared to the design code limitation requirement. As the extreme compression concrete strain was no longer 0.0035, the equivalent stress block empirical factors of α1 and β1 had to be calibrated to the new strain of 0.005. For reference, at a limiting extreme concrete strain of 0.0035, the α1 factor would be 0.79 and the β1 factor would be 0.87. The empirical factors are directly a function of the compressive strength of the utilized concrete. However, for a strain of 0.005, the newly calibrated empirical factors of α and β would be 0.66 0.98 for our analysis respectively. the equivalent stress block parameters α and β were obtained from tables within the ISIS Canada Design Manual #3. The updated stress block factors are based on different ratios of strain concrete over the strain in concrete at peak stress and the compressive strength of the concrete. Table 5-2 presents an updated comparison table.

Table 5-2. Ultimate Flexural Capacity Strain Calibrated

Specimen ID	M_Exp (kN.m)	M_Model (kN.m)	P_Exp (kN)	P_Model (kN)	Test / Model	εcu
S1-Control	188	188	150	150	1.00	0.005
S2-Rehabilitation	200	197	160	158	1.02	0.005

A comparison of the model and experimental data values presents a near-perfect match between the test and the model. The results validate the sound predictability of the model thus it can be utilized for a parametric study. As required by design code requirements, the extreme compression concrete strain will be limited to 00035 which is conservative in nature and therefore safe.

5.1.2. Control Specimen Service Deflection

Deflection at the serviceability limit state was modeled by satisfying the conditions of equilibrium, and the conditions of strain compatibility and by applying the assumptions stated earlier. Two equations of equilibrium had to be satisfied to proceed with predicting the deflection of the specimen at service. The first equation is the summation of the axial forces in the system that had to equal zero to satisfy static equilibrium. The second equation was that the sum of all the force moments had to equate to the service moment, i.e., the moment applied by the imparted live load

(wheel load) on the system. Equations 5-7 and 5-8 portray the conditions for equilibrium that had to be satisfied to proceed with numerical modeling of the service deflection.

$$\Sigma Fx = 0: F_c + F_{s1} - F_{ps} - F_{s2} - F_{s3} = 0 \tag{5-7}$$

$$\Sigma M = M_s = P_s \, x \, L \tag{5-8}$$

Where: Fx is the axial force in the system (kN)

Fc is the compressive concrete force applied through its centroid (kN)

Fs1 is the steel reinforcing bar in compression force (kN)

Fps is the prestressing steel tendon force (kN)

Fs2 is the steel reinforcing bar layer #1 in tension force (kN)

Fs3 is the steel reinforcing bar layer #2 in tension force (kN)

Ms is the imparted service moment (kN.m)

Ps is the loading actuator live load (kN)

L is the load lever arm (m)

The forces in the above equations of equilibrium were broken down into stresses multiplied by their respective areas. The stress for each reinforcing material based on Hooke's law is equal to the modulus of elasticity of the material multiplied by the associated material strain. Based on the conditions of strain compatibility, curvature (ψ) is the slope of the strain diagram. Therefore, the strain could be rewritten as a function of curvature. Equations 5-9, 5-10, 5-11, 5-12, and 5-13 were substituted in for each respective material strain in the above force components.

$$\psi = \varepsilon_c \, x \, c \tag{5-9}$$

$$\psi = \varepsilon_{s1}\, x\, (c - d_{s1})$$

(5-10)

$$\psi = \varepsilon_{ps}\, x\, (d_{ps} - c)$$

(5-11)

$$\psi = \varepsilon_{s2}\, x\, (d_{s2} - c)$$

(5-12)

$$\psi = \varepsilon_{s3}\, x\, (d_{s3} - c)$$

(5-13)

Where: ψ is the curvature (1/mm)

εc is the concrete strain

εs1 is the compression steel strain

εps is the steel tendon strain

εs2 is the tension steel layer 1 strain

εs3 is the tension steel layer 2 strain

Fs3 is the steel reinforcing bar layer #2 in tension force (kN)

Ms is the imparted service moment (kN.m)

Curvature was isolated in both equations as a function of the remaining components of the forces. Thus, there were two equations of equilibrium and two unknowns. The first unknown was curvature (ψ) that was isolated alone and the cantilever concrete neutral axis (c). To establish a curvature diagram to proceed with the moment area method to calculate deflection numerically, iteration was used to solve for the curvature at five locations of the cantilever for each load case. As the cantilever was non-prismatic, both the moment along the cantilever was changing with the

change in lever arm and the change of stiffness/rigidity (EI) for the same load case. Iteration would begin with choosing a neutral axis depth for one location and then inputting this value into both equations of equilibrium. Iteration would keep changing the value until both curvatures from both equations matched and this was the curvature for this location for this load case. As the cantilever is non-prismatic this iterative procedure was conducted for five locations for each load case establishing a curvature diagram (M/EI) diagram for the respective load case. Figure 5-4 presents a flowchart illustrating the process of numerically modeling the deflection from establishing a curvature diagram for each load case.

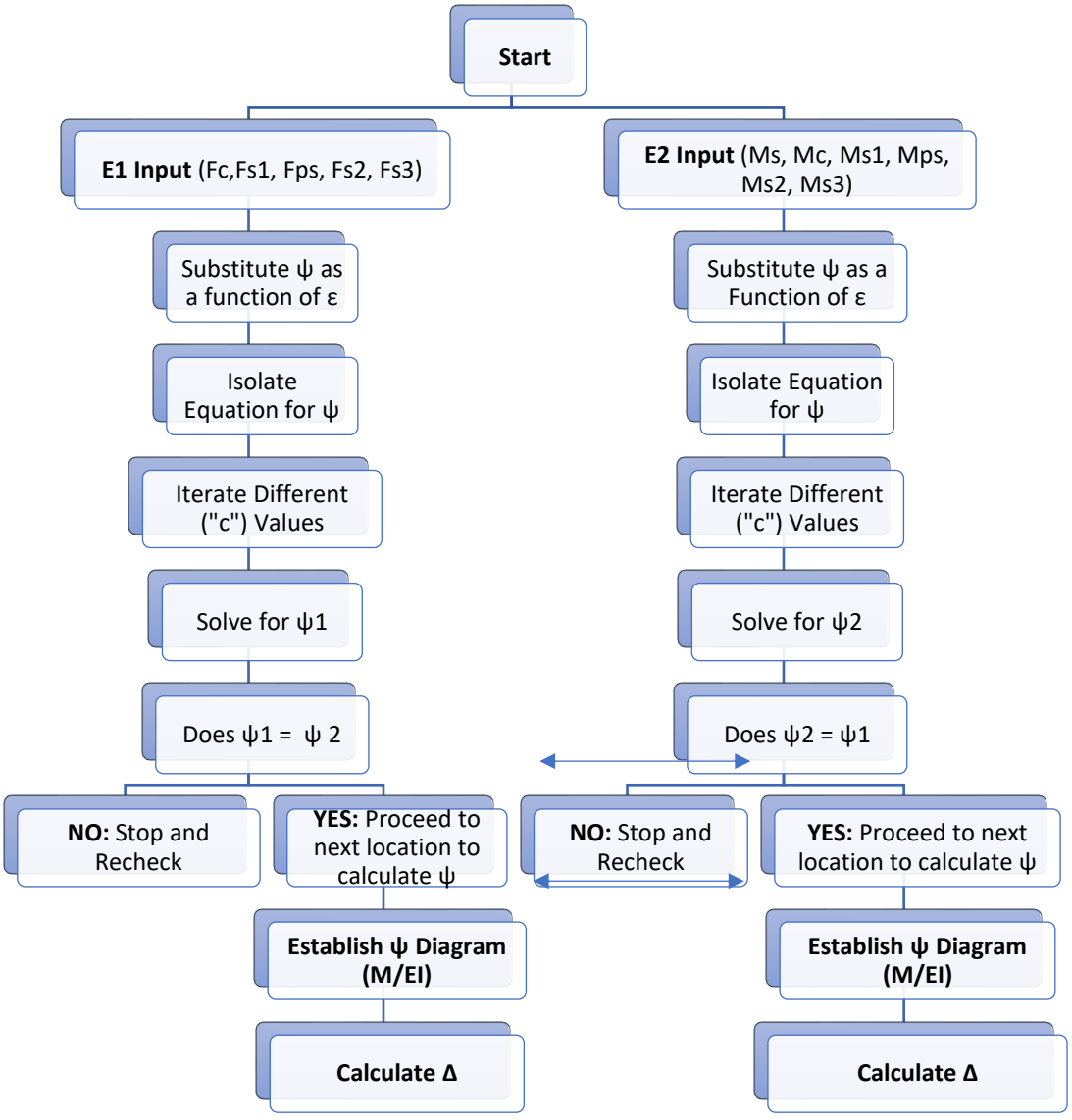

Figure 5-4. Concrete Cantilever Service Deflection Modeling Process

The deflection of the control specimen was modeled numerically for three distinct load cases. The first load case was the control specimen under service, i.e., a loading actuator magnitude of 65 kN. The second load case was the specimen post-service, i.e., a loading actuator magnitude of 85 kN. The third load case was the specimen pre-service, i.e., a loading actuator magnitude of 55 kN. For all three load cases, the compressive stress of the concrete was within the linear region and below the max peak stress of the stress-strain relationship sustaining the validity of the assumed linear triangular distribution for stress. All strain values were below 1000 micro-strain (0.001) for all three load cases. Figure 5-5 presents the curvature diagram for the 65 kN load case.

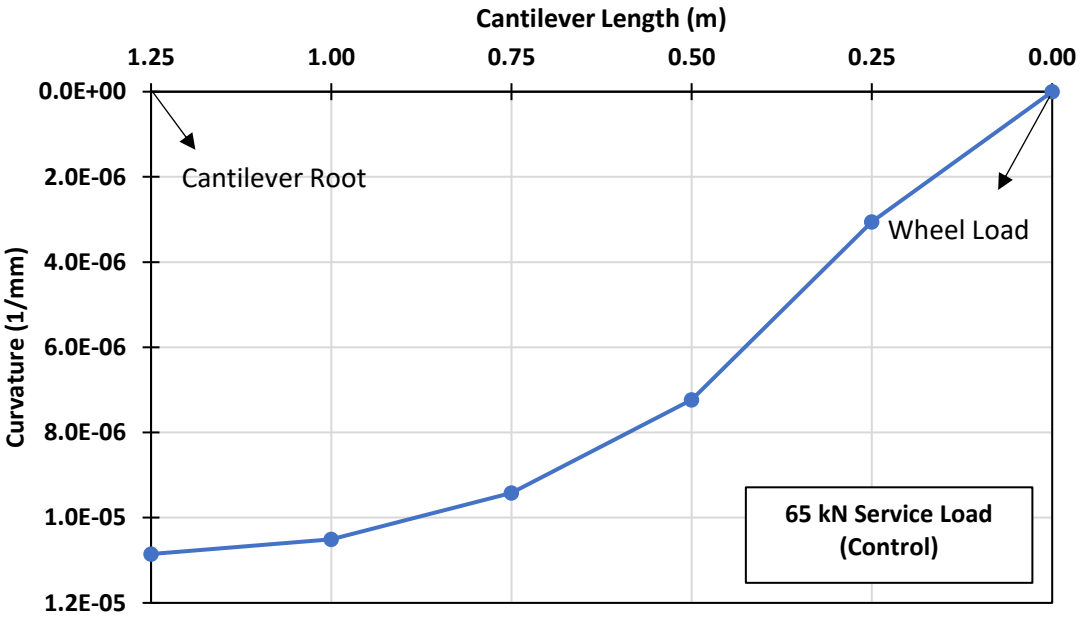

Figure 5-5. Control Specimen 65 kN Load Case Curvature Diagram

The curvature diagram was divided into five simple geometric shapes applying the second moment-area theorem. The model was used to predict the deflection underneath the wheel load and at 0.75 m from the wheel load for each load case. Thus, there were two points to create the model deflected shape curve per load case. The model-deflected shape was created and verified with the experimental data. The experimental data for verification was based on data from a sensor underneath the experimental load and a sensor at 0.75 m from the load. Table 5-3 presents a

comparison of the deflection magnitudes at the 65 kN load case between the experimental value and the numerical model prediction. The concrete strain level for this load case was 0.0007 <0.001.

Table 5-3. Control Specimen 65 kN Load Case Deflection Magnitudes

Deflection Location	Experimental Test (mm)	Analytical Model (mm)	Test/Model
At Wheel Load	6.02	7.03	0.86
At 0.75 m	1.59	1.31	1.21
At Cantilever Root	0	0	1

Figure 5-6 presents the deflected shape curves for the 65 kN load case based on the analytical model prediction and from the experimental test data.

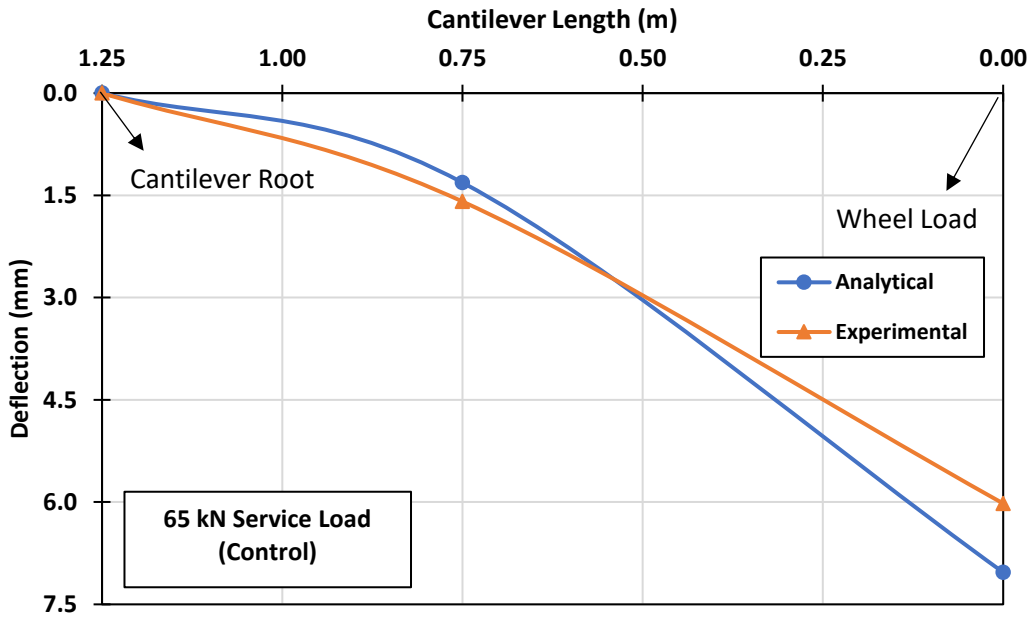

Figure 5-6. Control Specimen 65 kN Load Case Deflection Curves

Figure 5-7 presents the curvature diagram for the 85 kN (post-service) load case.

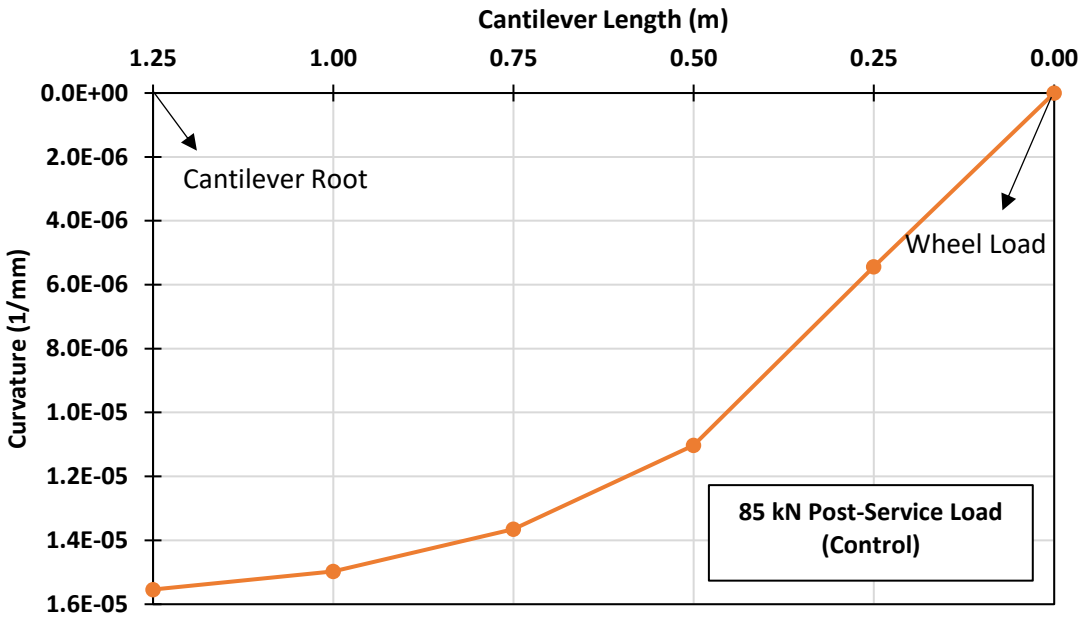

Figure 5-7. Control Specimen 85 kN Load Case Curvature Diagram

Table 5-4 presents a comparison of the deflection magnitudes at the 85 kN load case between the experimental value and the numerical model prediction. The concrete strain level for this load case was 0.0009 <0.001.

Table 5-4. Control Specimen 85 kN Load Case Deflection Magnitudes

Deflection Location	Experimental Test (mm)	Analytical Model (mm)	Test/Model
At Wheel Load	9.35	10.24	0.91
At 0.75 m	2.43	1.88	1.29
At Cantilever Root	0	0	1

Figure 5-8 presents the deflected shape curves for the 85 kN load case based on the analytical model prediction and from the experimental test data.

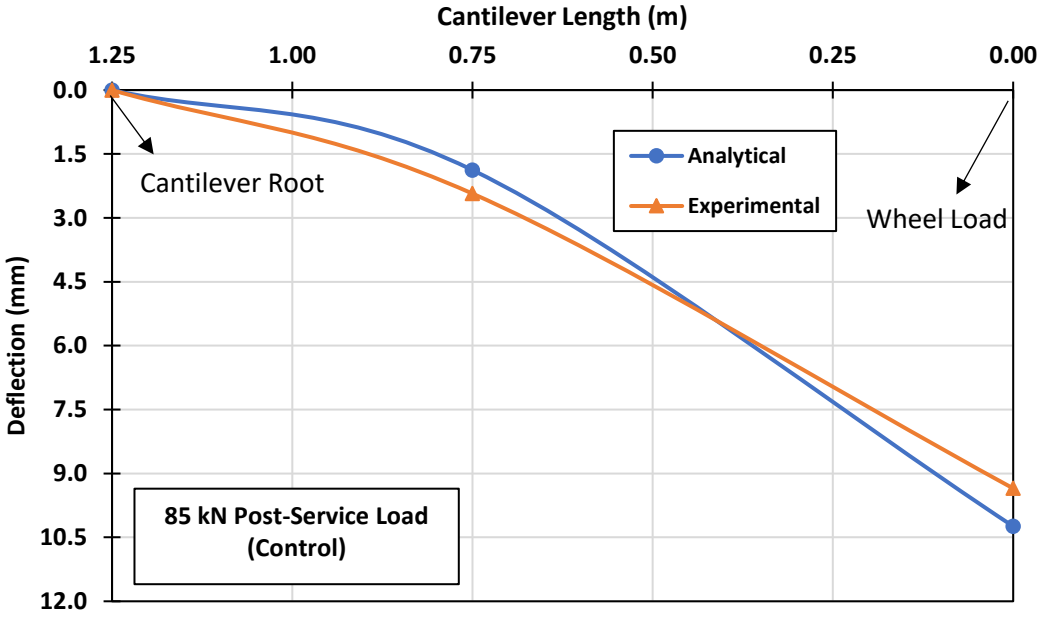

Figure 5-8. Control Specimen 85 kN Load Case Deflection Curves

Figure 5-9 presents the curvature diagram for the 55 kN (pre-service) load case.

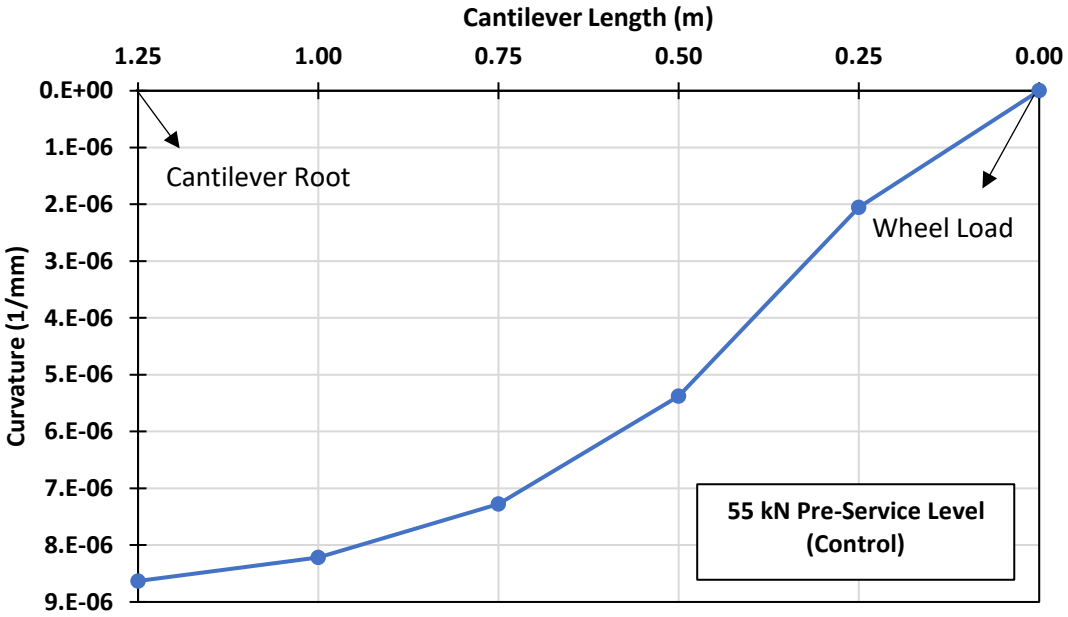

Figure 5-9. Control Specimen 55 kN Load Case Curvature Diagram

Table 5-5 presents a comparison of the deflection magnitudes at the 55 kN load case between the experimental value and the numerical model prediction. The concrete strain level for this load case was 0.0006 <0.001.

Table 5-5. Control Specimen 55 kN Load Case Deflection Magnitudes

Deflection Location	Experimental Test (mm)	Analytical Model (mm)	Test/Model
At Wheel Load	4.79	5.44	0.88
At 0.75 m	1.31	1.03	1.27
At Cantilever Root	0	0	1

Figure 5-10 presents the deflected shape curves for the 55 kN load case based on the analytical model prediction and from the experimental test data.

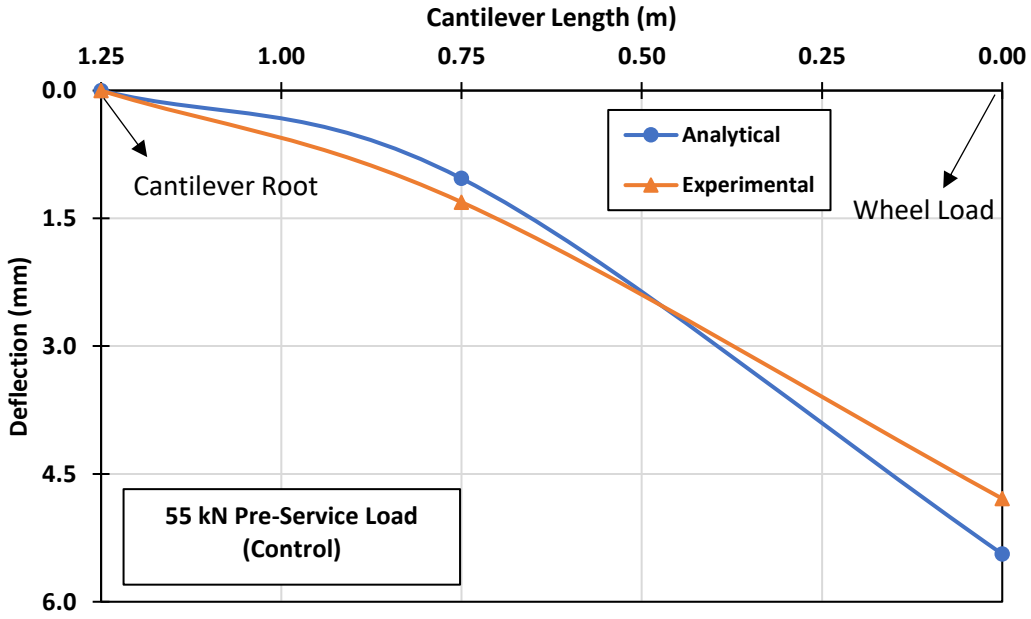

Figure 5-10. Control Specimen 55 kN Load Case Deflection Curves

The comparison of the model service deflection at three different load cases within the concrete linear stress region against the experimental data yielded a few important findings. The model overpredicts the deflection of the concrete cantilever for all three load cases underneath the load, i.e., the test/model ratio is less than one. A test/model ratio of less than one indicates that the concrete cantilever is deflecting less than predicted in reality and thus is safer for design purposes. However, at 0.75 m from the wheel load location, which is closer to the cantilever load, the model underpredicts the deflection. This is not ideal but reasonable given the assumptions made for the model. The model does not see the imperfections in the lab as there are tolerances to the sensors. Additionally, the model assumes a perfect cantilever where the cantilever root does not move, and the base of the cantilever is fully supported. However, in the lab, there was movement observed. The results are very reasonable and the experimental test results validate the predictability of the model. The most important deflection magnitude for a cantilever is the magnitude at the free end where max deflection is observed. Thus, the model has been validated and is sound for predicting the deflection at simulated service for the concrete cantilever. Figure 5-11 presents a summary of the analytical model versus experimental test data deflection curves for all three load cases for the control specimen.

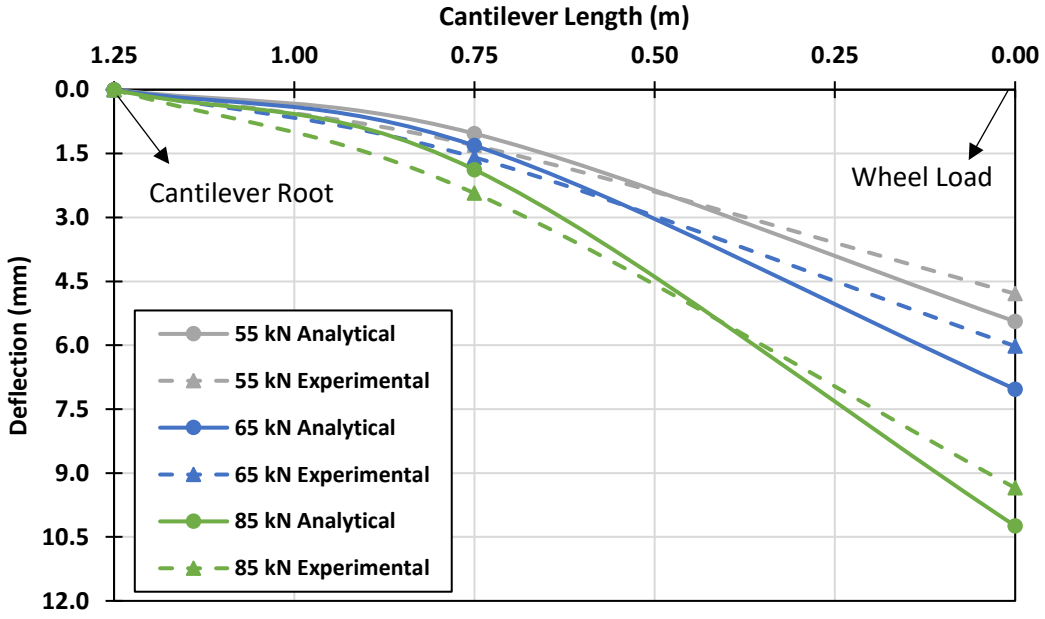

Figure 5-11. Control Specimen Model Deflection Curves Summary

5.1.3. CFRP Rehabilitation Specimen Service Deflection

Modeling the deflection at simulated service conditions for the CFRP rehabilitation specimen underwent the same procedure that was outlined for the control specimen. The conditions of equilibrium and the conditions of strain compatibility had to be met with the addition of the force contribution from the CFRP tendons. Therefore, the flowchart in Figure 5-4 was also followed. Similarly, the deflection of the rehabilitation specimen was modeled numerically for the same three load cases. The first load case was the specimen under service, i.e., a loading actuator magnitude of 65 kN. The second load case was the specimen post-service, i.e., a loading actuator magnitude of 85 kN. The third load case was the specimen pre-service, i.e., a loading actuator magnitude of 55 kN. For all three load cases, the compressive stress of the concrete was within the linear region and below the max peak stress of the stress-strain relationship sustaining the validity of the assumed linear triangular distribution for stress. All strain values were below 1000 micro-strain (0.0010) for all three load cases. Figure 5-12 presents the curvature diagram for the 65 kN load case.

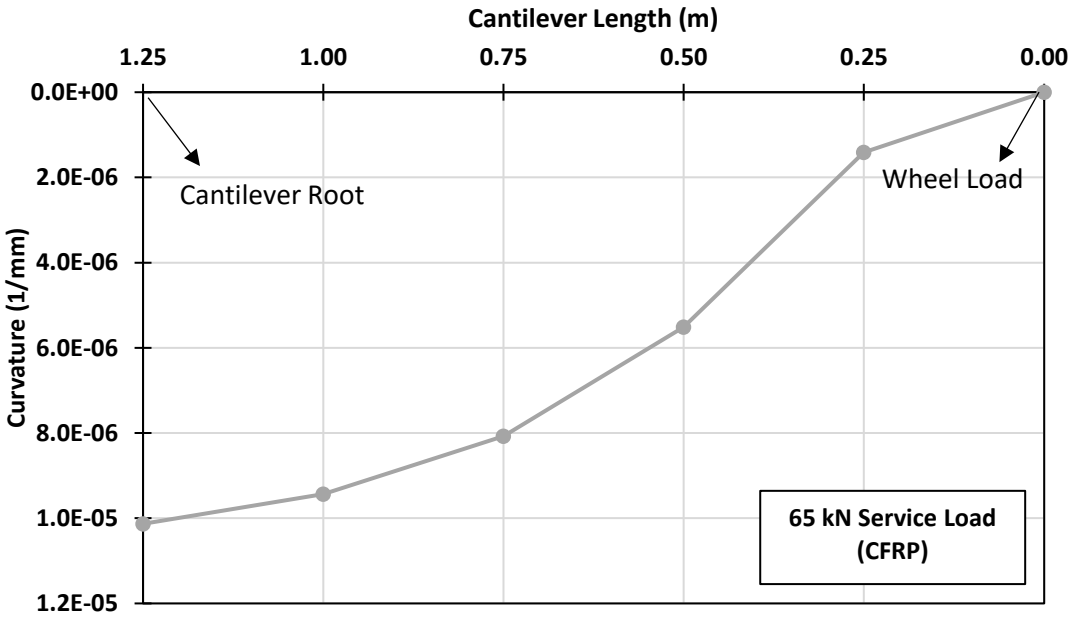

Figure 5-12. Rehabilitation Specimen 65 kN Load Case Curvature Diagram

Identical to the control specimen process, the curvature diagram was divided into five simple geometric shapes applying the second moment-area theorem. The model was used to predict the deflection underneath the wheel load and at 0.75 m from the wheel load for each load case. Thus, there were two points to create the model deflected shape curve per load case. The the model-deflected shape was created and verified with the experimental data. The experimental data for verification was based on data from a sensor underneath the experimental load and a sensor at 0.75 m from the load. Table 5-6 presents a comparison of the deflection magnitudes at the 65 kN load case between the experimental value and the numerical model prediction. The concrete strain level for this load case was 0.0007 <0.001.

Table 5-6. Rehabilitation Specimen 65 kN Load Case Deflection Magnitudes

Deflection Location	**Experimental Test (mm)**	**Analytical Model (mm)**	**Test/Model**
At Wheel Load	4.99	6.08	0.82
At 0.75 m	1.41	1.19	1.18
At Cantilever Root	0	0	1

Figure 5-13 presents the deflected shape curves for the 65 kN load case based on the analytical model prediction and from the experimental test data.

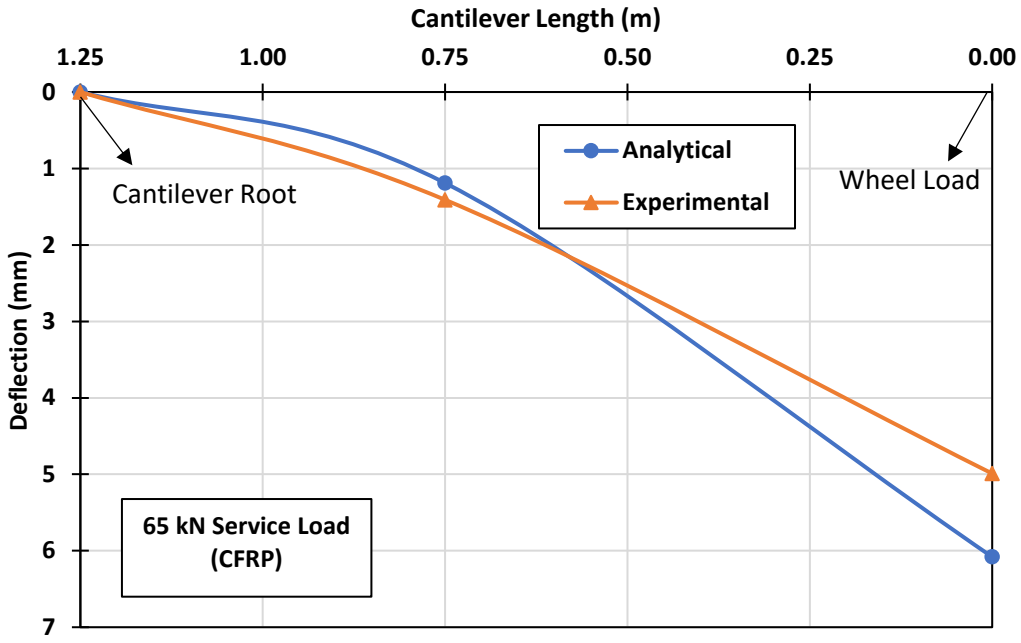

Figure 5-13. Rehabilitation Specimen 65 kN Load Case Deflection Curves

Figure 5-14 presents the curvature diagram for the 85 kN (post-service) load case.

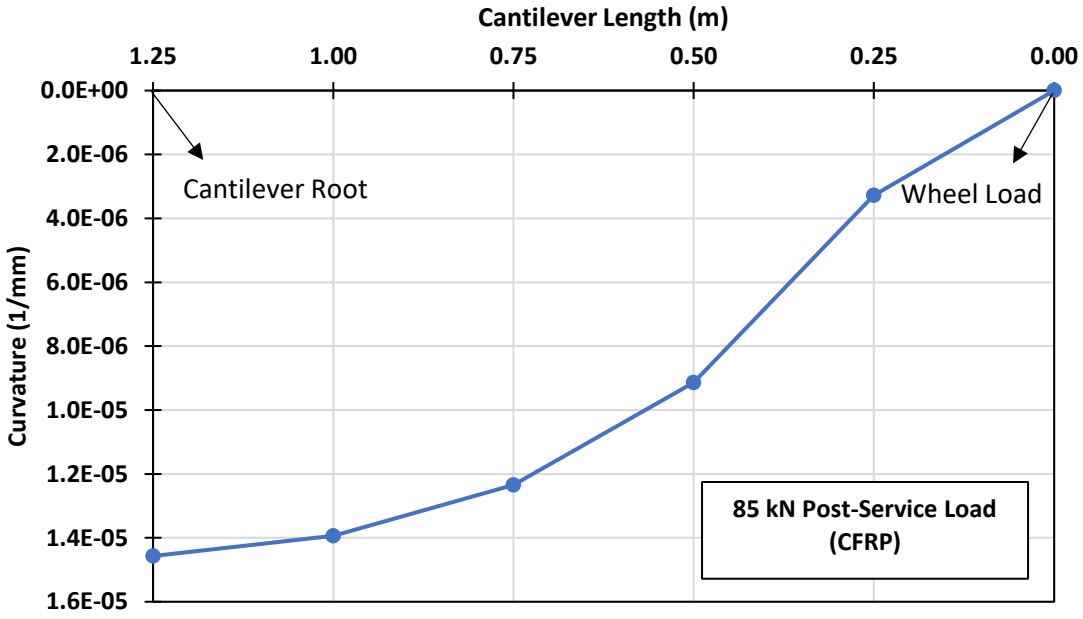

Figure 5-14. Rehabilitation Specimen 85 kN Load Case Curvature Diagram

Table 5-7 presents a comparison of the deflection magnitudes at the 85 kN load case between the experimental value and the numerical model prediction. The concrete strain level for this load case was 0.0009 <0.001.

Table 5-7. Rehabilitation Specimen 85 kN Load Case Deflection Magnitudes

Deflection Location	Experimental Test (mm)	Analytical Model (mm)	Test/Model
At Wheel Load	7.74	9.21	0.84
At 0.75 m	2.05	1.75	1.17
At Cantilever Root	0	0	1

Figure 5-15 presents the deflected shape curves for the 85 kN load case based on the analytical model prediction and from the experimental test data.

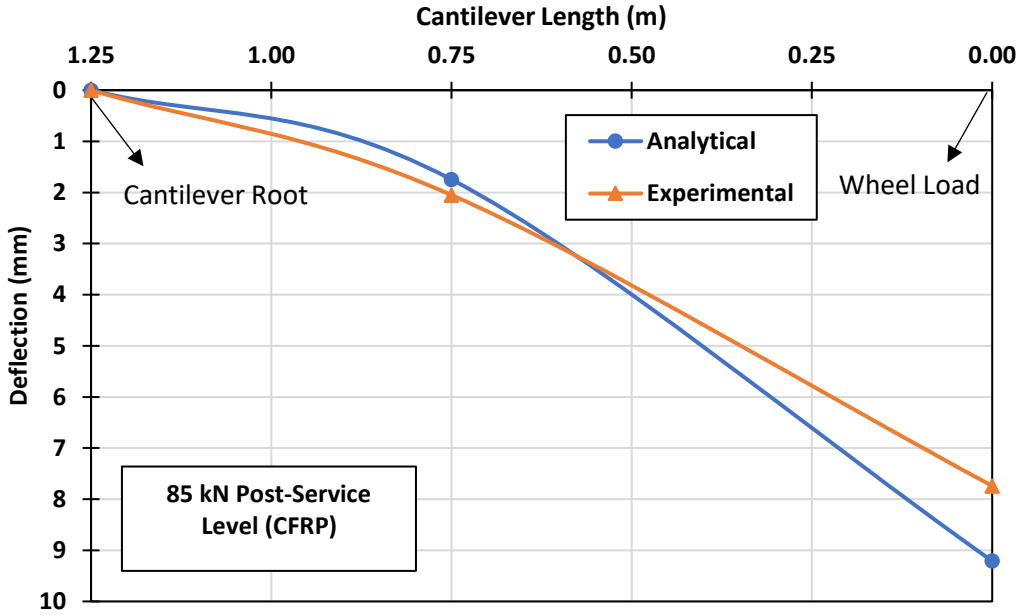

Figure 5-15. Rehabilitation Specimen 85 kN Load Case Deflection Curves

Figure 5-16 presents the curvature diagram for the 55 kN (pre-service) load case.

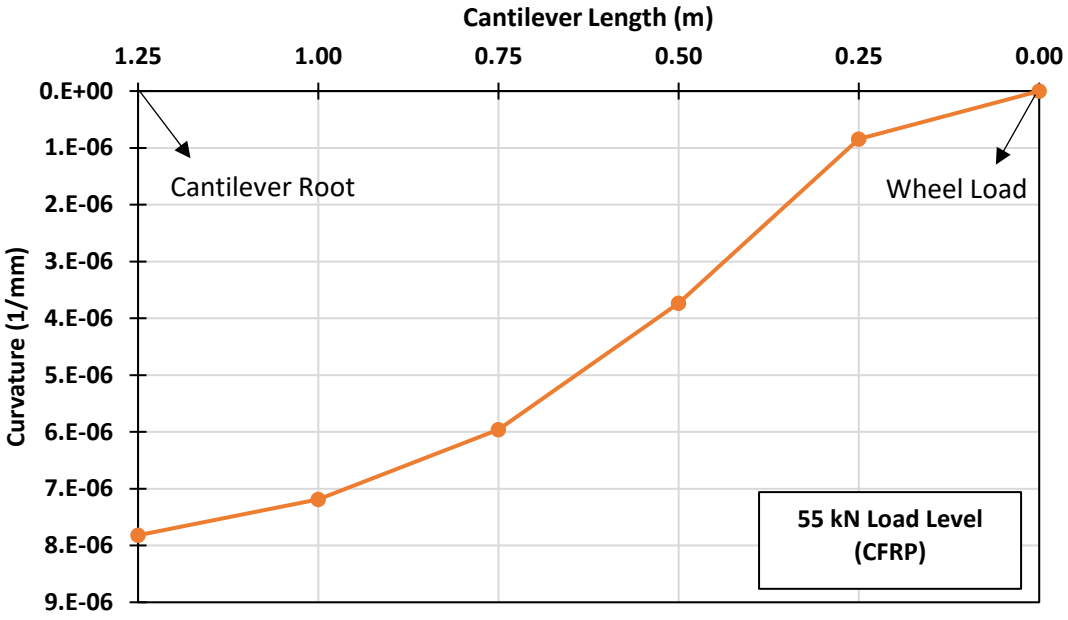

Figure 5-16. Rehabilitation Specimen 55 kN Load Case Curvature Diagram

Table 5-8 presents a comparison of the deflection magnitudes at the 55 kN load case between the experimental value and the numerical model prediction. The concrete strain level for this load case was 0.0006 <0.001.

Table 5-8. Rehabilitation Specimen 55 kN Load Case Deflection Magnitudes

Deflection Location	Experimental Test (mm)	Analytical Model (mm)	Test/Model
At Wheel Load	3.50	4.54	0.77
At 0.75 m	0.98	0.91	1.08
At Cantilever Root	0	0	1

Figure 5-17 presents the deflected shape curves for the 55 kN load case based on the analytical model prediction and from the experimental test data.

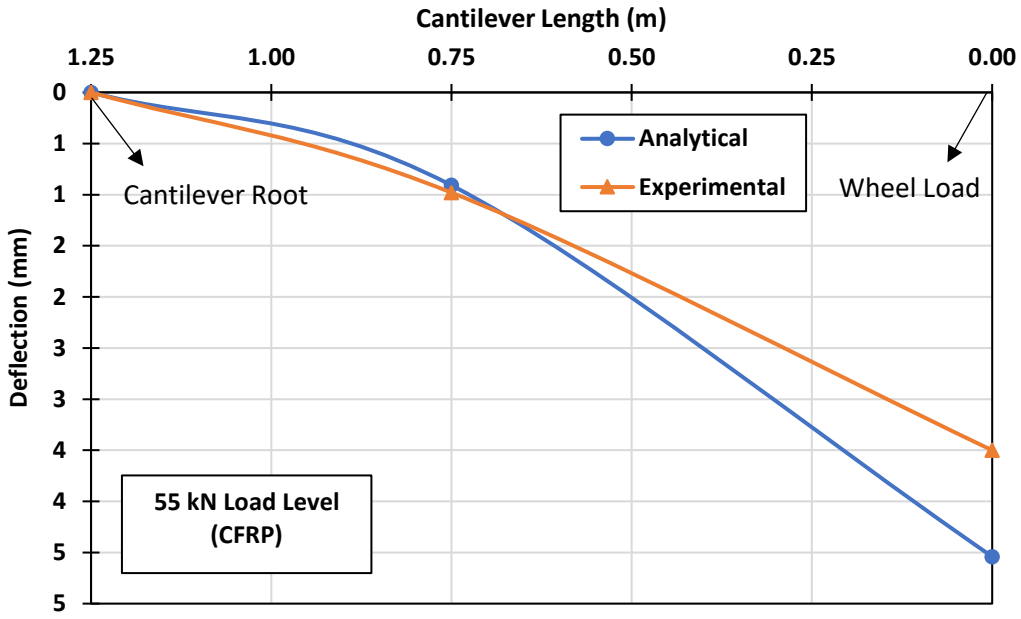

Figure 5-17. Rehabilitation Specimen 55 kN Load Case Deflection Curves

The comparison of the model deflection for the rehabilitation specimen at three load cases within the concrete linear stress region against the experimental data yielded a few important findings. Like the control specimen, the model overpredicts the deflection of the concrete cantilever for all three load cases underneath the load, i.e., the test/model ratio is less than one. A test/model ratio of less than one indicates that the concrete cantilever is deflecting less than predicted in reality and thus is safer for design purposes. However, at 0.75 m from the wheel load location, which is closer to the cantilever load, the model underpredicts the deflection. This is not ideal but reasonable given the assumptions made for the model. The model does not see the imperfections in the lab as there are tolerances to the sensors. Additionally, the model assumes a perfect cantilever where the cantilever root does not move, and the base of the cantilever is fully supported where in the lab there was movement observed. The results are very reasonable and the experimental test results validate the predictability of the model. The most important deflection magnitude for a cantilever is the magnitude at the free end where max deflection is observed. Thus, the model has been validated and is sound for predicting the deflection at the service state for the concrete cantilever.

Figure 5-18 presents a summary of the analytical model versus experimental test data deflection curves for all three load cases for the rehabilitation specimen.

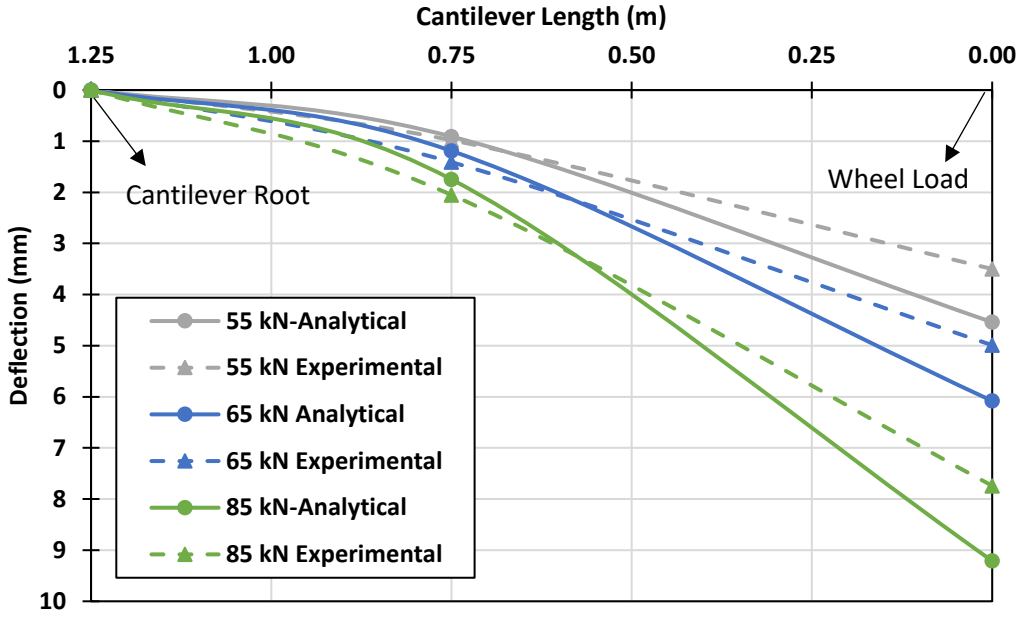

Figure 5-18. Rehabilitation Specimen Model Deflection Curves Summary

5.2. Existing Bridge Parametric Study

Following model verification with the experimental data and the sound predictability results, a parametric study was conducted. The parametric study encompassed applying the analytical model to a small representative section of the existing under consideration bridge structure that this research is based on. A 3.0 m section of the existing in-situ bridge cantilever wing is utilized as a representative section for the parametric study. The selection of the representative.0 m strip is similar in essence to the selection of a unit strip of slab cut out in a one-way concrete slab for purposes of analysis and design. Figure 5-19 presents a schematic of the 3.0 m cut-out.

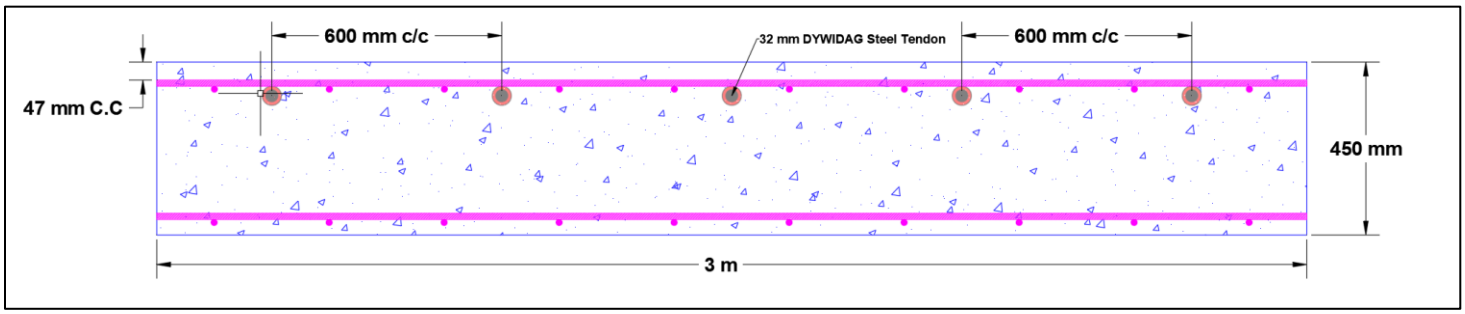

Figure 5-19. Existing Bridge Parametric Study Section

5.2.1. Flexural Capacity

The existing bridge deck depth of the cantilever wing varies from 225 mm at the free end to 450 mm at the top root. Transverse 32 mm PT steel bars spaced 600 mm on centre encased in grouted 50 mm corrugated metal ducts serve as the primary structural reinforcement resisting the vehicular traffic loads imparted on the cantilever wings. Calculation of the flexural capacity of the nominal slab cut out was based on the critical section of the cantilever illustrated in Figure 5-19. The unit section has five steel PT tendons within its influence zone. At a limiting design extreme compression concrete fibre strain of 0.0035, the model yields a moment capacity of 2656 kN.m for this section. To simulate damage conditions, it is assumed that from years of service and corrosion, one of the steel tendons has completely deteriorated. Thus, only four out of the five steel PT tendons are now contributing toward structural capacity per se. Given the damage, at a limiting design extreme compression concrete fibre strain of 0.0035, the model yields a moment capacity of 2469 kN.m for this section. Therefore, there was a loss of 187 kN.m at ultimate. To rehabilitate the structural capacity from the deteriorated lost steel tendon within its 600 mm influence zone, the proposed PT NSM CFRP rehabilitation methodology is implemented. One lost steel tendon corresponds to a loss of 806 mm2 of cross-sectional area. Therefore, we proposed the utilization of #4 (13 mm) CFRP rods which are the largest CFRP rod available in today's market. Each rod corresponds to a cross-sectional area of 126.7 mm2. Hence, six #4 (13 mm) CFRP rods were

utilized for rehabilitation. Figure 5-20 presents the parametric study section with a lost PT steel tendon and the implementation of six #4 (13mm) rods CFRP rods near-surface-mounted.

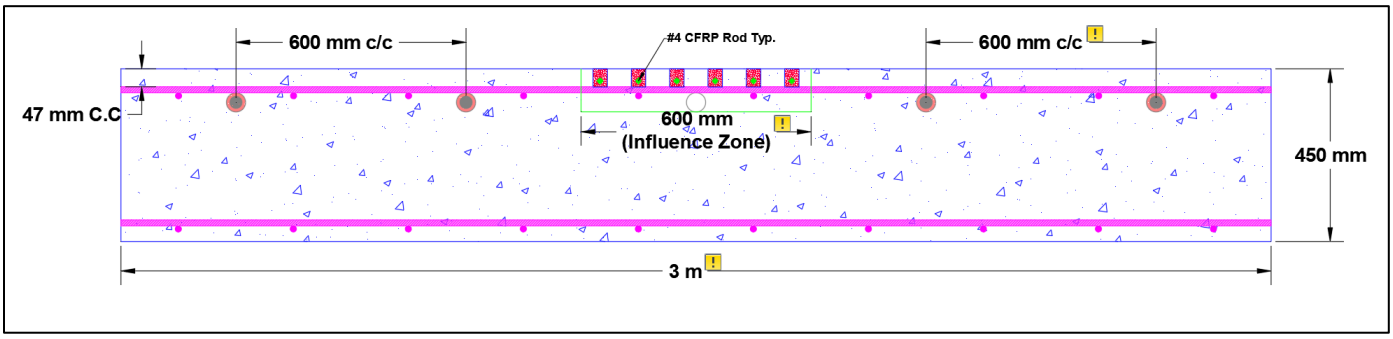

Figure 5-20. Existing Bridge Parametric Study Rehabilitated Section

Based on the results of the conducted experimental program in Chapter 4, the same proposed NSM CFRP detailing was used. Figure 5-21 presents a close-up of the proposed CFRP NSM detailing for the existing bridge under consideration parametric study.

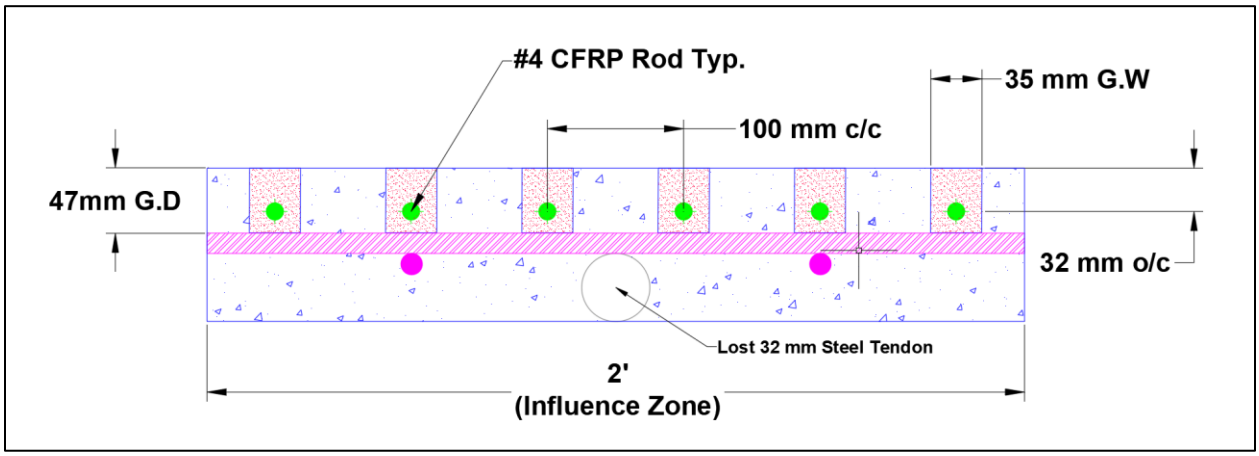

Figure 5-21. Existing Bridge Parametric Study CFRP NSM Detailing

Figure 5-21 showcases the proposed six #4 (13 mm) CFRP rods near-surface-mounted on the tensile side of the slab at 100 mm c/c apart and 32 mm o/c deep. The clear distance between each NSM groove is 62.5 mm which is reasonable from a realistic perspective of a contractor having to saw-cut these grooves. The groove width and depth were kept at 35 mm and 47 mm to avoid any bond slip failure and to ensure a good bond with the concrete substrate as proven experimentally.

Additionally, a cement-based grout would protect the CFRP from damaging ultraviolet rays. As the CHBDC does not have a clear detailing requirement for NSM CFRP for the rehabilitation of concrete structures, the above detailing is considered sound. With the addition of the six #4 (13 mm) CFRP rods, at a limiting design extreme compression concrete fibre strain of 0.0035, the model yields a moment capacity of 2661 kN.m for this section. Therefore, the lost moment capacity of the section was restored. Table 5-9 presents a summary of the flexural capacities for the three different scenarios of the existing bridge parametric study.

Table 5-9. Existing Bridge Parametric Study Flexural Capacity Summary

Section ID	Steel Tendons #	CFRP Tendons #	M_Model (kN.m)	εcu
Nominal	5	-	2656	0.0035
Damage	4	-	2469	0.0035
Rehabilitated	4	6	2661	0.0035

5.2.2. Deflection

The existing bridge deck has the original 32 mm transverse steel tendons post-tensioned at an effective force of 500 kN equivalent. The PT force was required to hold up the thin cantilever wings and control the deflection. The application of the wheel load relative to the cantilever root was 2.5 m away. The free end of the cantilever was another 1 m away. Thus, a total of 3.5 m. The service deflection will be modeled for the following three scenarios:

- Existing Bridge Nominal Parametric Study Section
- Existing Bridge Damage Parametric Study Section
- Existing Bridge Rehabilitated Parametric Study Section

The deflection of the concrete cantilever section at simulated service was calculated using the verified analytical model. The compression concrete strain at service was 0.0007, thus the assumed linear triangular distribution for the concrete compressive stress remained valid. The input parameters from the model to follow the Figure 5-4 process were the properties from the existing bridge structure to get the deflection underneath the wheel load but also at the free end of the cantilever. The wheel load would be loading the cantilever within the curb limits, thus on the real bridge, it would be handy to know both the deflection underneath the wheel load and at the free end of the cantilever that would experience max deflection. Max deflection at the free end is calculated using the second-moment area theorem and it is only the moment lever arm that changes to account for the increased deflection. Given the steel tendons were post-tensioned at a force of 500 kN, an equivalent force would have to be reintroduced into the system if that force was lost. However, based on the experimental results of the proposed CFRP mechanical anchor in Chapter 3, 50 kN is the limiting max effective prestressing force for each CFRP rod.

For scenario one, the nominal parametric study section, the model yields a deflection of 11.84 mm underneath the wheel load and 18.85 mm as the max deflection at the free end of the cantilever. This would correspond to five steel tendons with 500 kN of PT force in each tendon. For scenario two, the damage parametric study section, the model yields a deflection of 16.83 mm underneath the wheel load and 26.88 mm as the max deflection at the free end of the cantilever. This would correspond to four steel tendons with 500 kN of PT force in each tendon with one being lost due to deterioration. The proposed six #4 (13mm) CFRP rods had to be checked to determine the level of rehabilitation. The six CFRP rods were adequate at the ultimate level but had to be checked for service deflection. As indicated earlier, the max effective prestressing force was limited to 50 kN due to the anchorage effect, so a total of 300 kN. However, as the CFRP rods are near-surface-mounted, the increased lever arm, i.e., increased distance from the extreme compression concrete fibre would provide a bit of added service capacity. Table 5-10 presents a summary of the service deflections for the considered three case scenarios.

Table 5-10. Existing Bridge Parametric Study Service Deflection Summary

Section ID	Steel Tendons #	Steel PT Force (kN)	CFRP Tendons #	CFRP PT Force (kN)	Δ_Model Wheel Load (mm)	Δ_Model Free End (mm)	εc
Nominal	5	2500	-	-	11.84	18.85	0.0007
Damage	4	2000	-	-	16.83	26.88	0.0008
Rehabilitated	4	2000	6	300	12.74	20.28	0.0007

Figure 5-22 illustrates the deflected shape of the existing bridge concrete cantilever section based on the three case scenarios.

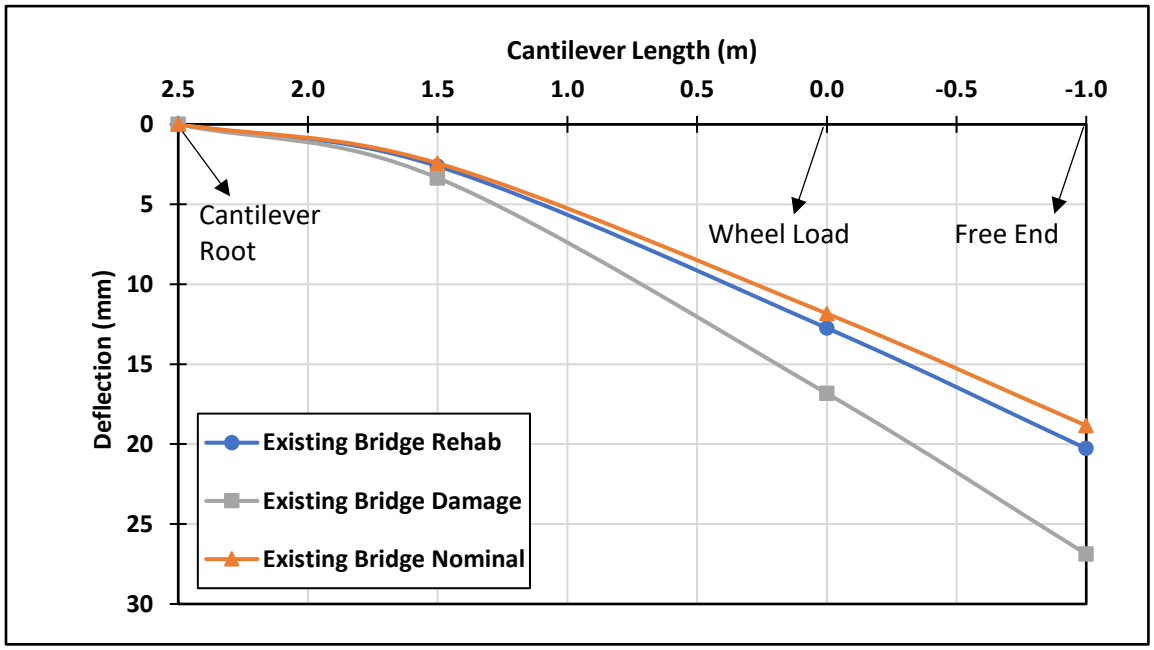

Figure 5-22. Existing Bridge Parametric Study Service Deflection Summary

The proposed PT CFRP rehabilitation methodology is very promising to restore the lost structural capacity in a PT concrete bridge cantilever wing slab. The implementation of six - #4 (13 mm) CFRP rods for the lost steel tendon due to deterioration was able to restore structural capacity at the ultimate. At the serviceability limit state, due to the limiting PT force of 50 kN per CFRP rod because of the anchor effect, the system was not able to restore completely the nominal deflection capacity of the system. However, these results are encouraging to improve the anchorage design to get more PT force out of it to fully restore the service deflection.

CHAPTER 6 CONCLUSIONS AND RECOMMENDATIONS

The purpose of the research was many-fold. The first was to determine the viability and suitability of a proposed mechanical strengthening system for post-tensioning unidirectional pultruded CFRP Rods. The second was to evaluate the performance and feasibility of utilizing the post-tensioned CFRP rods with permanent mechanical anchorage to rehabilitate deteriorated post-tensioned concrete bridge cantilever wing slabs. To achieve these goals, a comprehensive experimental program was established. A mechanical strengthening system for post-tensioning CFRP rods was proposed and developed. The strengthening system consisted of machining in-house a mechanical split wedge and barrel anchor. Experimental testing was conducted on the anchor to determine its viability for use in post-tensioned concrete bridge cantilever wing slabs. In total, seven mechanical anchorage specimens were fabricated and tested. The average maximum ultimate capacity of the anchorage system was around 100 kN. The test results of the anchorage system pertain quite exclusively to a #3 (10 mm) unidirectional CFRP rod. The following conclusions were drawn from the anchorage experimental program:

- The utilization of a stainless-steel barrel and soft aluminum slit aluminum wedges with a longitudinal circular profile was a suitable mechanical anchor to grip the #3 CFRP rod in this application.
- Even while using soft aluminum wedges for the gripping, the CFRP rod still failed due to pinching shear failure near the anchor at a load level less than the ultimate strength of the CFRP rod.
- Equi-distant spaced split wedges were needed to avoid anchorage component slippage.
- Lubrication on the outside of the wedges aids in the better insertion of the wedges for load-bearing capacity.
- An 80-kN presetting force was needed on the anchors to eliminate system slippage.
- A max safe effective anchorage jacking force of 50 kN only could be applied to be in conformance with CHBDC requirements.

After the completion of the anchorage experimental program, the mechanical anchor was utilized in the bridge cantilever wing slab experimental program. Two half-scale bridge cantilevers were fabricated and cast. The first is the control specimen with only steel post-tensioning. The second

specimen was a specimen that underwent simulated damage followed by PT CFRP rehabilitation. Simulated damage conditions entailed the loss of a 15 mm PT steel bar that was post-tensioned with 100 kN of force. The rehabilitation scheme entailed replacing the lost steel tendon with two 10 mm CFRP rods that were post-tensioned with 50 kN of force each. The CFRP rods were introduced for rehabilitation by near-surface mounting them into the tensile side of the concrete and bonding them to the concrete substrate but utilizing a cement-based grout. Both specimens were tested under a selected displacement-controlled loading protocol simulating service and ultimate conditions. The following were the conclusions and results drawn from the bridge cantilever wing slab experimental program:

- The failure mode of the control steel specimen was a flexural concrete crushing failure. The ultimate capacity of the cantilever was 187.5 kN.m. A secondary mode of failure was deformation-induced shear on the system.
- The failure mode of the CFRP rehabilitation specimen was a flexural concrete crushing failure. The ultimate capacity of the cantilever was 200 kN.m.
- The CFRP rehabilitation specimen restored/rehabilitated the lost structural capacity in the system after undergoing simulated damage with two 10 mm CFRP rods post-tensioned at 50 kN each.
- At service and at ultimate, the CFRP rehabilitation specimen deflected less than the control steel specimen.
- The crack widths at ultimate for the control steel specimen were around 2.5-3.0 mm.
- The crack widths at ultimate for the CFRP rehabilitation specimen were around 1.25-1.50 mm.
- At service and at ultimate the crack widths of the CFRP rehabilitation specimen were smaller in measurement than the control steel specimen.
- More cracks were present in the CFRP rehabilitation at service and at ultimate.
- More map cracking/spider web cracking/intertwining of cracks was present in the CFRP rehabilitation specimen at service and at ultimate.
- There was no slippage or movement in the permanent CFRP mechanical anchors while the bridge cantilever specimen was being tested.

- A bonded PT system for CFRP is recommended to lock the PT force in place and to reduce losses in the system compared with an un-bonded mechanical PT system.
- The proposed NSM groove detailing of a 35 mm wide by 47 mm deep groove with a CFRP rod placed 32 mm o/c in the groove resulted in no bond-slip failure or grout splitting at service or post-service. Minor grout splitting was only observed at the ultimate destruction of the specimens.
- The utilization of a cement-based grout for NSM grooves can be more efficient and cost-effective based on the groove dimensions.
- Post-tensioning CFRP for rehabilitation of PT bridge structures is needed to fully utilize the structural potential of the CFRP material and to reintroduce the lost pre-compression force into the concrete that was lost due to corrosion deterioration of steel tendons.

Following the bridge cantilever wing slab experimental program, an analytical model was developed. The purpose of the model was to predict the ultimate flexural capacity of the bridge cantilever specimen and the deflection of the specimens under service conditions. The model was verified with the experimental data and the model had sound predictability with the ratio between the test data and the analytical model being near one. The model was conservative at predicting the deflection under a wheel load at service and conservative at predicting the ultimate flexural capacity when using an extreme compression concrete fibre strain of 0.0035. The model was used for a parametric study applying it to a cantilever section of the existing bridge structure.

In addition to the conclusions drawn based on the experimental and analytical study, the following recommendations are suggested to expand on the research presented:

- Varying the radius of the linear circular profile of the mechanical anchor to obtain an optimum radius that balances between the required contact pressure and the tensile load capacity induced by the grip.
- Varying with different materials of various hardness for the split wedges in the mechanical anchor to see the effect on the ultimate tensile load capacity of the anchor.
- Conduct more static anchorage tests and associated fatigue tests.
- Conduct static anchorage tests with the same mechanical anchor but by utilizing CFRP rods produced by different manufacturers to assess the versatility of the anchor.

- Alter the current mechanical anchorage system to accommodate a #4 (13 mm) CFRP rod as the larger diameter would be more feasible to rehabilitate deteriorated larger diameter steel tendons currently in PT bridges.
- Begin proposing acceptance criteria for CFRP anchorage systems.
- Conduct fatigue testing and not just static testing on the bridge cantilever wing specimens.
- Varying the reinforcement ratio of the CFRP rods within the bridge cantilever specimen to determine how much more capacity can be obtained if looking for a rehabilitated plus upgraded section.
- Varying the NSM groove detailing by decreasing the depth of the NSM groove if the concrete cover is limited on an existing bridge deck.
- Begin proposing NSM groove detailing requirements in codes rather than just minimum groove dimensions.
- A non-linear model to represent the compressive stress of concrete is needed if predicting the deflection of a concrete cantilever past service limits is desired.

BIBLIOGRAPHY

Al-Mayah, A., Soudki, K., and Plumtree, A. 2001. “Mechanical behavior of CFRP rod anchors under tensile loading.” *Journal of Composites for Construction*, 5 (2), 128–135.

Al-Mayah, A., Soudki, K., and Plumtree, A. 2006. “Development and assessment of a new CFRP rod–anchor system for prestressed concrete.” *Applied Composite Materials*, 13 (5), 321–334.

Al-Mayah, A., Soudki, K., and Plumtree, A. 2013. “Simplified anchor system for CFRP rods.” *Journal of Composites for Construction*, 17 (5), 584–590.

American Concrete Institute, 222.2R-14. 2014. "*Report on Corrosion of Prestressing Steels*", Reported by ACI Committee 222, Farmington Hills MI.

American Concrete Institute, 423.3R-17. 2017. "*Recommendations for Concrete Members Prestressed with Single-Strand Unbonded Tendons*", Reported by ACI Committee 423, Farmington Hills MI.

American Concrete Institute, 423.7R-14. 2014. "*Specification for Unbonded Single-Strand Tendon Materials*", Reported by ACI Committee 423, Farmington Hills MI.

American Concrete Institute, 440.4R-11. 2011. "*Prestressing Concrete Structures with FRP Tendons*". Reported by ACI Committee 440, Farmington Hills MI.

ASTM D7205/D7205M-21. 2021. *Standard test method for tensile properties of fiber reinforced polymer matrix composite bars*. ASTM International. West Conshohocken, PA.

Benmokrane, B., Nazair, C., Seynave, X., and Manalo, A. 2017. “Comparison Between ASTM D7205 and CSA S806 Tensile-Testing Methods for Glass Fiber–Reinforced Polymer Bars.” *Journal of Composites for Construction*, 21 (5).

Canadian Standard Association, *CSA S6-19*, Canadian Highway Bridge Design Code. 2019. Toronto, Ontario.

Canadian Standard Association, *Commentary on CSA S6:19*, Canadian Highway Bridge Design Code. 2019. Toronto, Ontario.

Chajes, M., Rollins, T., Dai, H., and Murphy, T. 2019. "*Report on Techniques for Bridge Strengthening*." https://www.fhwa.dot.gov/bridge/pubs/hif18041.pdf.

De Lorenzis, L, and Teng, J.G. 2007. "Near-Surface Mounted FRP Reinforcement : An Emerging Technique for Strengthening Structures." *Composites*. *Part B, Engineering*, 38 (2), 119–143.

De Waal, Leo, et al. 2017. "FRP Strengthening of 60 Year Old Pre-Stressed Concrete Bridge Deck Units." *Engineering Structures*, 143, 346.

El-Haacha, R., and El-Soudki, K. 2013. "Prestressed near-Surface Mounted Fibre Reinforced Polymer Reinforcement for Concrete Structures — a Review 1." *Canadian Journal of Civil Engineering*, 40 (11), 1127–1139.

El-Hacha, R., and Gaafar, M. 2011. "Flexural Strengthening of Reinforced Concrete Beams Using Prestressed Near-Surface-Mounted CFRP Bars," *PCI Journal*, 56 (4),134-151.

El-Hacha, Raafat, et al. 2001. "Prestressed Fibre-Reinforced Polymer Laminates for Strengthening Structures." *Progress in Structural Engineering and Materials*, 3 (2),111–121.

El-Hacha, R., and Rizkalla, S.H. 2007. "*Case Histories and Use of FRP for Prestressing Applications*," SP-245, American Concrete Institute, Farmington Hills, Michigan, 143-164.

Federal Highway Administration (FHWA). 2016."*Count of Deficient Bridges by Functional Classification*," National Bridge Inventory.

fib (International Federation for Structural Concrete). 1993. *Recommendations for the acceptance of post-tensioning systems*. Lausanne, Switzerland: fib.

Grace, N.F., Jensen, E.A., Eamon, C.D., and Shi, X. 2012. “Life-Cycle Cost Analysis of Carbon Fiber-Reinforced Polymer Reinforced Concrete Bridges.” *ACI Structural Journal*, 109 (5), 697–697.

Grace, N.F., Jensen, E.A., Matsagar, V., and Penjendra, P. 2013. “Performance of an AASHTO Beam Bridge Prestressed with CFRP Tendons.” *Journal of Bridge Engineering*, 18 (2), 110–121.

Grace, N.F., Ushijima, K., Matsagar, V., and Wu, C. 2013. “Performance of AASHTO-Type Bridge Model Prestressed with Carbon Fiber-Reinforced Polymer Reinforcement.” *ACI Structural Journal*, 110 (3), 491–501.

Grace, N.F., et al. 2022. “Design, Construction, and Monitoring of US Longest Highway Bridge Span Prestressed with CFRP Strands.” *Journal of Bridge Engineering*, 27 (7).

Heydarinouri, H., Vidovic, A., Nussbaumer, A., and Ghafoori, E. 2021. "FE Analysis and Experimental Validation of Mechanical Wedge–barrel Anchors for CFRP Rods." *Composite Structures*, 275.

Heydarinouri, H., Motavalli, M., Nussbaumer, A., and Ghafoori, E. "Development of a Mechanical Wedge–Barrel Anchor for CFRP Rods: Static and Fatigue Behaviors." *Journal of Composites for Construction*, 25 (3).

ISIS Canada, Intelligent Sensing for Innovative Structures, A Canadian Network of Centres of Excellence. 2006. *Reinforcing Concrete Structures with Fibre-Reinforced Polymers*, Design Manual No. 3., Winnipeg, Manitoba.

Kim, Yail, et al. 2018. “Strengthening of a Bridge Using Post-Tensioned Near Surface-Mounted Carbon Fiber-Reinforced Polymer in Multi-Hazard Environment.” *ACI Structural Journal*, 115 (2), 451–462.

Kim, Yail J, et al. 2014. “Anchorage Configuration for Post-Tensioned NSM CFRP Upgrading Constructed Bridge Girders.” *Engineering Structures*, 79, 256–266.

Kim, Yail, et al. 2016. “Functional Performance of Bridge Girders Strengthened with Post-Tensioned Near-Surface-Mounted Carbon Fiber- Reinforced Polymer.” *ACI Structural Journal*, 113 (2), 239–250.

Kim, Yungon, et al. 2014. “Strengthening of Reinforced Concrete T-Beams Using Anchored CFRP Materials.” *ACI Structural Journal*, 111 (5), 1027–1035.

Lee, D., and Cheng, L. 2011. “Assessing the Strengthening Effect of Various Near-Surface-Mounted FRP Reinforcements on Concrete Bridge Slab Overhangs.” *Journal of Composites for Construction*, 15, (4) (2011): 615–624.

Michael, A., Ansley, M., O'Neill, C., and Hamilton, T. 2008. “Bridge Decks Strengthened with near-Surface Mounted Bars Embedded in Cement-based Grout”. *Composites Research Journal*, 2 (1), 47-54.

National Academic of Sciences, Engineering, and Medicine. 2021. *Repair and Maintenance of Post-Tensioned Concrete Bridges*. Washington, DC: The National Academic Press. https://doi.org/10.17226/26172.

Omran, H.Y, and El-Hacha, R. 2014. “Effects of Sustained Load and Freeze-Thaw Exposure on RC Beams Strengthened with Prestressed NSM-CFRP Strips.” *Advances in Structural Engineering*, 17 (12), 1801–1816.

Oudah, F., and El-Hacha, R. 2012. “Fatigue Behavior of RC Beams Strengthened with Prestressed NSM CFRP Rods.” *Composite Structures*, 94 (4), 1333–1342.

Post-Tensioning Institute, and Pawan R. Gupta. 2006. *Post-Tensioning Manual*. 6th ed. Farmington Hills, Michigan: PTI Post-Tensioning Institute.

Post-Tensioning Institute. 1998. “*Acceptance Standards for Post-Tensioning Systems*", Phoenix, Arizona.

Post-Tensioning Institute. 2019. *Specification for Multistrand and Grouted Post-Tensioning*, Farmington Hills, Michigan: PTI Post-Tensioning Institute.

Rostásy, F. S. 1998. “Draft guidelines for the acceptance testing of FRP posttensioning tendons.” *Journal of Composites for Construction*, 2 (1), 2–6.

Schmidt, J. W., Bennitz, A., Täljsten, B., Goltermann, P., and Pedersen, H. 2012. “Mechanical anchorage of FRP tendons—A literature review.” *Construction Building Materials,* 32, 110-121.

Schmidt, J. W., Bennitz, A., Täljsten, B., and Pedersen, H. 2010. “Development of mechanical anchor for CFRP tendons using integrated sleeve.” *Journal of Composites for Construction*, 14 (4), 397–405.

Schmidt, J. W., Smith, S.T., Täljsten, B., Bennitz, A., Goltermann, P., and Pedersen, H. 2011. “Numerical simulation and experimental validation of an integrated sleeve-wedge anchorage for CFRP rods.” *Journal of Composites for Construction*, 15 (3), 284–292.

Siwowski, Tomasz, et al. 2020. “Development and Implementation of CFRP Post-Tensioning System for Bridge Strengthening.” *Engineering Structures*, 20.

Sun, Wei, et al. 2016. “Behavior of Anchored Carbon Fiber-Reinforced Polymer Strips Used for Strengthening Concrete Structures.” ACI Materials Journal, 113 (2), 163– 172.

Taljsten, B., and Nordin, H. 2007. "*Concrete Beams Strengthened with External Prestressing Using External Tendons and Near-Surface-Mounted Reinforcement*," SP-245, American Concrete Institute, Farmington Hills, Michigan,143-164.

The Canadian Infrastructure Report Card. 2019. "*Monitoring the State of Canada's Core Public Infrastructure.*" canadianinfrastructure.ca/en/index.html.

Zhang, S.S, et al. 2017. "Reinforced Concrete Beams Strengthened in Flexure with near-Surface Mounted (NSM) CFRP Strips: Current Status and Research Needs." *Composites. Part B, Engineering*, 131, 30–42.

APPENDIX A MECHANICAL ANCHORAGE STATIC TEST RESULTS

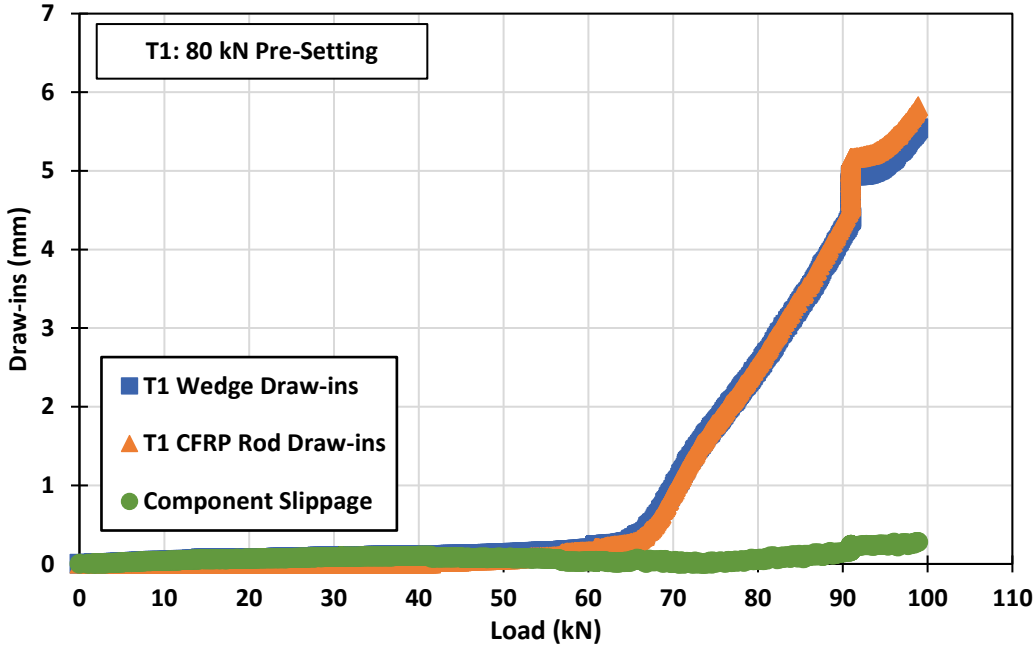

Figure A.1. Static Anchorage Test T1 Specimen Draw-ins

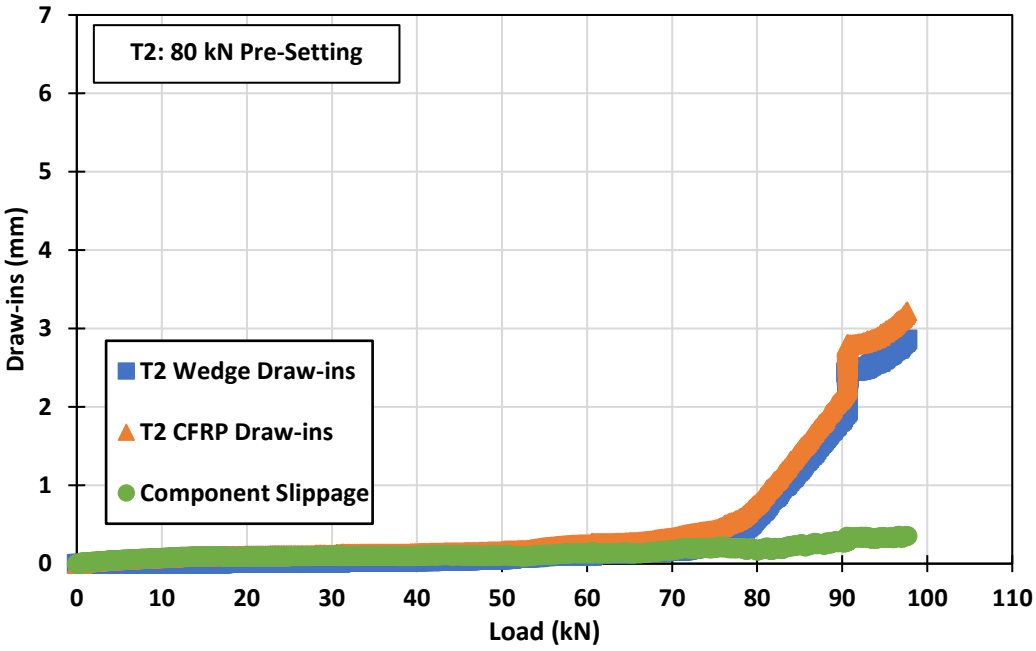

Figure A.2. Static Anchorage Test T2 Specimen Draw-ins

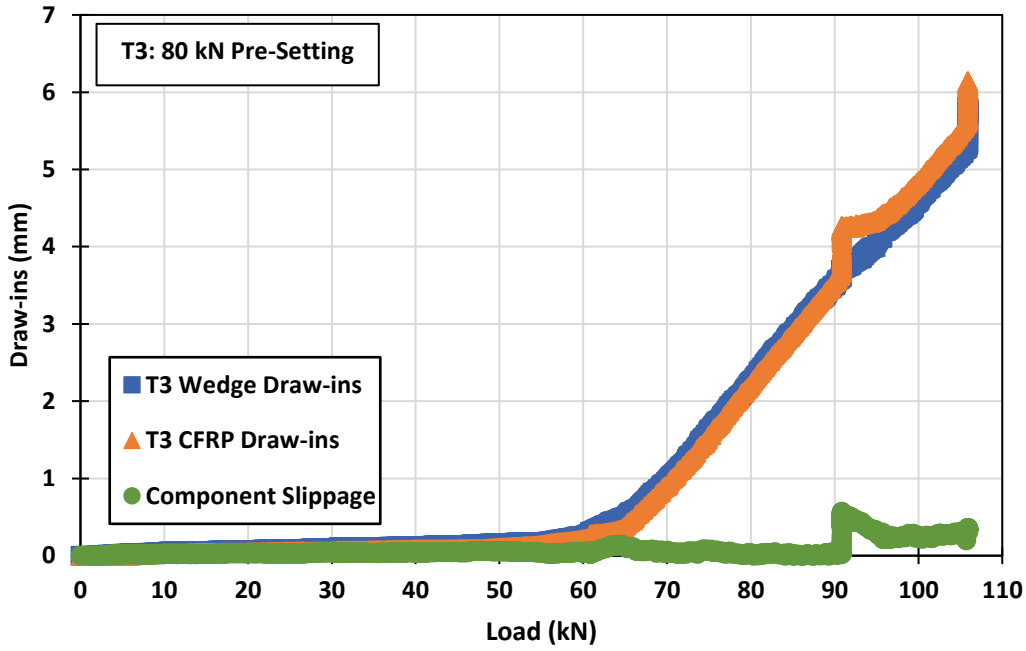

Figure A.3. Static Anchorage Test T3 Specimen Draw-ins

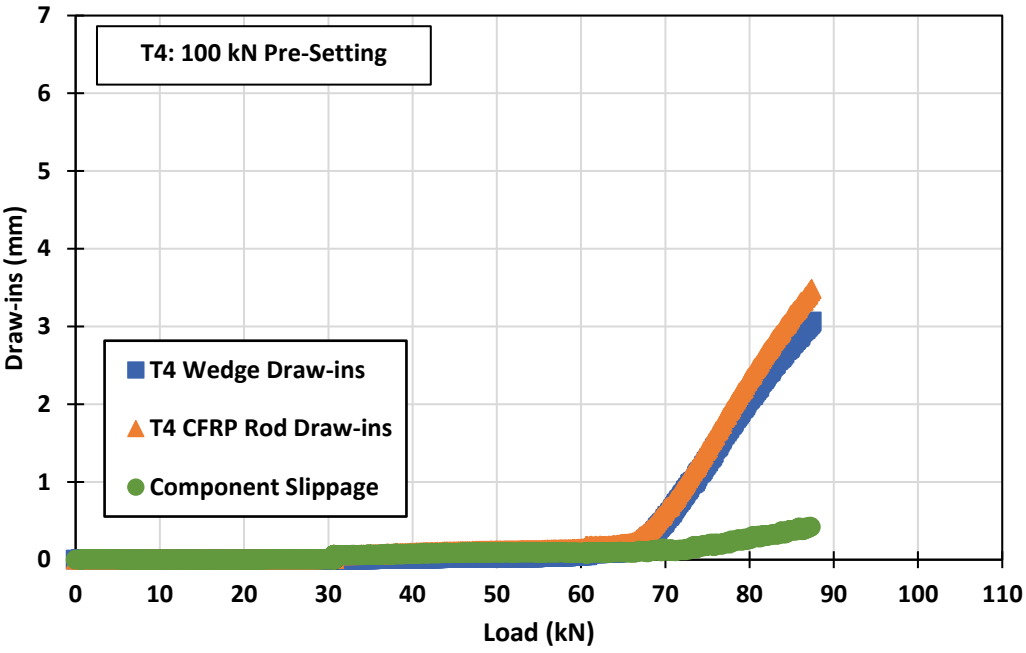

Figure A.4. Static Anchorage Test T4 Specimen Draw-ins

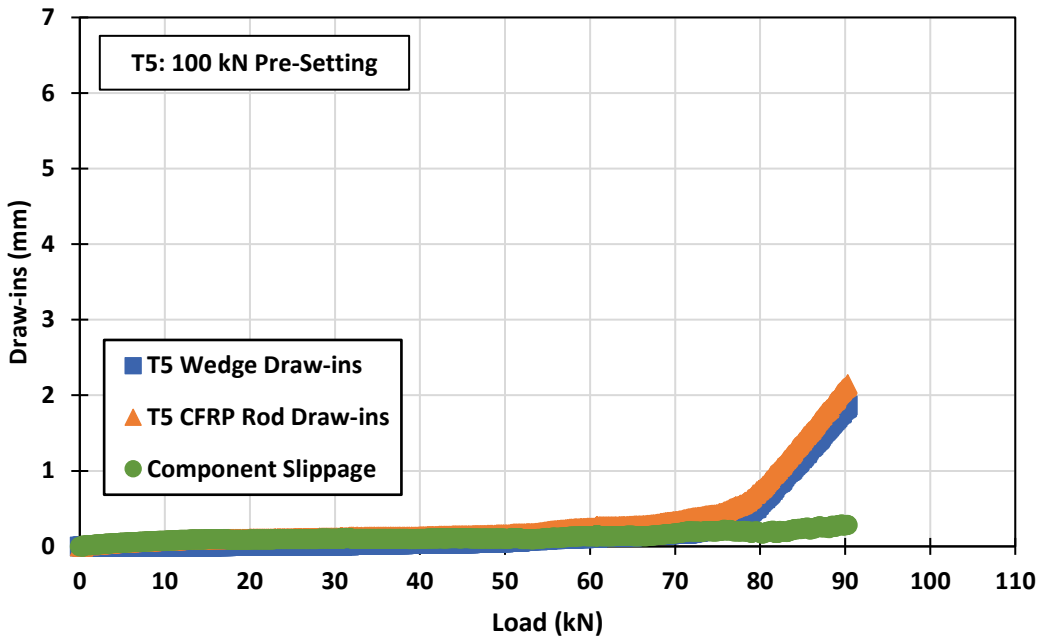

Figure A.5. Static Anchorage Test T5 Specimen Draw-ins

APPENDIX B BRIDGE CANTILEVER SPECIMEN POST-TENSIONING RECORD

Appendix B.1. Control Specimen Double Steel Tendon Pull

Date of Jack Calibration:	06-Jun-22	**Date of Stressing:**	07-Jun-22	**Stressing Mode:**	Free End Only	**Concrete Strength**	38.5	MPa	**Date of Grouting:**	08-Jun-22

Tendon 1A: Jack 1

Load Stage	Load Increment	Load (kN)	Theoretical Elongation (mm)	Minimum Tolerance (mm)	Maximum Tolerance (mm)	Actual Elongation (mm)	Theoretical Micro-Strain (με)	Actual Micro-Strain (με)	Theoretical Gauge Pressure (psi)	Actual Gauge Pressure (psi)
1	20%	10	1.16	1.08	1.24	1.07	276	311	318	500
2	40%	20	2.32	2.15	2.48	2.37	551	595	636	800
3	60%	30	3.47	3.23	3.72	3.91	827	900	954	1200
4	80%	40	4.63	4.31	4.95	4.76	1102	1207	1272	1600
5	100%	50	5.79	5.38	6.19	6.80	1378	1511	1590	2000

Tendon 3C: Jack 2

Load Stage	Load Increment	Load (kN)	Theoretical Elongation (mm)	Minimum Tolerance (mm)	Maximum Tolerance (mm)	Actual Elongation (mm)	Theoretical Micro-Strain (με)	Actual Micro-Strain (με)	Theoretical Gauge Pressure (psi)	Actual Gauge Pressure (psi)
1	20%	10	1.16	1.08	1.24	1.05	276	322	318	500
2	40%	20	2.32	2.15	2.48	2.35	551	632	636	800
3	60%	30	3.47	3.23	3.72	3.90	827	931	954	1200
4	80%	40	4.63	4.31	4.95	4.75	1102	1247	1272	1600
5	100%	50	5.79	5.38	6.19	6.80	1378	1558	1590	2000

Tendon 2B:

Load Stage	Load Increment	Load (kN)	Micro-Strain (με)
1	20%	10	-11
2	40%	20	-33
3	60%	30	-45
4	80%	40	-58
5	100%	50	-71

Double Tension Micro-Strain Readings

Tendon ID	At 100 kN (με)	At Pump Stabilization (με)	At Nut Tightening (με)	At Release (με)	60 mins. After Release (με)	24 hours After Release (με)	Final Effective Load (kN)
Tendon 1	1511	1641	1838	1791	1772	1672	60.67
Tendon 3	1558	1686	1855	1790	1772	1672	60.67

Appendix B.2. Control Specimen Single Steel Tendon Pull

Date of Jack Calibration:	06-Jun-22	**Date of Stressing:**	07-Jun-22	**Stressing Mode:**	Free End Only	**Concrete Strength**	38.5	MPa	**Date of Grouting:**	08-Jun-22

Steel Tendon 2B: Jack 1

Load Stage	Load Increment	Load (kN)	Theoretical Elongation (mm)	Minimum Tolerance (mm)	Maximum Tolerance (mm)	Actual Elongation (mm)	Theoretical Micro-Strain (με)	Actual Micro-Strain (με)	Theoretical Gauge Pressure (psi)	Actual Gauge Pressure (psi)
1	20%	20	2.32	2.15	2.48	1.79	551	552	636	600
2	40%	40	4.63	4.31	4.95	3.81	1102	1100	1272	1450
3	60%	60	6.95	6.46	7.43	6.02	1654	1663	1908	2200
4	80%	80	9.26	8.61	9.91	7.87	2205	2206	2544	2800
5	100%	100	11.58	10.76	12.39	9.90	2756	2757	3180	3400

Steel Tendon 1A:

Load Stage	Load Increment	Load (kN)	Micro-Strain (με)
1	20%	20	18
2	40%	40	20
3	60%	60	39
4	80%	80	42
5	100%	100	0

Steel Tendon 3C:

Load Stage	Load Increment	Load (kN)	Micro-Strain (με)
1	20%	20	-37
2	40%	40	-54
3	60%	60	-63
4	80%	80	-72
5	100%	100	-78

Single Tension Micro-Strain Readings

Tendon Label	At 100 kN (με)	At Pump Stabilization (με)	At Nut Tightening (με)	At Release (με)	60 mins. After Release (με)	24 hours After Release (με)	Final Effective Load (kN)
Tendon 2	2757	2845	2990	2849	2828	2794	101.38

Appendix B.3. Rehab Specimen Double Steel Tendon Pull

Date of Jack Calibration:	06-Jun-22	**Date of Stressing:**	04-Aug-22	**Stressing Mode:**	Free End Only	**Concrete Strength**	39.8	MPa	**Date of Grouting:**	05-Aug-22

Tendon 1A: Jack 1

Load Stage	Load Increment	Load (kN)	Theoretical Elongation (mm)	Minimum Tolerance (mm)	Maximum Tolerance (mm)	Actual Elongation (mm)	Theoretical Micro-Strain (με)	Actual Micro-Strain (με)	Theoretical Gauge Pressure (psi)	Actual Gauge Pressure (psi)
1	20%	10	1.16	1.08	1.24	1.02	276	196	318	500
2	40%	20	2.32	2.15	2.48	2.03	551	444	636	900
3	60%	30	3.47	3.23	3.72	3.05	827	766	954	1250
4	80%	40	4.63	4.31	4.95	4.19	1102	1130	1272	1800
5	100%	50	5.79	5.38	6.19	5.51	1378	1479	1590	2000

Tendon 3C: Jack 2

Load Stage	Load Increment	Load (kN)	Theoretical Elongation (mm)	Minimum Tolerance (mm)	Maximum Tolerance (mm)	Actual Elongation (mm)	Theoretical Micro-Strain (με)	Actual Micro-Strain (με)	Theoretical Gauge Pressure (psi)	Actual Gauge Pressure (psi)
1	20%	10	1.16	1.08	1.24	1.02	276	184	318	500
2	40%	20	2.32	2.15	2.48	2.03	551	517	636	900
3	60%	30	3.47	3.23	3.72	3.05	827	786	954	1250
4	80%	40	4.63	4.31	4.95	4.27	1102	1106	1272	1800
5	100%	50	5.79	5.38	6.19	5.72	1378	1487	1590	2000

Steel Tendon Double Pull Micro-Strain Readings

Tendon Label	At 100 kN (με)	At Pump Stabilization (με)	At Nut Tightening (με)	At Release (με)	60 mins. After Release (με)	24 hours After Release (με)	Final Effective Load (kN)
Steel Tendon 1	1479	1679	1856	1728	1687	1654	60.02
Steel Tendon 2	1487	1687	1860	1767	1693	1658	60.16

Appendix B.4. Rehab Specimen Double CFRP Tendon Pull

Date of Jack Calibration:	06-Jun-22	**Date of Stressing:**	16-Aug-22	**Stressing Mode:**	Free End Only	**Concrete Strength**	39.8	MPa	**Date of Grouting:**	17-Aug-22

CFRP Tendon 1: Jack 1

Load Stage	Load Increment	Load (kN)	Theoretical Elongation (mm)	Minimum Tolerance (mm)	Maximum Tolerance (mm)	Actual Elongation (mm)	Theoretical Micro-Strain (με)	Actual Micro-Strain (με)	Theoretical Gauge Pressure (psi)	Actual Gauge Pressure (psi)
1	20%	10	4.75	4.42	5.09	4.06	1132	1074	318	500
2	40%	20	9.51	8.84	10.17	8.00	2263	2149	636	900
3	60%	30	14.26	13.26	15.26	14.15	3395	3394	954	1250
4	80%	40	19.01	17.68	20.34	19.81	4527	4570	1272	1800
5	100%	50	23.77	22.10	25.43	24.00	5659	5574	1590	2000

CFRP Tendon 2: Jack 2

Load Stage	Load Increment	Load (kN)	Theoretical Elongation (mm)	Minimum Tolerance (mm)	Maximum Tolerance (mm)	Actual Elongation (mm)	Theoretical Micro-Strain (με)	Actual Micro-Strain (με)	Theoretical Gauge Pressure (psi)	Actual Gauge Pressure (psi)
1	20%	10	4.75	4.42	5.09	4.06	1132	1039	318	500
2	40%	20	9.51	8.84	10.17	7.77	2263	2075	636	900
3	60%	30	14.26	13.26	15.26	14.20	3395	3179	954	1250
4	80%	40	19.01	17.68	20.34	19.94	4527	4223	1272	1800
5	100%	50	23.77	22.10	25.43	24.26	5659	5194	1590	2000

Steel Tendon 1A:

Load Stage	Load Increment	Load (kN)	Micro-Strain (με)
1	20%	10	-7
2	40%	20	-13
3	60%	30	-18
4	80%	40	-23
5	100%	50	-27

Steel Tendon 3C:

Load Stage	Load Increment	Load (kN)	Micro-Strain (με)
1	20%	10	-9
2	40%	20	-14
3	60%	30	-18
4	80%	40	-23
5	100%	50	-26

CFRP Tendon Double Pull Micro-Strain Readings

Tendon Label	At 50 kN (με)	At Pump Stabilization (με)	At Nut Tightening (με)	At Release (με)	60 mins. After Release (με)	24 hours After Release (με)	Re-Tension (με)	Final Effective Load (kN)
CFRP Tendon 1	5574	5715	5750	5599	5307	4940	5750	50.81
CFRP Tendon 2	5194	5320	5644	5237	4999	4782	5723	50.57

APPENDIX C CONTROL SPECIMEN LOADING PROTOCOL AND TESTING OBSERVATIONS

1. **Load Step #1:** Uncracked Moment Region: 25 kN.
    a. **Cycle 1:** No observed cracks.
    b. **Cycle 2:** No observed cracks.
    c. **Cycle 3:** No observed cracks.
    d. **Cycle 4:** No observed cracks.
    e. **Cycle 5:** No observed cracks.
    f. **Notes:** No major concerns, specimen rebounding/retracting elastically when unloaded.

2. **Load Step #2:** f_cr: Onset of Cracking Region: 35 kN.
    a. **Cycle 1:** No observed cracks.
    b. **Cycle 2:** One 0.05 mm hairline crack on the top slab appears at approximately 70” from the free end.
    c. **Cycle 3:** No additional formation of cracks.
    d. **Cycle 4:** No additional formation of cracks.
    e. **Cycle 5:** No additional formation of cracks.
    f. **Notes:** First hairline crack remains at the same width of 0.05 mm. The cracks disappear when the specimen is being unloaded and reappears when back at a load level of 35 kN.

3. **Load Step #3:** Elastic Cracked Moment Region: 45 kN.
    a. **Cycle 1:** New hairline cracks on the top slab (tensile region) measuring 0.05 mm in width approximately. The previous crack is relatively the same width. New cracks at 66” and 71” respectively from the cantilever free end.
    b. **Cycle 2:** No new cracks. Existing cracks measure in width approximately 0.05 mm to 0.1 mm.
    c. **Cycle 3:** No new cracks.
    d. **Cycle 4:** No new cracks.
    e. **Cycle 5:** No new cracks.

f. **Notes:** No major changes were observed on this loading step. A few more hairline cracks have formed as noted in the first 2 cycles but cracks relatively disappear when the specimen is being unloaded and reappear when back at the load level of 45 kN.

4. **Load Step #4:** Elastic Cracked Moment Region: 55 kN.
    a. **Cycle 1:** New cracks have formed on the top slab (tensile region) and existing cracks have grown in width measuring approximately 0.10 – 0.15 mm. New crack locations are at 41", 47", 55", and 61" respectively from the cantilever free end.
    b. **Cycle 2:** New hairline cracks formed on the top slab (tensile region). Existing cracks still measure approximately 0.10 to 0.15 mm in width.
    c. **Cycle 3:** No new cracks, first cracks measuring 0.15 mm.
    d. **Cycle 4:** No new cracks, an extension of existing cracks over the top slab. The first cracks measured 0.15 mm.
    e. **Cycle 5:** No new cracks, an extension of existing cracks over the top slab.
    f. **Notes:** Many new hairline cracks in this loading step measuring 0.05 mm. The original cracks in the previous load steps measure 0.15 mm in width approximately.

5. **Break Time:** During a break, the specimen was loaded to 40 kN. Maintenance vehicle wheel load.
    a. **Cycle 1:** No new cracks. Existing cracks remain at the same width as before.
    b. **Cycle 2:** No new cracks. Existing cracks remain at the same width as before.
    c. **Notes:** No major observations. Specimen rebounding elastically when unloaded.

6. **Load Step #5:** Service Load: 65 kN.
    a. **Cycle 1:** No new cracks. Extension of top slab tensile cracks (measure approximately 0.05 mm. Original cracks measuring up to 0.20 mm in width.
    b. **Cycle 2:** No new cracks. Extension of top slab tensile cracks (measure approximately 0.05 mm. Original cracks measuring up to 0.20 mm in width.
    c. **Cycle 3:** No new cracks.

d. **Cycle 4:** No new cracks.
e. **Cycle 5:** No new cracks.
f. **Notes:** No major differences from the last load step, just more hairline extensions of existing cracks over the top slab. Cracks close all the way when unloaded.

7. **Load Step #6:** 85 kN (End of Testing Day #1).
    a. **Cycle 1:** New cracks form. Cracks now span from 36" from cantilever free to 77" respectively. Extension of existing cracks and existing cracks grow to measure approximately 0.20-0.25 mm in width. Cracks roughly every 6" o/c correlating to locations of lateral 10M reinforcing bars.
    b. **Cycle 2:** New cracks form. Cracks now span from 36" from cantilever free to 77" respectively. Extension of existing cracks and existing cracks grow to measure approximately 0.20-0.25 mm in width. Cracks roughly every 6" o/c correlating to locations of lateral 10M reinforcing bars.
    c. **Cycle 3:** No new cracks but an extension of existing cracks over the top slab and hairline cracks migrating down toward the neutral axis.
    d. **Cycle 4:** No new cracks but an extension of existing cracks over the top slab and hairline cracks migrating down toward the neutral axis.
    e. **Cycle 5:** No new cracks but an extension of existing cracks over the top slab and hairline cracks migrating down toward the neutral axis.
    f. **Notes:** New cracks and extension of existing cracks. Cracks do close all the way when unloaded.

8. **Load Step #7:** Beginning of Testing Day #2: 100 kN.
    a. **Cycle 1:** Extension of existing cracks on top slab. Cracks now vary in width from 0.2 mm to 0.4 mm.
    b. **Cycle 2:** Extension of existing cracks on top slab. Cracks now vary in width from 0.2 mm to 0.4 mm.
    c. **Cycle 3:** No new cracks.
    d. **Notes:** Cracks intertwine with each other. Upon unloading the specimen, cracks are still not visible.

9. **Load Step #8:** 115 kN.
    a. **Cycle 1:** Extension of existing cracks on top slab. Cracks now vary in width from 0.2 mm to 0.5 mm.
    b. **Cycle 2:** Extension of existing cracks on top slab. Cracks now vary in width from 0.2 mm to 0.5 mm.
    c. **Cycle 3:** No new cracks.
    d. **Notes:** This is the load step where when unloading the specimen, the cracks are now visible and can be measured, at approximately 0.05-0.1 mm.

10. **Load Step #9:** 140 kN (Permanent Damage State).
    a. **Cycle 1:** New cracks formed but still within the 36" to 77" range from cantilever free end. Extension of existing cracks on the top slab and towards the neutral axis on side of the cantilever. The first original cracks now measure 0.75 mm – 1.00 mm. When unloading, cracks measure 0.20-0.25 mm in width.
    b. **Cycle 2:** Extension of cracks. Cracks now measure up to 1.10 mm. When unloaded, cracks measure 0.20-0.30 mm.
    c. **Cycle 3:** New hairline cracks on top slab and extension down to neutral axis. At the cantilever root, noticing gapping form at the fulcrum on the compression side.
    d. **Notes:** Major deflection observed, when unloaded the specimen retracts but cracks are now permanent and visible. Noticeable that ultimate failure is soon. Minor map spalling of concrete apparent on cantilever soffit.

11. **Ultimate Destruction Loading: 0-150kN:**
    a. Cracks measuring 2.50 – 3.00 mm, major deflection. The primary mode of failure: is concrete crushing at the cantilever root followed by shear failure as the second mode of failure due to continuous deflection. Spalling of concrete on soffit at around 135-150 kN range.

APPENDIX D CFRP SPECIMEN LOADING PROTOCOL AND TESTING OBSERVATIONS

1. **Load Step #1:** Uncracked Moment Region: 25 kN.
    a. **Cycle 1:** No observed cracks.
    b. **Cycle 2:** No observed cracks.
    c. **Cycle 3:** No observed cracks.
    d. **Cycle 4:** No observed cracks.
    e. **Cycle 5:** No observed cracks.
    f. **Notes:** No major concerns, specimen rebounding/retracting elastically when unloaded.

2. **Load Step #2:** 35 kN.
    a. **Cycle 1:** No observed cracks.
    b. **Cycle 2:** No observed cracks.
    c. **Cycle 3:** No observed cracks.
    d. **Cycle 4:** No observed cracks.
    e. **Cycle 5:** No observed cracks.
    f. **Notes:** No major concerns, specimen rebounding/retracting elastically when unloaded.

3. **Load Step #3:** f_cr: Onset of Cracking Region: 45 kN.
    a. **Cycle 1:** The first onset of cracking appears based on a visual. Hairline cracks have formed.
    b. **Cycle 2:** More hairline cracks. Crack locations range from 61” to 71” respectively from the cantilever free end.
    c. **Cycle 3:** More hairline cracks. Crack locations range from 56” to 71” respectively from the cantilever free end.
    d. **Cycle 4:** New hairline cracks across the top slab at 55” from the cantilever free end.
    e. **Cycle 5:** No new cracks.

f. **Notes:** No major changes were observed on this loading step. The onset of cracking commences with many hairline cracks forming. The cracks disappear when the specimen is being unloaded and reappear when back at the load level of 45 kN.

4. **Load Step #4:** Elastic Cracked Moment Region: 55 kN.
    a. **Cycle 1:** New cracks have formed on the top slab (tensile region) and existing cracks have grown in width measuring approximately 0.02 – 0.05 mm. New crack locations from 54" to 71" respectively from the cantilever free end.
    b. **Cycle 2:** New hairline cracks formed on the top slab (tensile region). Existing cracks still measure approximately 0.02 to 0.05 mm in width.
    c. **Cycle 3:** No new cracks.
    d. **Cycle 4:** No new cracks.
    e. **Cycle 5:** No new cracks.
    f. **Notes:** Many new hairline cracks in this loading step measuring 0.05 mm.

5. **Break Time:** During the break, the specimen loaded to 40 kN. Maintenance vehicle wheel load.
    a. **Cycle 1:** No new cracks. Existing cracks remain at the same width as before.
    b. **Cycle 2:** No new cracks. Existing cracks remain at the same width as before.
    c. **Notes:** No major observations. Specimen rebounding elastically when unloaded.

6. **Load Step #5:** Service Load: 65 kN.
    a. **Cycle 1:** New cracks have formed on the top slab (tensile region) and existing cracks have grown in width measuring approximately 0.05 mm. New crack locations from 47" to 71" respectively from the cantilever free end.
    b. **Cycle 2:** No new cracks. Extension of top slab tensile cracks (measure approximately 0.05 mm. Original cracks measuring up to 0.10 mm in width.
    c. **Cycle 3:** No new cracks.
    d. **Cycle 4:** No new cracks.
    e. **Cycle 5:** No new cracks.

f. **Notes:** No major differences from the last load step, just more hairline extensions of existing cracks over the top slab. Cracks close all the way when unloaded. More map cracking in CFRP rehab. the specimen at service than the control but crack widths are smaller. No evidence of grout splitting in NSM grooves. The grooves are in good condition. No slippage or movement at live and dead anchors.

7. **Load Step #6:** 85 kN (End of Testing Day #1).
    a. **Cycle 1:** New cracks form. Cracks still span from 47" from cantilever free to 77" respectively. Extension of existing cracks and existing cracks grow to measure approximately 0.10 mm in width. Cracks roughly every 6" o/c correlating to locations of lateral 10M reinforcing bars. Most cracks are within the 0.05 mm to 0.10 mm range approximately.
    b. **Cycle 2:** New cracks form. Cracks still span from 36" from cantilever free to 77" respectively. Extension of existing cracks and existing cracks grow to measure approximately 0.10 mm in width. Cracks roughly every 6" o/c correlating to locations of lateral 10M reinforcing bars.
    c. **Cycle 3:** No new cracks but an extension of existing cracks over the top slab and hairline cracks migrating down toward the neutral axis.
    d. **Cycle 4:** No new cracks but an extension of existing cracks over the top slab and hairline cracks migrating down toward the neutral axis.
    e. **Cycle 5:** No new cracks but an extension of existing cracks over the top slab and hairline cracks migrating down toward the neutral axis.
    f. **Notes:** New cracks and extension of existing cracks. Cracks do close all the way when unloaded. NSM grooves remain in good condition, intact, and with no evidence of splitting or CFRP rod bond slip. No slippage or movement in live and dead anchors.

8. **Load Step #7:** Beginning of Testing Day #2: 100 kN.
    a. **Cycle 1:** Extension of existing cracks on top slab. Cracks now vary in width from 0.15 mm to 0.20 mm.

b. **Cycle 2:** Extension of existing cracks on top slab. Cracks now vary in width from 0.15 mm to 0.20 mm.
c. **Cycle 3:** No new cracks.
d. **Notes:** Cracks intertwine with each other. Spider web/map cracking is evident. Upon unloading the specimen, cracks are still not visible. NSM grooves remain in good condition, intact, and with no evidence of splitting or CFRP rod bond slip. No slippage or movement in live and dead anchors.

9. **Load Step #8:** 115 kN.
    a. **Cycle 1:** Intertwining of existing cracks on top slab. Cracks now vary in width from 0.1 mm to 0.3 mm.
    b. **Cycle 2:** Extension of existing cracks on top slab. Cracks now vary in width from 0.1 mm to 0.3 mm.
    c. **Cycle 3:** No new cracks.
    d. **Notes:** This is the load step where when unloading the specimen, the cracks are now visible but cannot be measured yet. NSM grooves remain in good condition, intact, and with no evidence of splitting or CFRP rod bond slip. No slippage or movement in live and dead anchors.

10. **Load Step #9:** 140 kN
    a. **Cycle 1:** New cracks formed but still within the 36” to 77” range from cantilever free end. Extension of existing cracks on the top slab and towards the neutral axis on side of the cantilever. The first original cracks now measure 0.5 mm to 0.6 mm. When unloading, cracks measure 0.05-0.1 mm in width.
    b. **Cycle 2:** Extension of cracks. Cracks now measure up from 0.1 mm to 0.75 mm. When unloaded, cracks measure 0.05-0.01 mm.
    c. **Cycle 3:** No new cracks.
    d. **Notes:** Major deflection observed, when unloaded the specimen retracts but cracks are now permanent and visible. No noticeable failure yet. NSM grooves remain in good condition, intact, and with no evidence of splitting or CFRP rod

bond slip. No slippage or movement in live and dead anchors.

11. Load Step #10: 160 kN

- **a. Cycle 1:** Extension of existing cracks on the top slab and towards the neutral axis on side of the cantilever. The first original cracks now measure up to 1.25 mm. Crack widths range from 0.20 to 1.25 mm. Crack locations from 36” to 77” respectively from the cantilever free end. When unloading, some cracks are permanent measuring 0.4 mm in width.
- **b. Cycle 2:** Extension of cracks. Cracks now measure up to 1.25 mm. Ultimate failure was apparent. Map spalling of concrete apparent on the soffit.
- **c. Notes:** Noticeable failure apparent, the onset of groove grout splitting commencing at cantilever root. No slippage or movement in live and dead anchors.

12. Ultimate Destruction Loading: 0-160kN:

- **a.** Cracks measuring 1.25-1.50 mm, major deflection. The primary mode of failure: is concrete crushing at the cantilever root. No observed shear failure from deformation. Crack widths are not wide but there are more of them than the control. NSM groove splitting occurred minorly at the cantilever root at ultimate only, otherwise, the grooves were in good condition. A good bond between NSM CFRP and concrete. No slippage or movement in live and dead anchors.

APPENDIX E BRIDGE CANTILEVER SPECIMEN LOAD-DEFLECTION CURVES

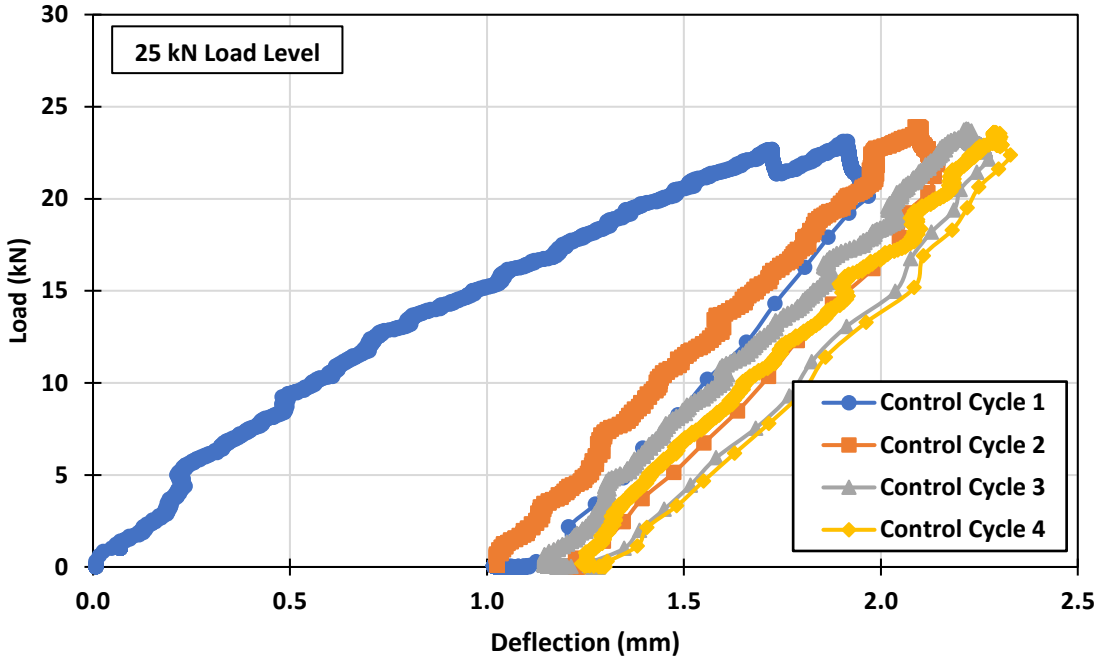

Figure E.1. Control Specimen 25 kN Load-Deflection Curve

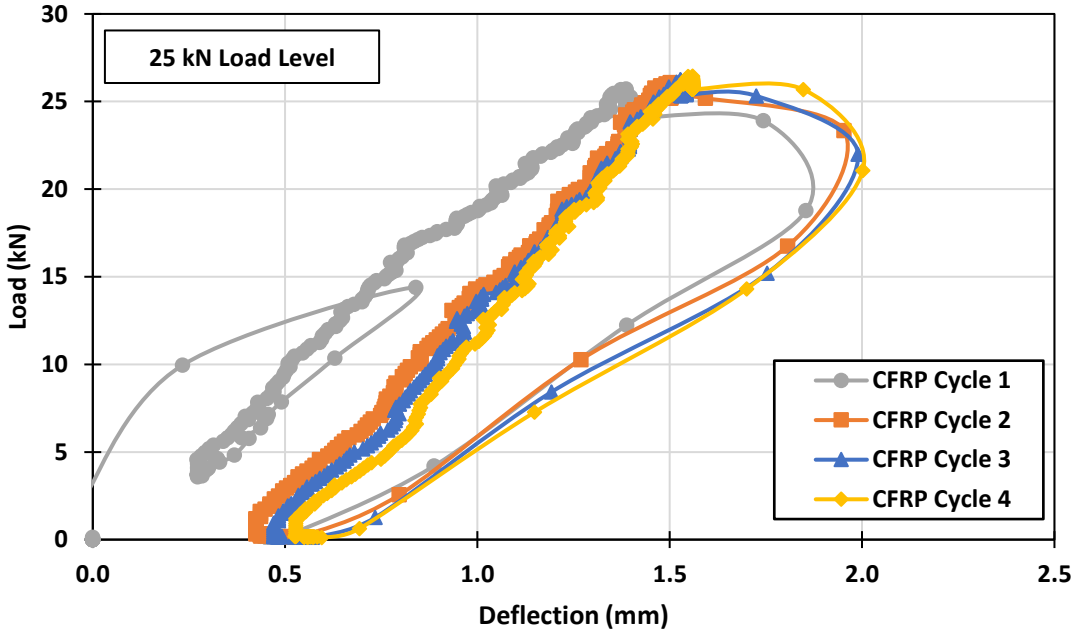

Figure E.2. Rehabilitation Specimen 25 kN Load-Deflection Curve

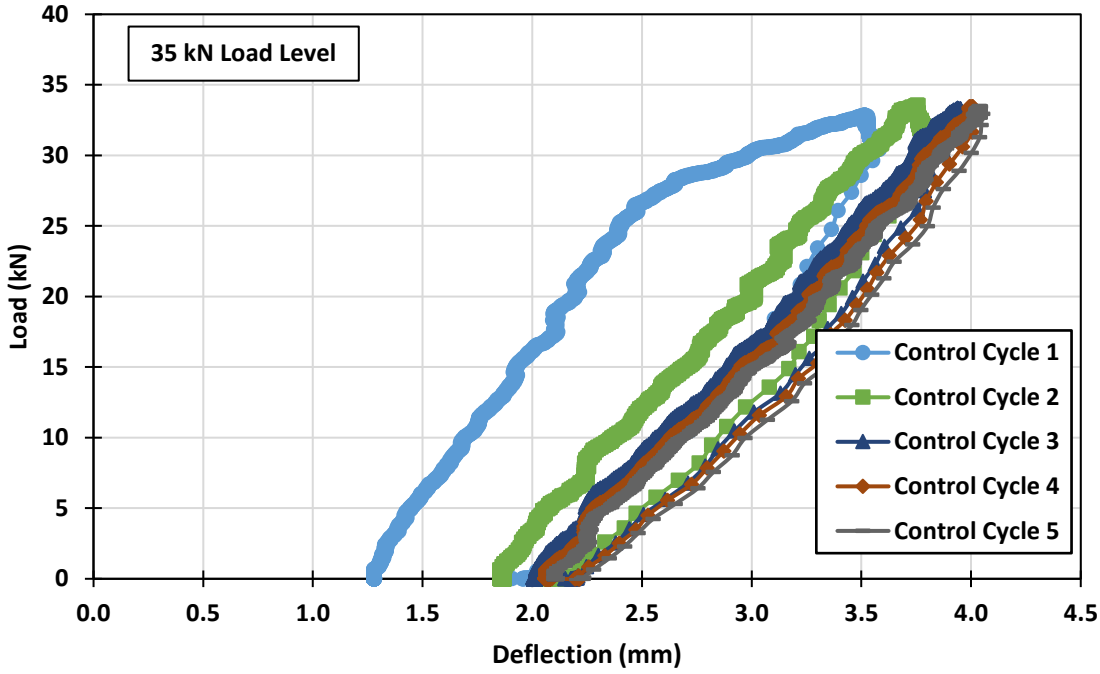

Figure E.3. Control Specimen 35 kN Load-Deflection Curve

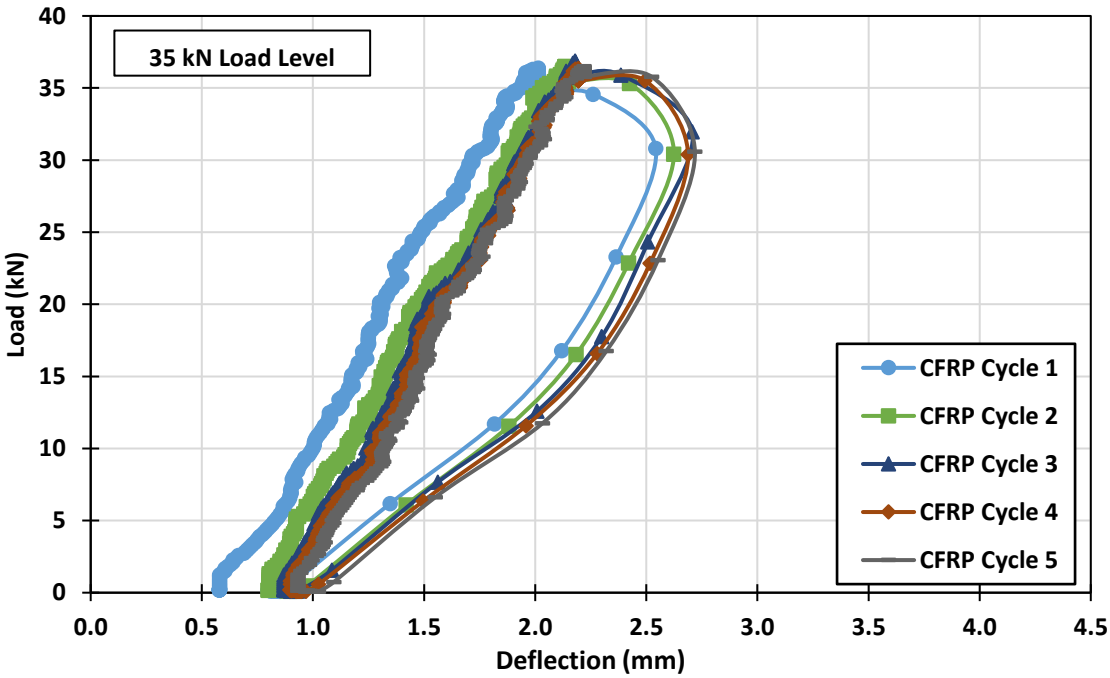

Figure E.4. Rehabilitation Specimen 35 kN Load-Deflection Curve

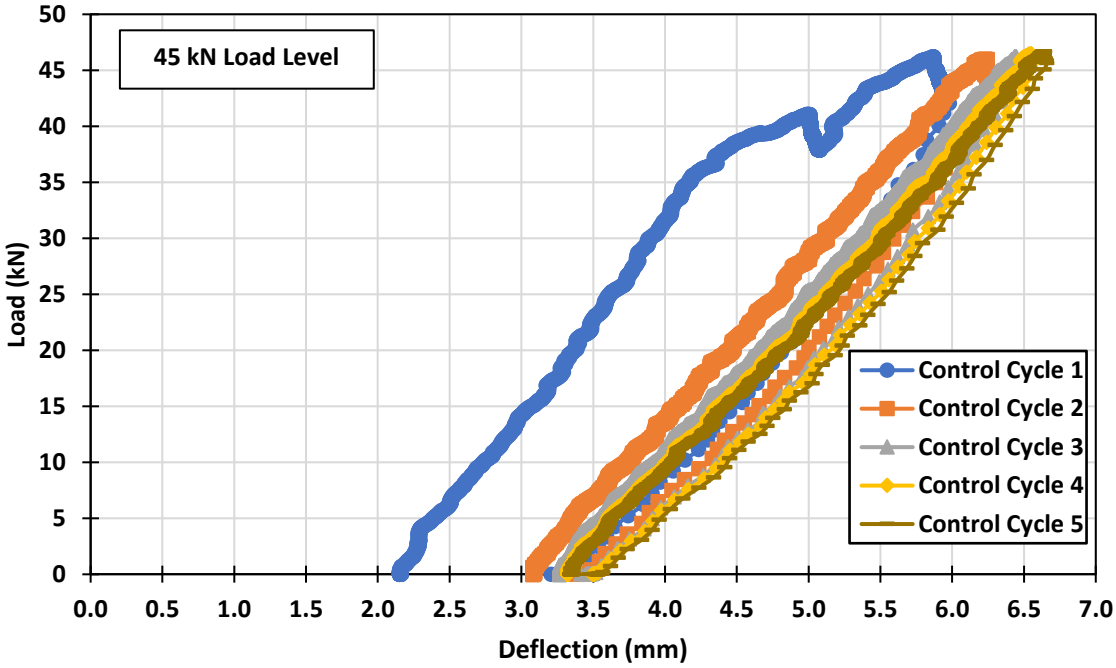

Figure E.5. Control Specimen 45 kN Load-Deflection Curve

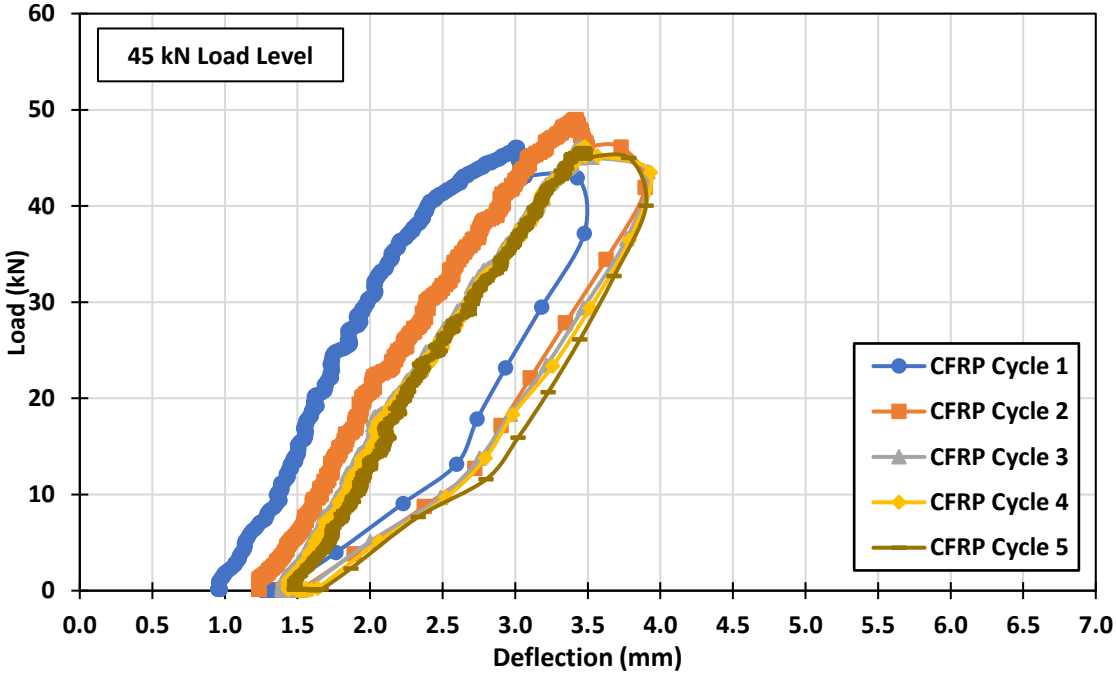

Figure E.6. Rehabilitation Specimen 45 kN Load-Deflection Curve

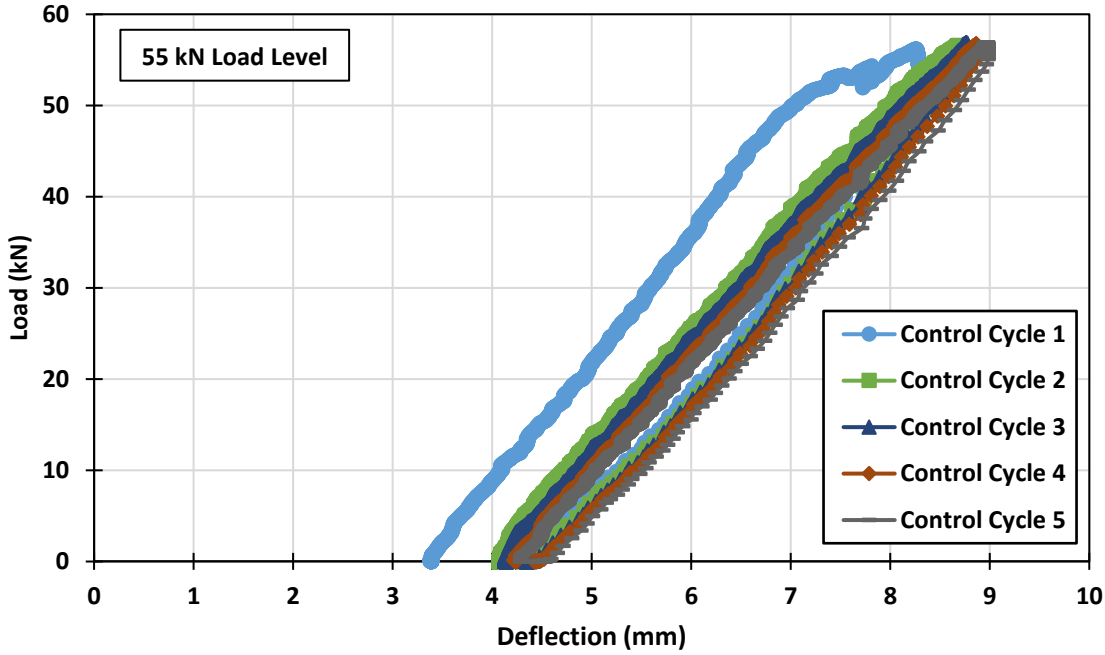

Figure E.7. Control Specimen 55 kN Load-Deflection Curve

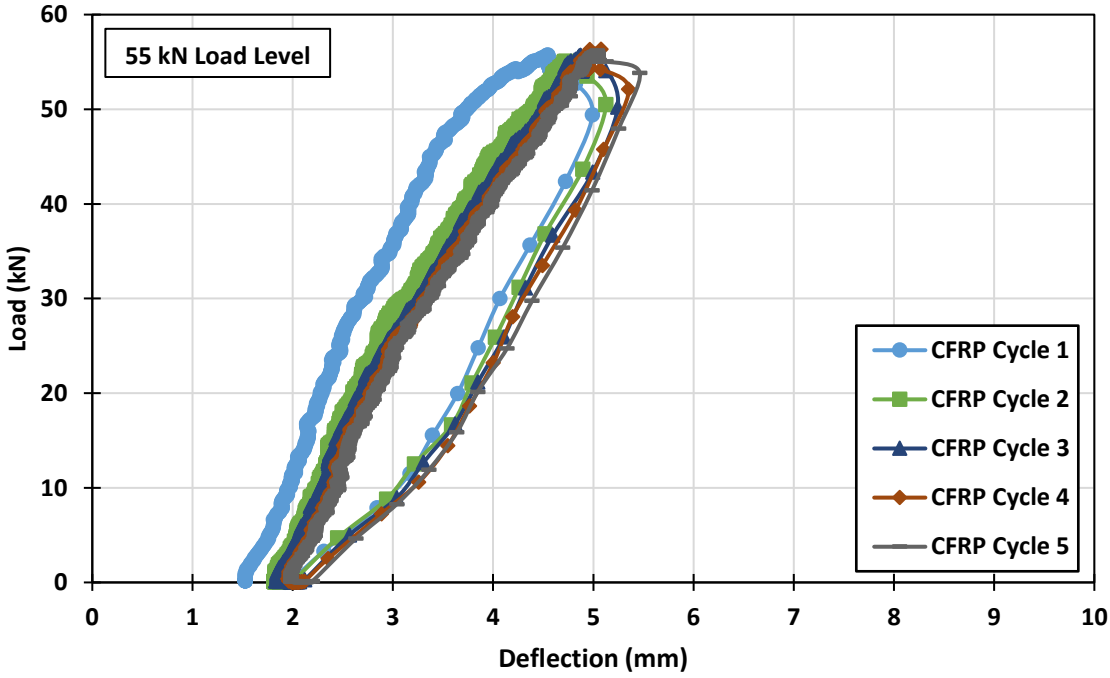

Figure E.8. Rehabilitation Specimen 55 kN Load-Deflection Curve

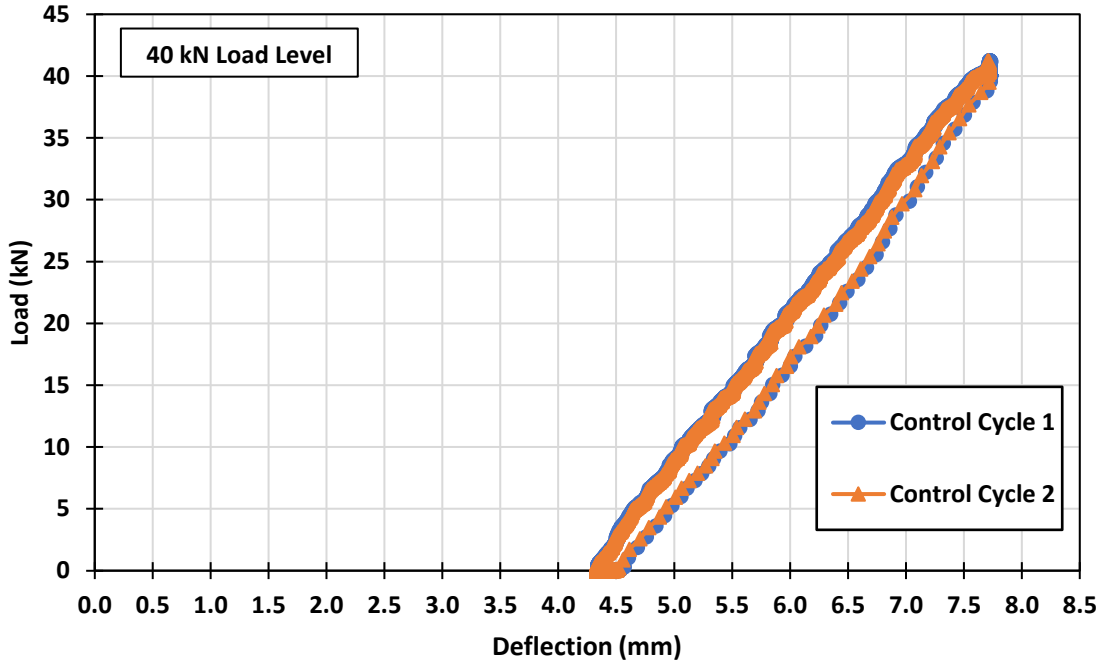

Figure E.9. Control Specimen 40 kN Load-Deflection Curve

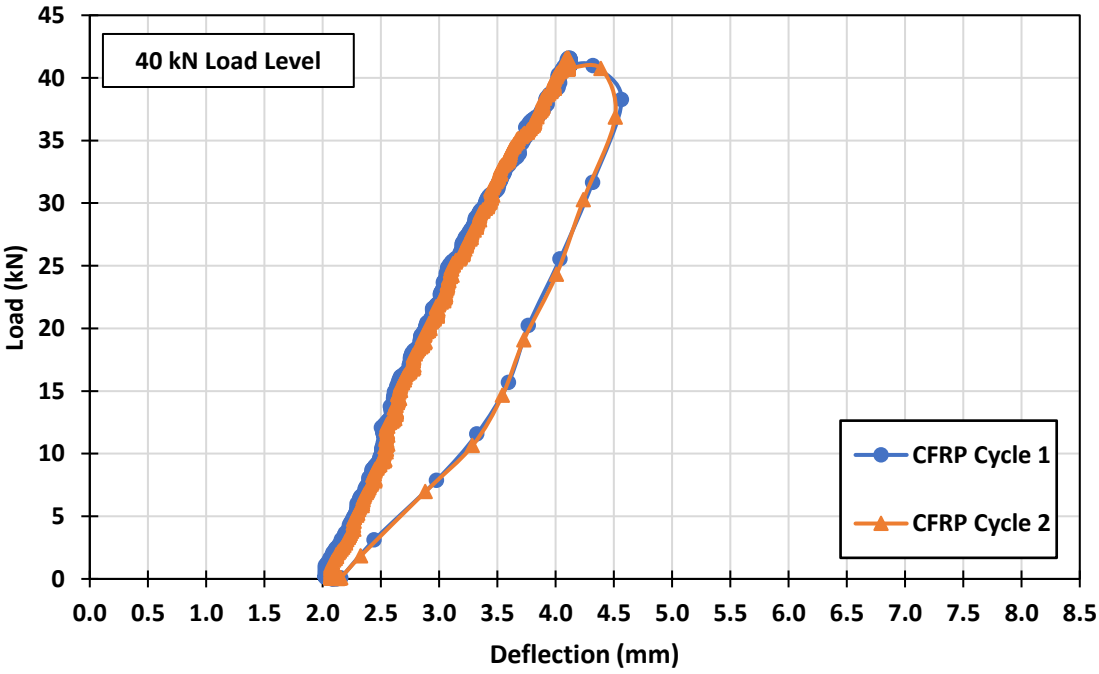

Figure E.10. Rehabilitation Specimen 40 kN Load-Deflection Curve

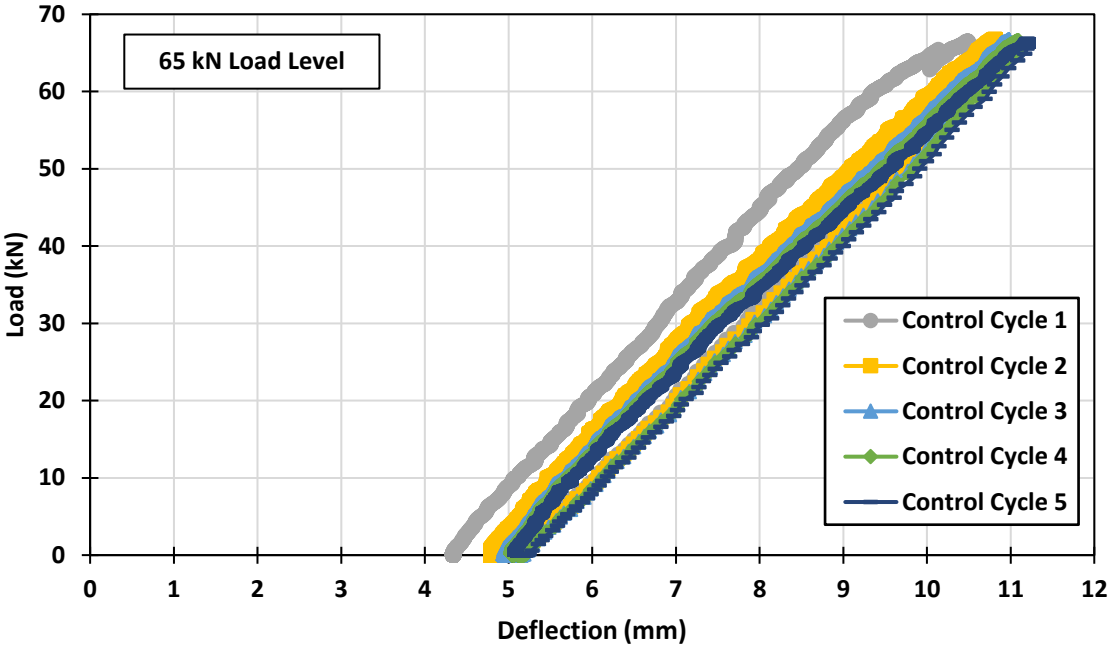

Figure E.11. Control Specimen 65 kN Load-Deflection Curve

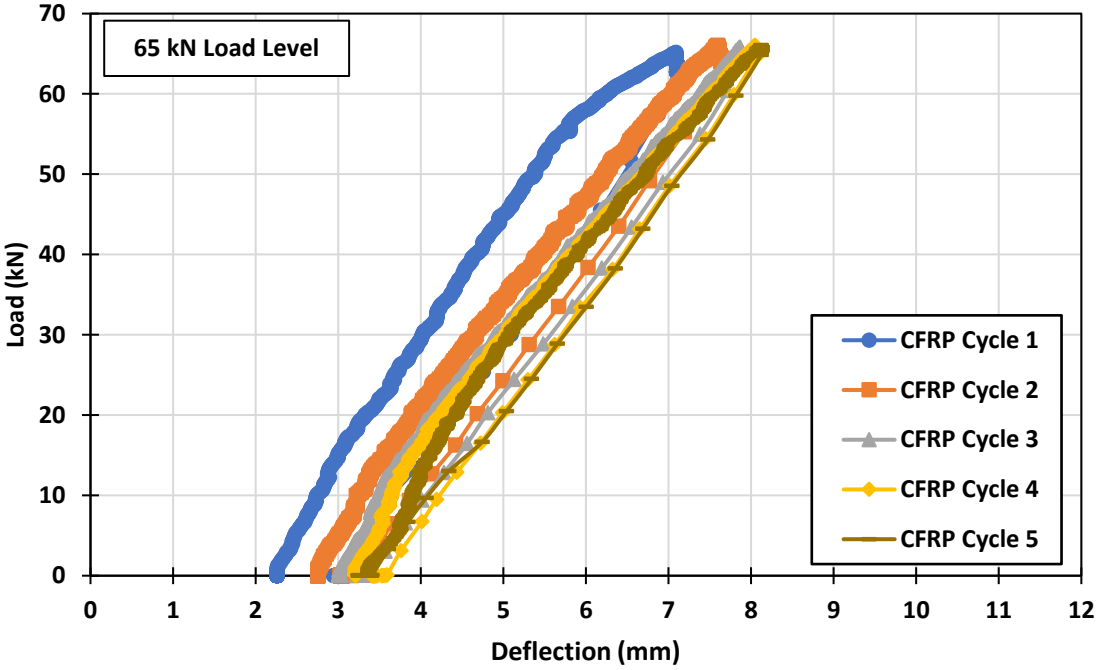

Figure E.12. Rehabilitation Specimen 65 kN Load-Deflection Curve

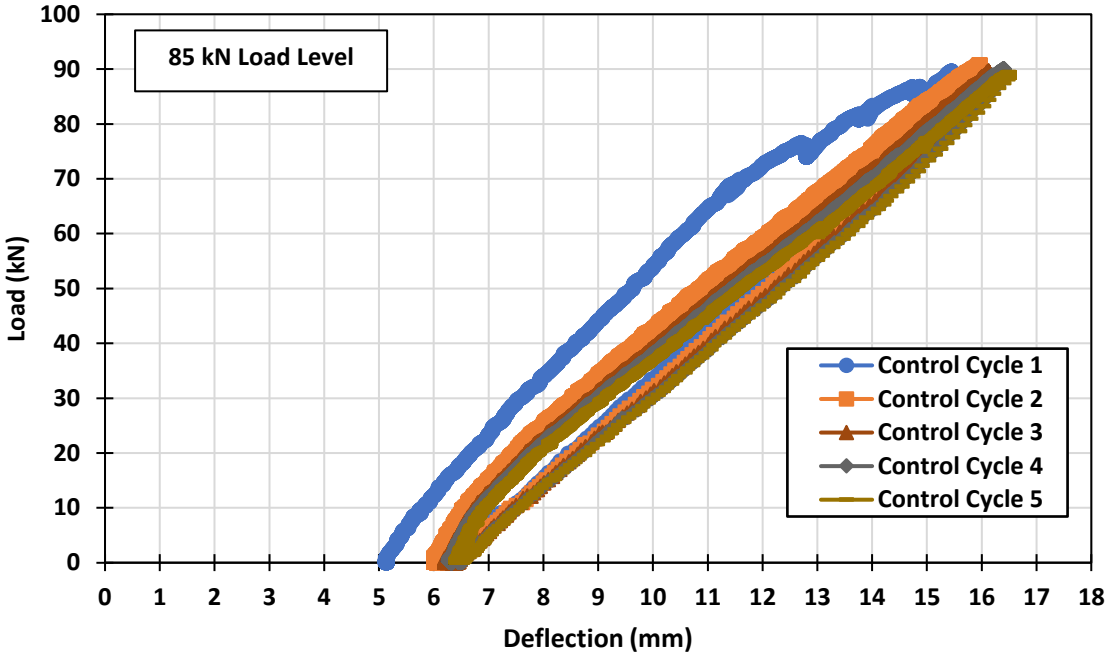

Figure E.13. Control Specimen 85 kN Load-Deflection Curve

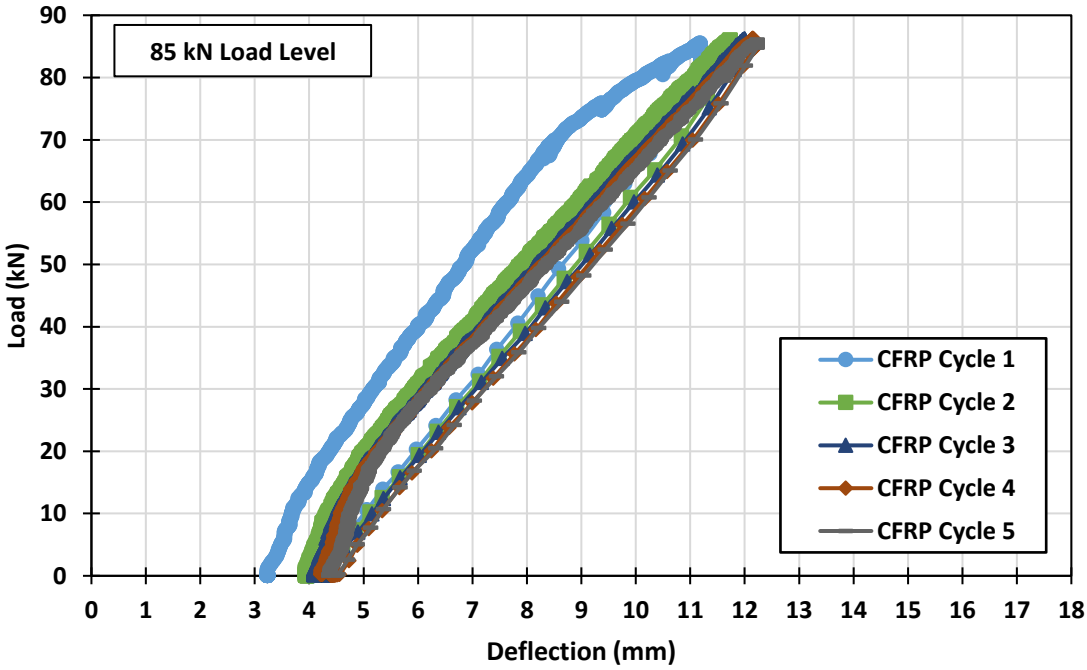

Figure E.14. Rehabilitation Specimen 85 kN Load-Deflection Curve

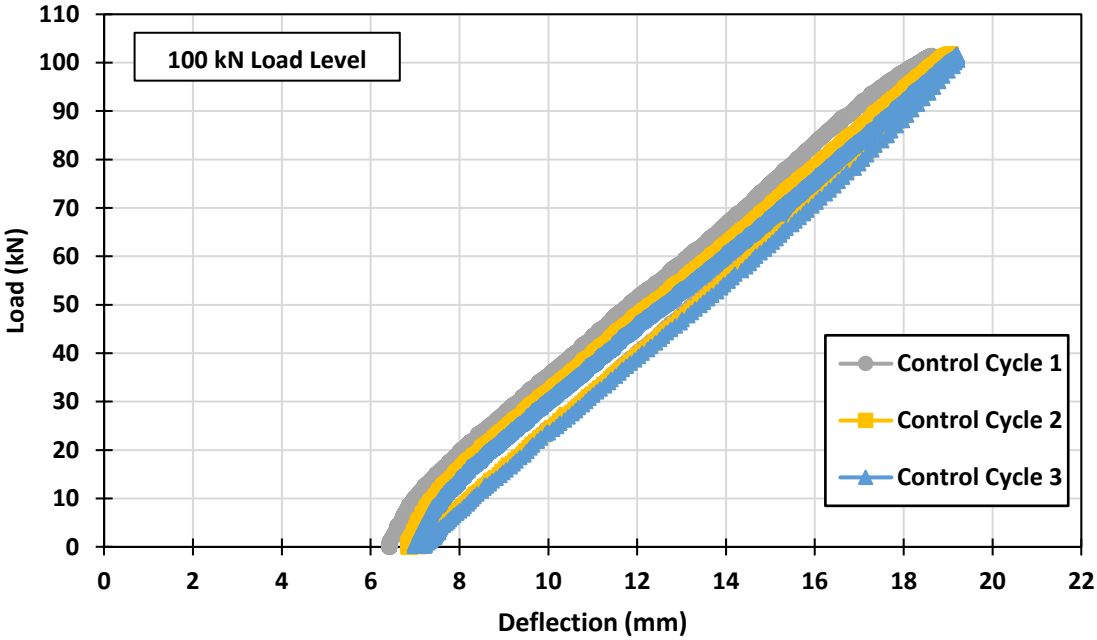

Figure E.15. Control Specimen 100 kN Load-Deflection Curve

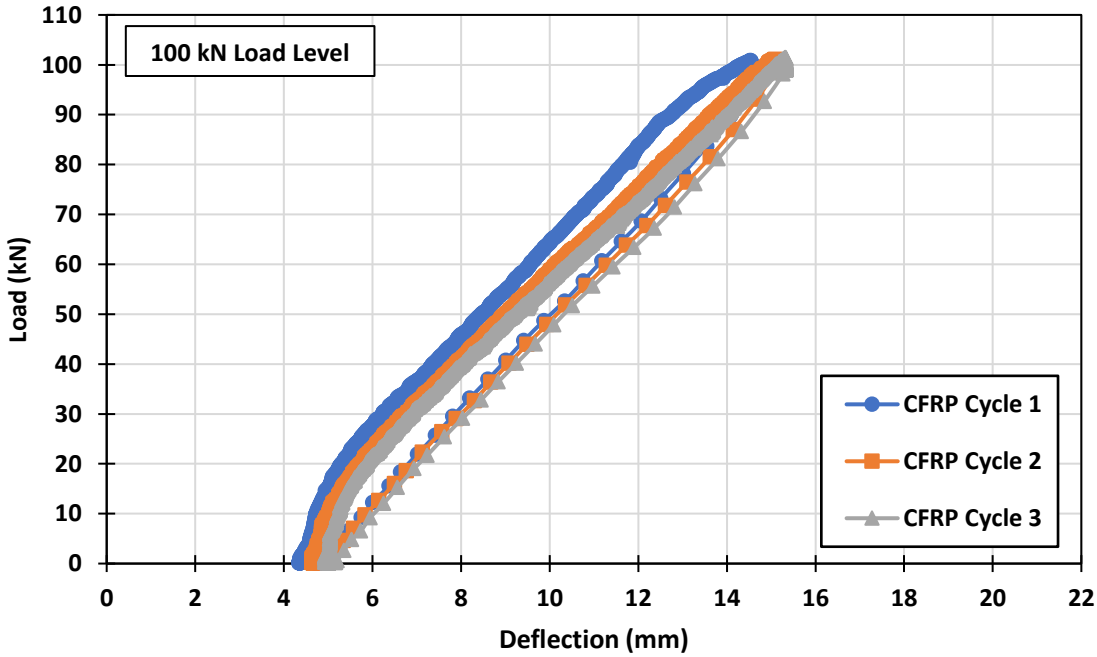

Figure E.16. Rehabilitation Specimen 100 kN Load-Deflection Curve

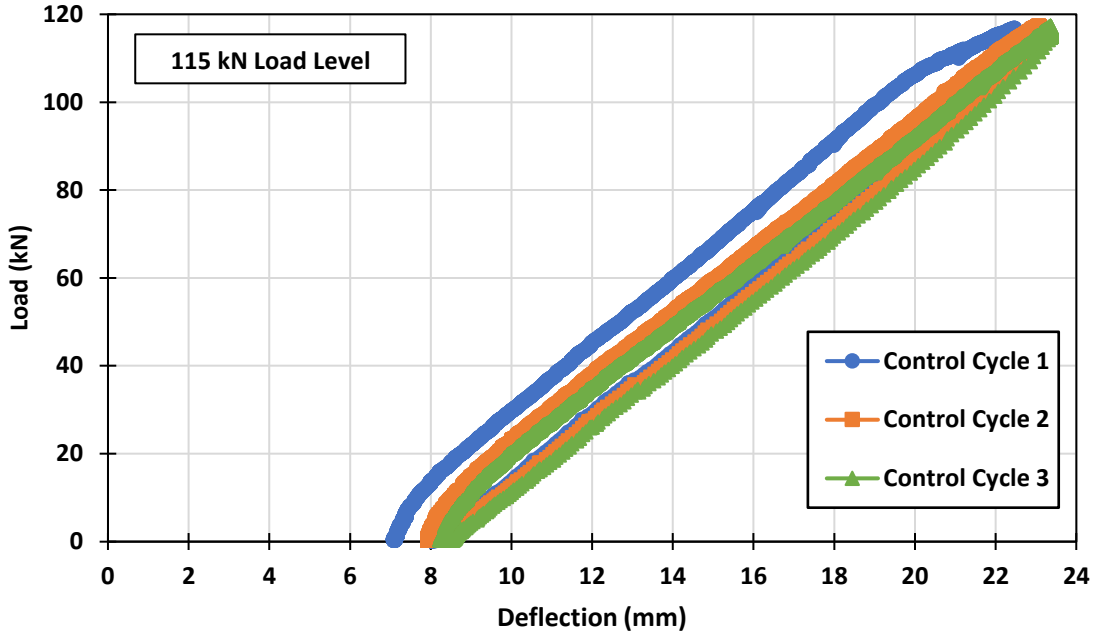

Figure E.17. Control Specimen 115 kN Load-Deflection Curve

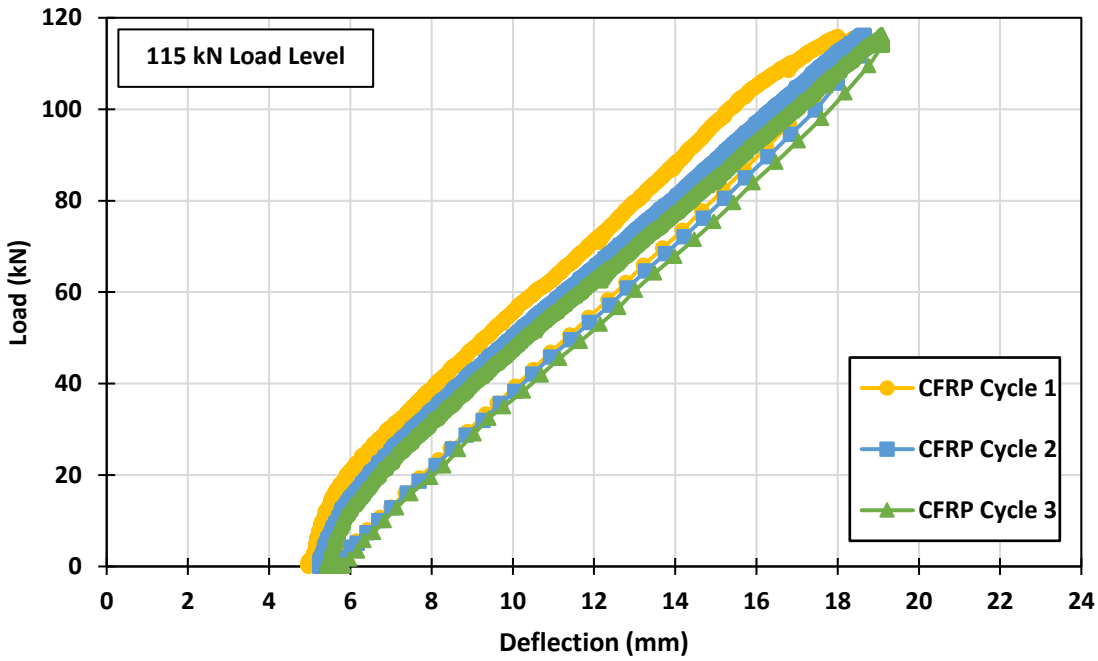

Figure E.18. Rehabilitation Specimen 115 kN Load-Deflection Curve

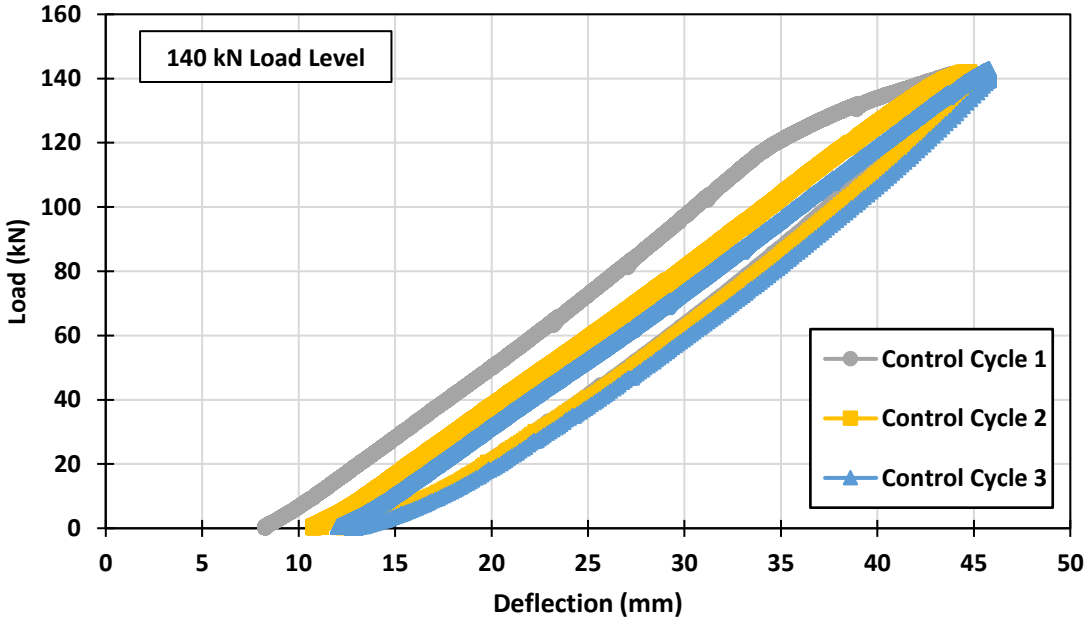

Figure E.19. Control Specimen 140 kN Load-Deflection Curve

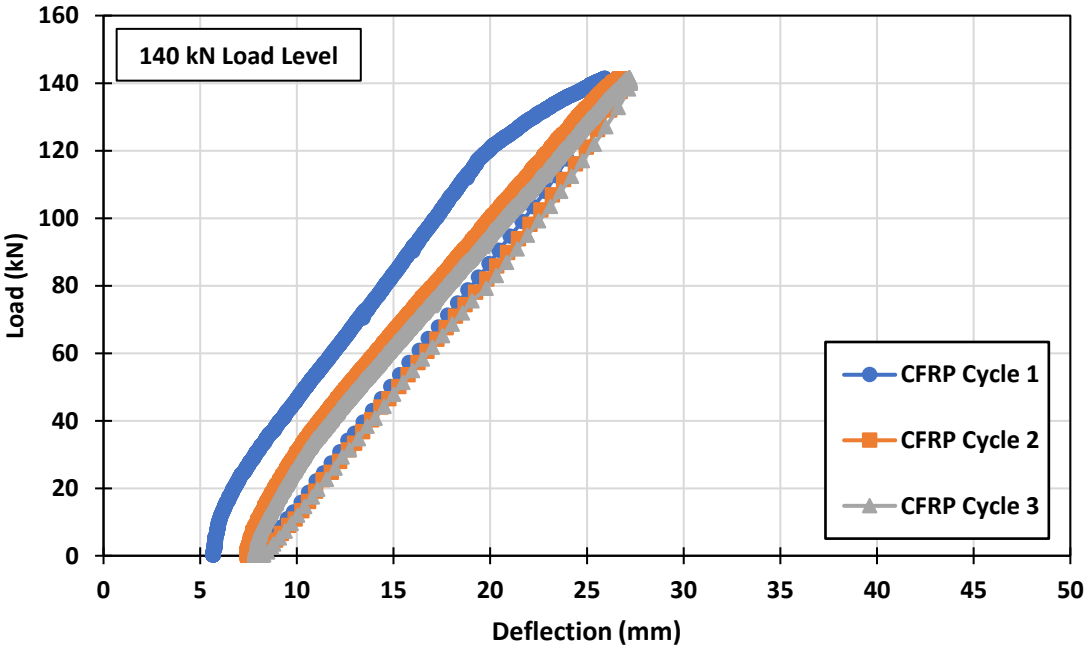

Figure E.20. Rehabilitation Specimen 140 kN Load-Deflection Curve

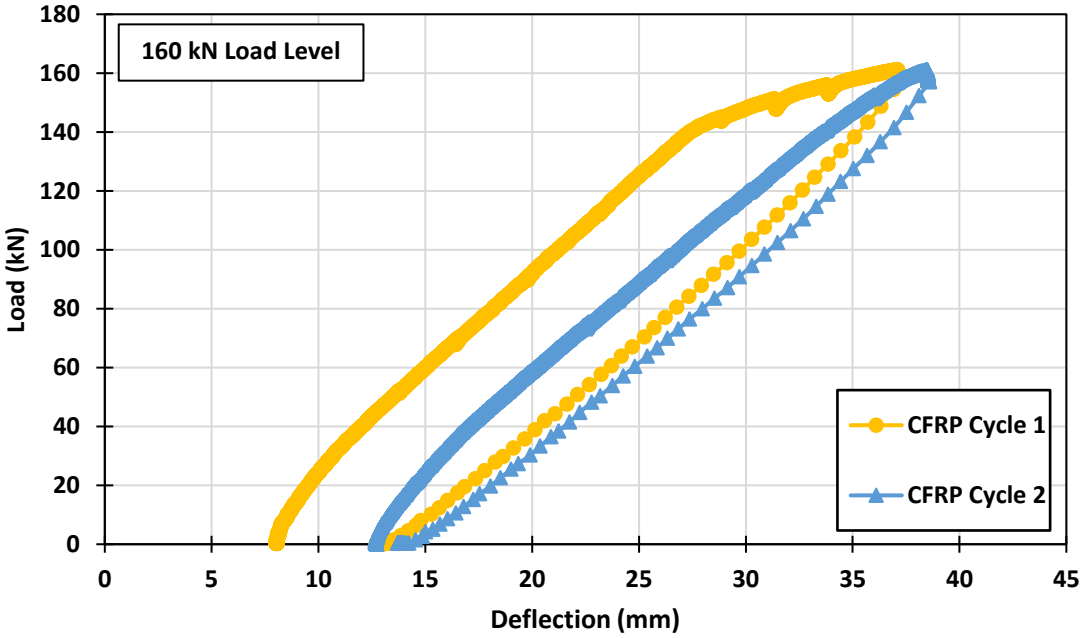

Figure E.21. Rehabilitation Specimen 160 kN Load-Deflection Curve

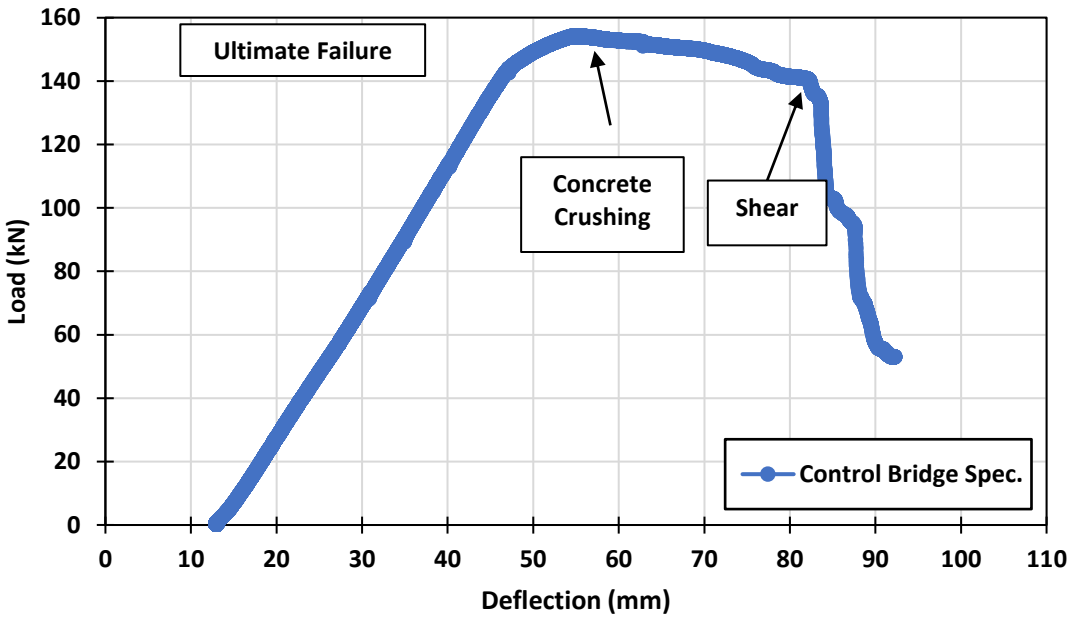

Figure E.22. Control Specimen Ultimate Load-Deflection Curve

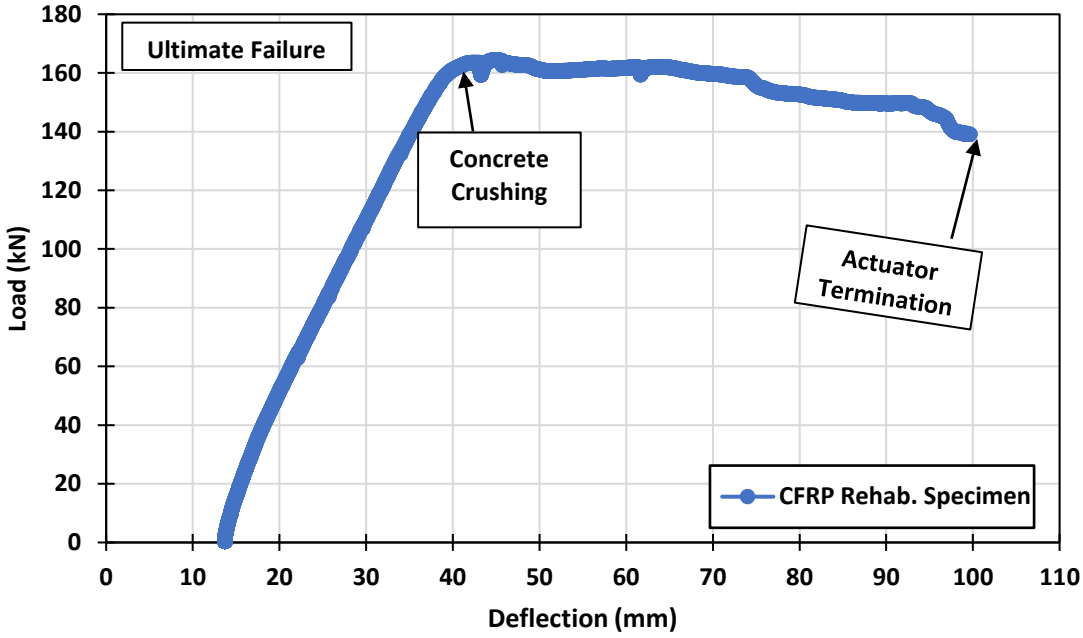

Figure E.23. Rehabilitation Specimen Ultimate Load-Deflection Curve